Deformation under the constant stress state and its effect on stress-strain behaviour of Fraser River Sand

by

Takahiro Shozen

B.Sc.Engg., Kansai University, 1991

A THESIS SUBMITTED IN PARTIAL FULFILMENT OF THE REQUIREMENTS FOR THE DEGREE OF MASTER OF APPLIED SCIENCE

in

THE FACULTY OF GRADUATE STUDIES

Department of Civil Engineering

We accept this thesis as conforming to the required standard.

THE UNIVERSITY OF BRITISH COLUMBIA

March 2001

In presenting this thesis in partial fulfilment of the requirements for an advanced degree at the University of British Columbia, I agree that the Library shall make it freely available for reference and study. I further agree that permission for extensive copying of this thesis for scholarly purposes may be granted by the head of my department or by his or her representatives. It is understood that copying or publication of this thesis for financial gain shall not be allowed without my written permission.

Department of Civil Eng.

The University of British Columbia
Vancouver, Canada

Date Mar 6th 2001

Abstract

This study was carried out to improve our understanding of the behaviour of Fraser River Sand during and after ageing

The main objectives of this study are (a) the effects of ageing time under constant stress state on the stiffness of sand and (b) the effects of stress path during subsequent shear. Identical soil samples were aged under constant stresses for 1, 10, 100 and 1,000 minutes prior to shear along a variety of stress paths. The effects of the levels of confining stress and initial effective stress ratio on changes in stiffness due to ageing under a given stress path were also investigated.

The effect of ageing time is recognized regardless of the condition applied under the triaxial test. The magnitude of the considerable increase occurs in shear modulus with increased holding duration. In addition, this increase becomes more significant when the ageing stress ratio is higher. Also, the ageing time effect seems to remain only within a small strain.

The effects of applied stress paths are also observed. However, this effect is strongly dependant on the initial stress ratios.

Table of Contents

CHAPTER 4

Table of Figures

Acknowledgements

I wish to express my sincere gratitude to my supervisors Dr.J.A.Howie and Dr.Y.P.Vaid for their support, guidance and encouragement during this research. The helpful discussions with my colleagues in the geotechnical research group at University of British Columbia, especially S. Sivathayalan and A. Eliadorani, are also appreciated.

The help of Civil Engineering Department mechanical and electronics workshop, especially, by Harald Schrempp and John Wong is gratefully acknowledged.

Financial support provided by the University of British Columbia and the Natural Science and Engineering Research Council of Canada and are acknowledged with deep appreciation.

CHAPTER 1

Introduction

Creep behaviour and ageing in soils has been recognized by many researchers who have studied their effects on the deformation characteristics of soils. The primary interest has been in the creep behaviour of clay. This may be because the settlements that occur under constant stress state are large and may reach unacceptable levels. On the other hand, the creep in sand is very small compared to those in clay.

The effect of time on the properties of sand has been recognized in the results of in-situ tests. The densification of foundation soils is often carried out in order to improve ground conditions. The cone penetration tip resistance increases with time after ground compaction, as indicated by measurements conducted at varying times after compaction (Mitchell and Solymar, 1984). In the past 15 years, creep of sand has gained more interest amongst researchers. Several laboratory studies have been carried out on the topic as transducers have become capable of measuring strain in the small range. The main interest in these studies has been the creep observed during pauses in shearing. However, the increase in moduli with ageing and time have not been systematically quantified.

This thesis presents an experimental study of the effects of ageing time on stiffness of Fraser River Sand in the triaxial test. The main object of the study was to delineate the strain development due to ageing under a constant stress state, and to investigate its effect on stress strain response during shearing. Each sand specimen was aged for a different period prior to the shear stage. The effects of ageing on stiffness were assessed under a variety of stress paths during shear. The influence of the level of initial confining stress and static shear stress ratio on stiffness increase due to ageing were also investigated.

CHAPTER 2

Literature Review

Time effects on the small strain modulus in soil have been recognized as an important factor in the characterization of the material properties for design of foundations. In clay, the slow continued compression that continues after the excess pore pressure has substantially dissipated is called secondary compression. The exact cause of secondary compression is not known. It is probably caused by continued reorientation of particles, possibly influenced by the extrusion of water which is held by attractive forces from the soil particles. (Lambe, 1969). Mitchell (1976) suggests that secondary compression involves a time-dependent adjustment of the soil structure and can be considered as a creep-type phenomenon. Secondary compression has been recognized for many years as an important contribution to total compression. Since secondary consolidation in clay results in significant deformation and changes in soil properties, many studies have been carried out providing results useful to practice. On the contrary, in sand under the stress state commonly encountered, pore pressure dissipation takes place rapidly and the deformation generated after primary consolidation may be very small. In addition, there is no clear evidence of the existence of interparticle forces in sand. Therefore, the effect of secondary compression in sand has not been studied until recently. Unless high stresses are imposed on samples, secondary compression is generally not a concern in granular material. For sand with strong mineral particles, this phenomenon becomes important only at stresses greater than 14MPa (Lambe, 1969). However, the ageing effect in sand has been recognized in field observation. The penetration resistance increases with time after compaction. The ageing behaviour and its effect are not well understood in granular materials. Several researchers have conducted experiments on various kinds of soils. This chapter will present a review of the current understanding of ageing of granular material based on field observation through in situ testing and on research in laboratory tests.

2.1 Field Evidence of Ageing

Changes in penetration resistance with time after deposition or disturbance have been recognized for some time. Mitchell and Solymar (1984) presented evidence of time-dependent penetration resistance after compaction by vibro and dynamic compaction. Figure 2.1 shows the result of the static cone resistance before densification compared to the results 9 days and 11 weeks after compaction. The penetration resistance after 9 days was actually smaller than its value before densification. This was attributed to disturbance of the sand structure. However, the cone resistance after 11 weeks increased significantly from the value before densification. Mitchell suggested that the most probable mechanism for the observed phenomenon seemed to be interparticle bonding due to the formation of silica acid gel films on the particle surface.

Charlie (1992) presented results of cone penetration tests conducted at various times

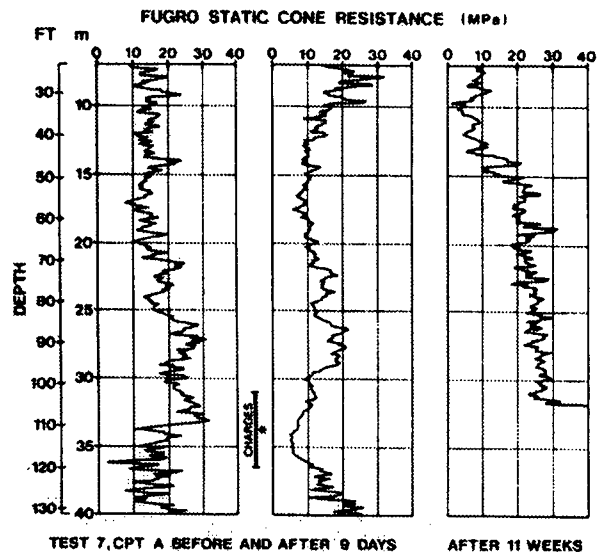

Figure 2.1 Penetration Resistance of Thick Sand Layer at Two Times After Disturbance (Mitchell and Solymar, 1984)

after ground improvement by blasting. He analyzed data from three different depth ranges for the purpose of comparison. The depth ranges for zones A, B and C were depth 0m-1.5m, 1.5m-5.1m and 5.1m or deeper respectively. One week after blasting, the average tip resistance in all zones was reduced by 46%. Eighteen weeks after blasting, the average increase in all zones over the value one week after blasting was 12%.

Schmertmann (1991) also presented evidence of increasing penetration resistance with time after dynamic compaction. Schmertmann suggested that a dispersive particle reorentation take place in all soils with time and that this results in an increase in particle friction causing a gain in modulus and strength with time. He suggested that this is also applicable to clay samples (Schmertmann, 1981). Whether clay or sand, Schmertman argued that the frictional gain is the reason for increase in modulus and strength with time. As far as the material fabric is concerned, it is worthwhile to point out that, under constant consolidation stresses, both G_0 and E_0 increase with time when subject to drained creep. The stiffness increase is much more pronounced in fine grained soils (Jamiolkowski, 1998).

Mesri (1990) suggested that the drained ageing of clean sands develops increased frictional resistance through macrointerlocking of particles and microinterlocking of surface roughness.

Berardi et al (1991) presented data obtained from two depth ranges in the silica sand and gravel deposit at the Sicilian shore of the Messina Strait in Italy. Comparisons of small strain shear modulus calculated from shear wave velocity seismic tests were made for two different strata. The shallow stratum was of Holocene age while the other belonged to the Pleistocene period. Both Holocene and Pleistocene materials had very similar mineralogical composition, grading and in-situ density. The measured normalized shear modulus of Pleistocene material was 4 times higher than that of the Holocene material. The large differences in shear modulus between two strata can be attributed to their different age. This large increase, however, was not obtained in the measurement in SPT resistance.

2.2 Laboratory evidence of ageing of sand samples

Tatsuoka (1998) presented the results of laboratory testing on Hostun Sand. Plane strain compression tests were performed by Casacliu et al. (1998) and Matsushita et al. (1998a, b). Hostun Sand is a quartz-rich, sub-angular, poorly-graded medium-grained sand with D_{50}=0.31mm, C_u=1.94, G_s=2.65, e_{max}=0.95 and e_{min}=0.55. This is very similar to Fraser River Sand. Void ratios of samples were around 0.615, which represents a relative density of about 80%. The stress history applied to the sample was very complicated. After saturation, samples were consolidated isotropically to p'=29kPa, followed by plane strain compression

(PSC) to a stress state with the lateral stress σ'_h=29kPa and the vertical stress σ'_v=88.2kPa. Specimens were then anisotropically consolidated at K=1/3 (R=3.0) up to a stress state of σ'_h=352kPa, σ'_v=1.18MPa with the vertical strain rate ε_v=0.0125%/min. After a pause of about three minutes, a set of specimens was then subjected to drained PSC at σ'_h=392kPa to ultimate state at constant but different axial strain rates. At various stages of the test, the

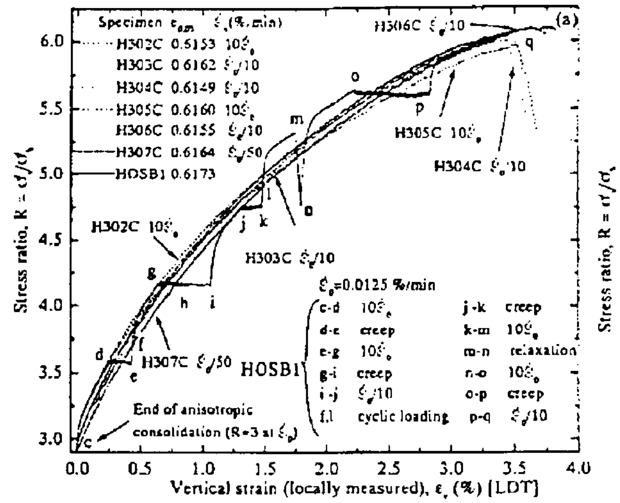

Figure 2.2 Effect of Ageing and Stress Relaxation in drained PSC tests on Houstun sand, Overall relationship between stress ratio R and axial strain ε_v (Tatsuoka, 1998)

stress ratio was held constant and the sample was allowed to strain. A typical result for the sample HOSB1 is shown in Figure 2.2. After each pause, the recommencement of loading resulted in a very stiff response. However, the stress-strain curve quickly returned to the original virgin curve as the incremental strain level increased to about 0.1%. Two different vertical strain rates were applied to the HOSB1. The strain rate difference showed the difference in the recovery of the virgin stress-strain curve: the faster the rate of strain, the higher the stress ratio at a given strain. This simply showed that the applied strain rate has some influence on the stress-strain curve in drained tests.

Daramola (1980) also observed time-dependent increase in stiffness in triaxial tests on sand specimens. Ham River Sand was used as a testing material. Four samples were prepared with an identical density in the dense state. The imposed effective confining pressure was 400kPa. One sample was sheared immediately after completion of consolidation and others were left under the consolidation pressure for durations of 10, 30 and 158 days respectively. All samples were sheared at an axial strain rate of 0.05%/min., which was slow enough for complete drainage to occur during shear. Figure 2.3 shows that the sample aged longer has a stiffer response until an axial strain of about 2.0%. When the axial strain was more than 2.0%, the stress-strain curves for 0 and 10 days crossed over. The explanation of this was

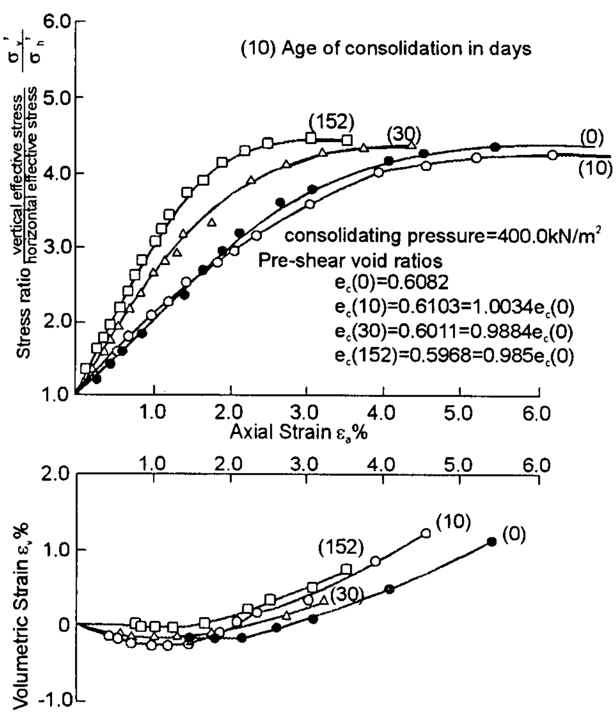

Figure 2.3 The Effect of the Age of Consolidation on Stress Strain Characteristic of Ham River Sand (Daramola, 1980)

that the relative density for unaged samples was higher than the others. The stress-strain curve was a function of relative density when the samples were not aged for a long time. However, once samples had aged longer than a certain time, relative density was not the main factor controlling stress-strain response in the small strain range. The ageing did not show significant influence on strength, which is measured at large axial strain. Volumetric strain developments for samples were also shown in the same figure. The longer aged samples had less contractive volumetric deformation during shear. Figure 2.4 shows the actual increase in

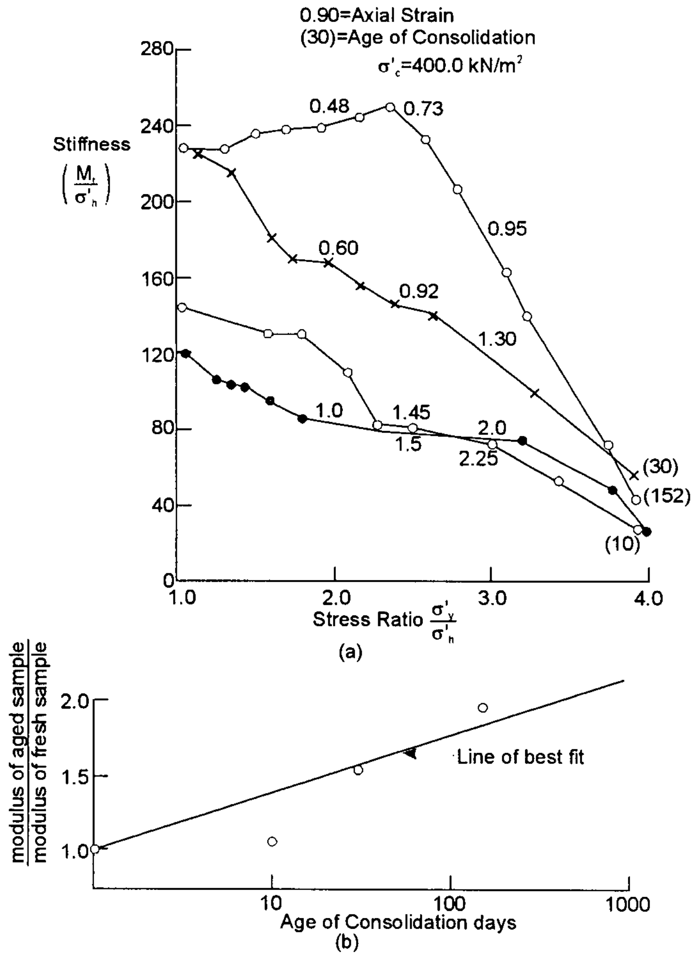

Figure 2.4 Variations of Resistance to Deformation with Consolidation Age (Dararmola, 1980)

secant modulus of aged samples relative to fresh samples. From his results, the estimated modulus will increase approximately by 50% for every log cycle of ageing. At this rate, the estimated modulus for 300 years ageing would be 3.5 times that of a freshly deposited sample at the same density.

Whitman (1964) carried out oedometer tests on a dry quartz sand to study the effect of time. The loading was held constant for a rest period during the compression test and was then resumed. The ratio of re-compression modulus with a 15 min rest to compression modulus for the first and second loading is much more than that for ones without a rest period.

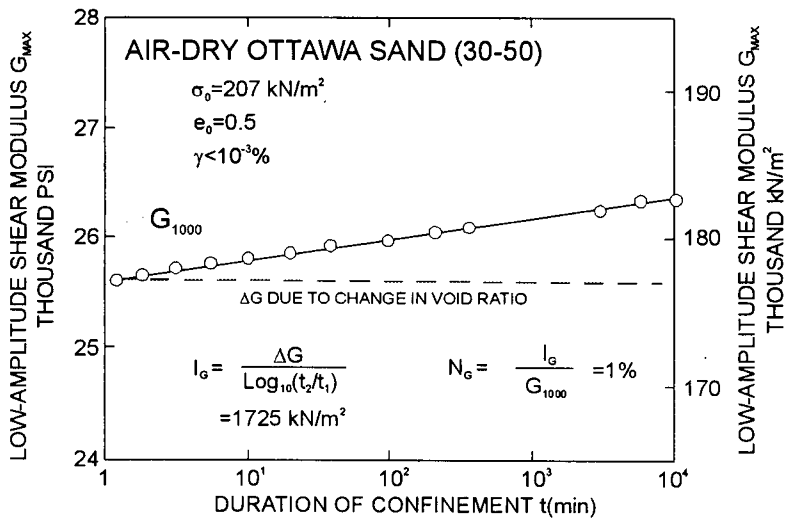

Figure 2.5 Typical Modulus change with Time for Sand (Anderson and Stokoe, 1978)

Anderson and Stokoe (1978) also studied the effect of ageing time on the shear moduli of coarse-grained soils using the resonant column test. Figure 2.5 shows the result of this test. The material used was air-dry Ottawa Sand under the hydrostatic condition with σ_0=207kPa. The shear modulus for 1,000 minutes holding duration (G_{1000}) was the first measurement and was used as the reference value of the stiffness. After a certain time of ageing, the shear modulus was measured. In Figure 2.5, a linear increase in modulus with the logarithm of time was observed for about 10,000 min. The rate of increase expressed as N_G was about 1% of G_{1000} per log cycle of ageing time. Interestingly, the magnitude of the long-term effect seems to be relatively independent of D_{50} until a value of D_{50} less than about 0.05mm. However, it is not known whether this is the case for sand other then Ottawa sand. Fahey (1998) pointed out that the shear modulus measured on an undisturbed sample was significantly greater than one predicted by using laboratory results. This was also confirmed by Murashev (1997). Fahey concluded that in-situ measurements of modulus were necessary unless very high quality undisturbed samples were available.

2.3 Creep phenomena

Creep is a phenomenon in which small deformation occurs with elapsed time under a constant stress state. Usually this term is used for the longer duration in the natural environment such as days and years. Some researchers use a term "ageing" or "time effect" as well. However, these terms are used not for the description of deformation taking place under the constant stress state but for its influence on modulus or behaviour in shear testing following a rest period. Creep used here simply indicates that deformation taking place under the constant stress state regardless of its length.

Creep phenomena are not described in all studies presented in this chapter. The influence of time is presented by describing the increase of modulus in the shearing test

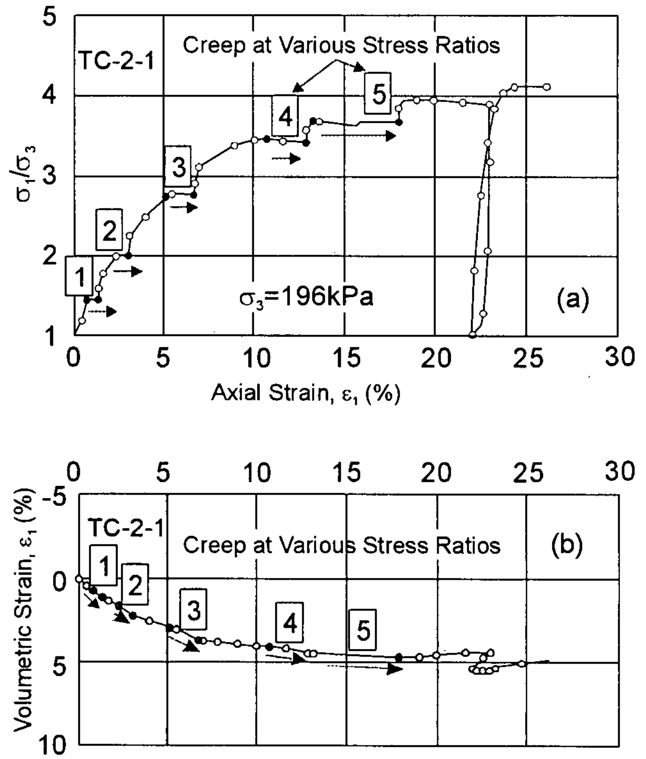

Figure 2.6 Results of Triaxial Compression Creep Tests (a) Stress Ratio versus Axial Strain. (b) Volumetric Strain versus Axial Strain for Antelope Valley Sand (Lade, 1998)

following the duration of the rest period. Lade (1998) presented the behavior of a granular sample. Material used in his research had a specific gravity of 2.81, and e_{max} and e_{min} of 1.24 and 0.98 respectively under dry conditions. The vertical load was applied to the triaxial specimen either by load control for the creep tests or by deformation control for the conventional triaxial compression tests. The void ratio of samples after the completion of saturation was in the range between 0.95 and 0.98. Creep behaviour is examined under two different conditions. One is creep under the isotropic stress state. The samples are isotropically compressed. During this process, the all-around pressure is maintained constant during creep deformation. In other cases, the creep phenomenon is observed under shearing. An example is shown in Figure 2.6. After completion of consolidation, conventional triaxial compression tests were carried out. At a selected stage of loading, the stress ratio was held constant. In order to measure axial and lateral strain, two telescopes and pins, which are attached to a membrane, are used for measuring actual deformation directly. According to this paper, the axial deformations measured by a dial gauge and by using telescopes show excellent agreement in reading, which can be seen in Figure 2.7 as system 1 and 2

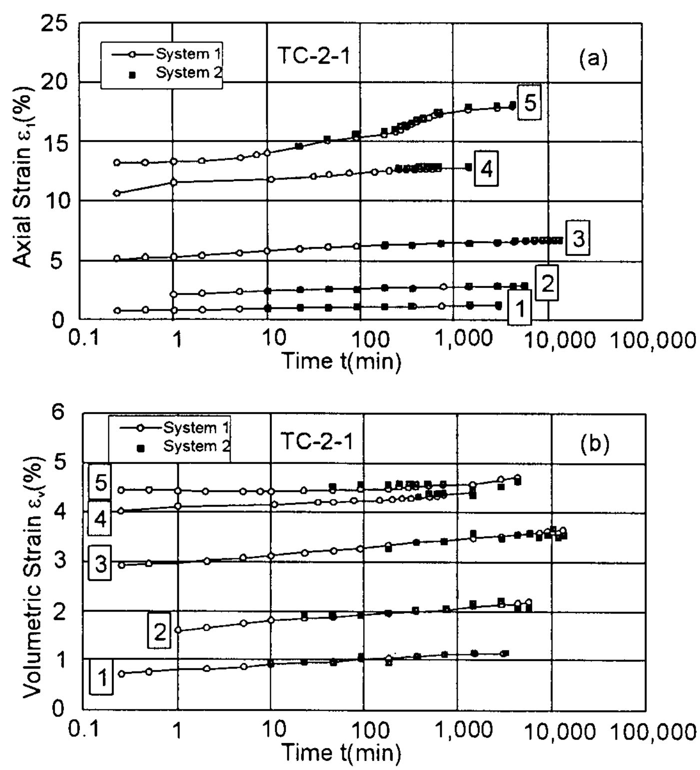

Figure 2.7 Results of Triaxial Compression Creep Tests (a) Axial Strain versus Log(time) (b) Volumetric Strain versus Log(time) (Lade, 1998)

respectively. As seen in Figure 2.7, axial and volumetric strains develop linearly against log time under isotropic stresses. In the case of the anisotropic stress state, axial strain and volumetric strain also develop linearly against the log time. However, when the stress ratio, σ'_1/σ'_3, becomes close to failure, the developments of both strains are no longer keeping a linear relationship.

Also, creep develops in a different manner depending on the angularity of soil particles. The time dependent behaviour of rounded Ottawa sand is qualitatively similar to the test data and observation presented for the angular tailing sand. However, the magnitude of creep deformations and the influences of confining stress, relative density, stress ratio and increment are less pronounced for the rounded sand in comparison to that for the angular sand (Mejia et al, 1989). Samples used for this research were prepared at a relative density of 60%.

Creep behaviour is also recognized in in-situ tests. Figure 2.8 shows a typical Full-

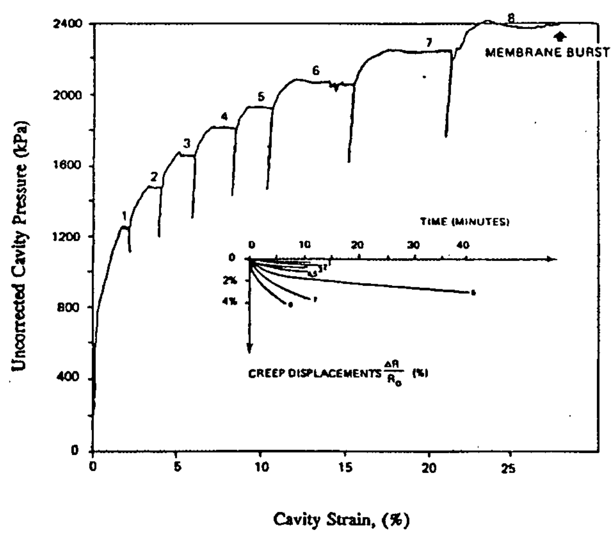

Figure 2.8 FEDPM Pressure-Expansion Curve With Multiple Creep Phases, Leidschendam Site (Howie, 1990)

Displacement Pressuremeter test result. As was noted in Mejia's work, the creep deformation for the given holding duration became larger at higher applied stress ratios. The one difference between the triaxial test and the PM test is the amount of creep observed. Nutt (1995) showed that in the pressuremeter test, the rate of strain development was controlled by the magnitude of ψ/ψ_l, where ψ was a current cavity pressure and ψ_l was the limit pressure. In the pressure meter test, the soil adjacent to the membrane attains a failure stress ratio early in the expansion and the amount of soil contributing to creep increases as the cavity pressure increases.

2.4 Recent research on the small strain behaviour of granular soils

In recent years, there has been growing acceptance that under working load soil below foundations is experiencing strain less than 0.5% with average strains typically below about 0.1% (Burland, 1989). In addition, attempts to model sand response under earthquake loading has led to increased study of the factors affecting the small strain stiffness of sand. There appears to be growing acceptance of a conceptual framework dividing the deformation into three regions of strain. Jardine (1992) described them as Zone 1 to 3.

Zone 1 corresponds to the region where behaviour is perfectly linear elastic. This was also taken to be the zone where axial strains were less than 0.001%. Zone 2 is the region in which stress-strain behaviour is non-linear but complete loading-unloading cycles show fully recoverable behaviour. This zone was defined by axial strain of between 0.001% and 0.1%. Zone 3 is outside of those two previous regions, i.e. ε_{axial}>0.1%. In the identical way, Atkinson and Sallfors(1991) also described those regions as very small strain, small and large strain respectively. Very small strain corresponds to the range of strain generally less than 0.001% where G'_0 is very nearly constant with strain. G'_0 is a shear modulus measured up to the critical strain ε_c. Small strain corresponds to the range of strain from 0.001% to 1% where the stress-strain curve is highly non-linear and G' depends on strain. Large strain corresponds to strains generally larger than about 1% where the soil is approaching failure and the shear stiffness becomes small. The only difference between two descriptions is the boundary between small and large strain. Jardine defines it as 0.1% while Atkinson selects 1%. Atkinson defines "small strain" as between 0.001% and 1% and other is between 0.001% to 0.1%.

Recently, local axial transducers have become sufficiently accurate to enable direct comparison between dynamic and continuous loading stiffness (Jovicic and Coop, 1997). Therefore, most research on stiffness has focused on the behaviour in Zone 1, or very small strain, which is the region in which G_{max} can be specified because of the characteristic of dynamic loading tests such as resonant column or bender element tests. The behaviour in the range of small strain [0.001% to 1%] is not well established in those studies. In addition, those studies do not seem to include the effect of ageing on shear modulus.

2.5 Proposed Research

Previous research has shown that time under sustained stress, which may be called ageing, plays a significant role for soil stiffness. It does not appear to have much effect on strength. The mechanism by which stiffness increases over time is poorly understood. In sands, creep during ageing rapidly reduces to a small amount. Since the pore pressure in the granular soil dissipates in seconds, the ageing phenomenon, in granular soils, has been neglected and its influence has not been investigated in detail. Recent research has indicated that sand stress-strain response is strain-rate dependent but the effect seems to be small. In addition, the research performed recently focused on the very small strain, which is less than 0.001%, and there are not many studies associated with small strain yet presented.

Much of the research for effect of time on stiffness has focused on the small strain modulus under conditions of repeated loading, i.e. resonant column apparatus. Laboratory research has typically followed similar test methods. Samples are typically subjected to several periods of creep. The effect of the previous creep phase on the current phase is unknown.

In this thesis, the effect of ageing on stiffness of very loose sand is studied under triaxial conditions for ageing time up to 10,000 minutes. Several samples were also prepared in the medium dense state in order to observe the influence of the holding duration on different densities. Tests at other initial conditions such as different stress ratios and different confining stresses are also performed for comparison purposes. In addition, the effect of imposed stress paths after ageing is investigated.

Chapter 3 will explain about the apparatus used in this study and how to correct for compliance in the triaxial tests. Chapter 4 will present the test results and findings from this study. Chapter 5 shows the conclusion for this study.

CHAPTER 3

Experimental Aspects

3.1 Introduction

The laboratory test program was designed to study the effect of periods of ageing at a constant stress ratio on the subsequent stress-strain response of the samples. The effect of variation of stress paths on the stress-strain response after ageing was also studied by applying four different stress paths of loading. The tests were carried out on very loose and medium dense Fraser River Sand under fully drained conditions. To achieve the above objectives, the following characteristics were required of the test:

- Homogeneous loose samples prepared to a repeatable void ratio;
- Independent control of axial load and confining stress to allow tight control of stress ratio;
- Ability to measure overall strain during consolidation and subsequent shearing
- Ability to measure strains over a smaller strain range to a higher degree of precision and accuracy to allow study of creep and initial stiffness at axial strains less than 0.5%;
- Stability of measurements over holding periods of up to 10,000 minutes (1

week).

All testing was carried out in the UBC geotechnical research laboratory using the triaxial apparatus. This chapter describes the apparatus and transducers used and discusses several test limitations and methods for adjustment of data to account for such limitations. The material properties of the Fraser River Sand and sample preparation technique are also described.

3.2 Testing Apparatus

All tests were conducted using a triaxial cell. The testing equipment can be seen in Figure 3.1. The apparatus included an axial load generator, cell pressure generator, back pressure generator and five transducers. The sample, which is 13cm high and 6.4cm in diameter, was confined in a latex rubber membrane submerged under de-aired water in a triaxial cell. Back pressure and confining pressures were applied by fluid pressure and the sample axial load was applied through a loading ram connected to a double acting piston. Five transducers were used to monitor axial displacement, volume change, cell pressure, pore pressure and axial load. Those readings were recorded and stored in a computer attached to the apparatus. Two pneumatic controllers were attached to this apparatus. One was for axial loading and the other was for confining pressure. A pneumatic controller is a device attached directly to a pressure regulator, which adjusts the supply of pressure in accordance with a pre-programmed procedure. The desired stress path is achieved by individually controlling σ'_1 and σ'_3 throughout the test.

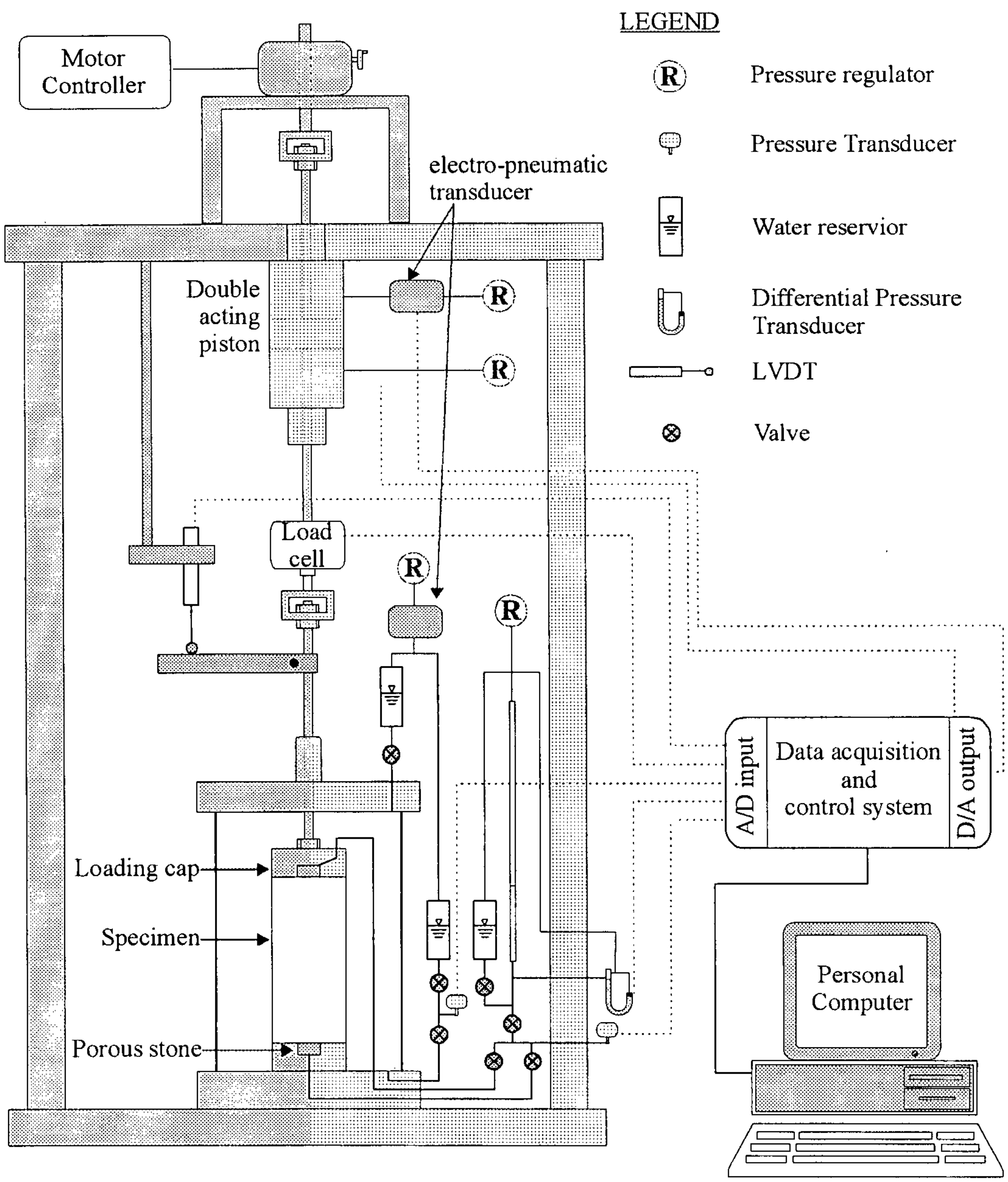

Figure 3.1 Testing Apparatus

3.3 Instrumentation and Test Control

In this section, the special aspects of the apparatus and the resolution of each transducer are discussed. Axial load and cell pressure were applied using a pneumatic controller. In such tests, the applied load or pressure sometimes exceeds the desired values. If this happens, the specimen experiences unloading. In the tests reported here, this was avoided

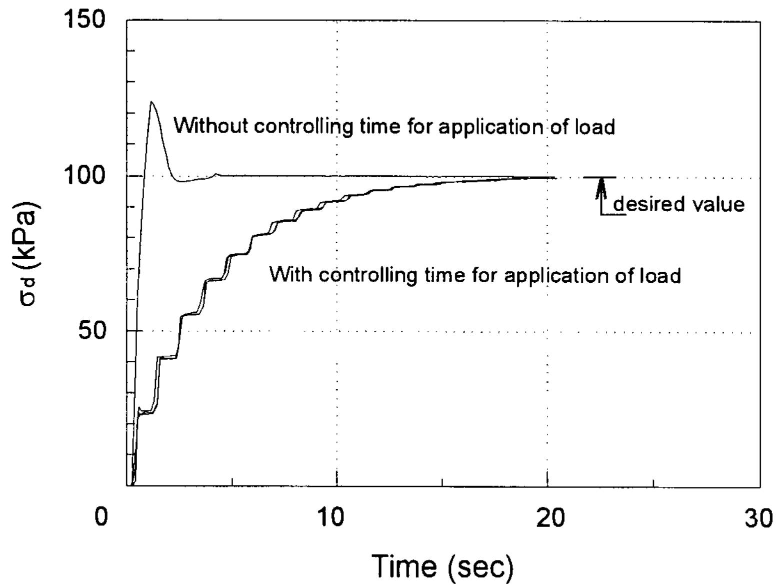

Figure 3.2 Approaching to the Desired Stress

by applying small increments of loads at constant time intervals and by monitoring the pressure difference from the actual desired value. Figure 3.2 shows the results of stress applications towards the desired value. Also, this figure shows the effect of interval difference for the application of stress. When the loading is applied without time control, the application of loading fails to stop when the current stress state reaches the desired state. Once load application was controlled by time interval, the applied stresses did not exceed the desired value. In addition, the length of the interval seemed to be unimportant provided the time interval was set. The interval applied for this series of tests was 0.5sec.

The resolution for each transducer, which is given in Table 1, is seen in Figure 3.3 to 3.5. All data recorded is with the same settings under all pressures applied. The constant stress state is referred to as the zero reading. Samples were left for about 6,000 seconds. Scatter is seen in all transducers. This shows the short term resolution of transducers. Two axial transducers with different resolutions are used for the tests depending on the test purposes. One was for the measurement for small strain and the other was for large strain. The transducer for monitoring small strain had a maximum range of 6 mm corresponding to 5% axial strain relative to the initial dimension of the sample. This transducer was used for monitoring the strain developed during an ageing test, expected to generate very small axial strain. However, 5% in the axial strain was not large enough to get the 130mm-sample to reach a point of dilation. In this case, the longer transducer was used for measuring a strain. The resolution of the transducer for axial measurement was about 0.002% to 0.004% for a short LVDT and 0.0025% to 0.0050% for the longer LVDT. More accuracy could be expected for the shorter LVDT for the measurement in the short term. However, the applied resolution for this research was 0.002% to 0.004%, since this particular transducer seemed to have a shift in the long term measurement. The resolution for the transducer for volumetric strain was about 0.001%. The differential transducer was used to measure volume change. The resolution of axial loading was about 0.1kPa. Resolution of the transducers used to monitor cell and pore pressure was 0.25kPa. Again, like the transducer for axial strain, both transducers could measure smaller values for a short time. Since the shift was recognized in both transducers for a long term measurement, the resolutions for these transducers were

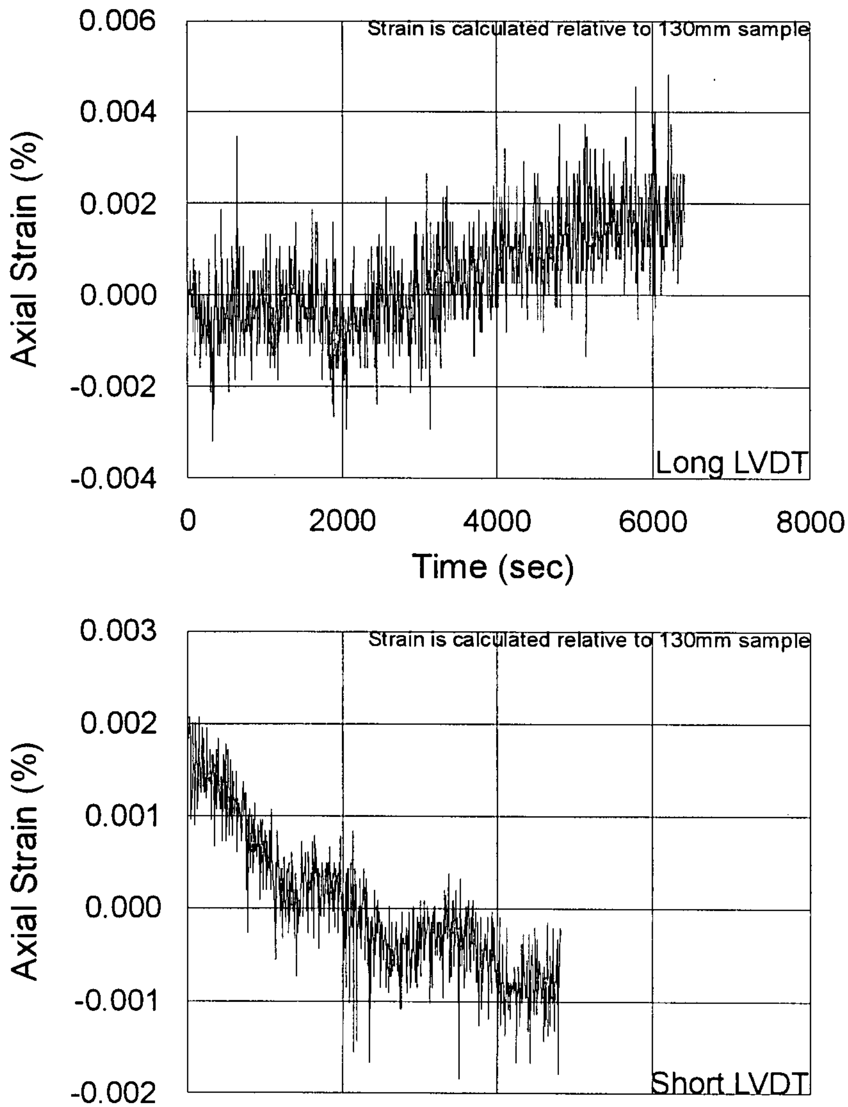

Figure 3.3 Resolution for Axial Strain Transducers

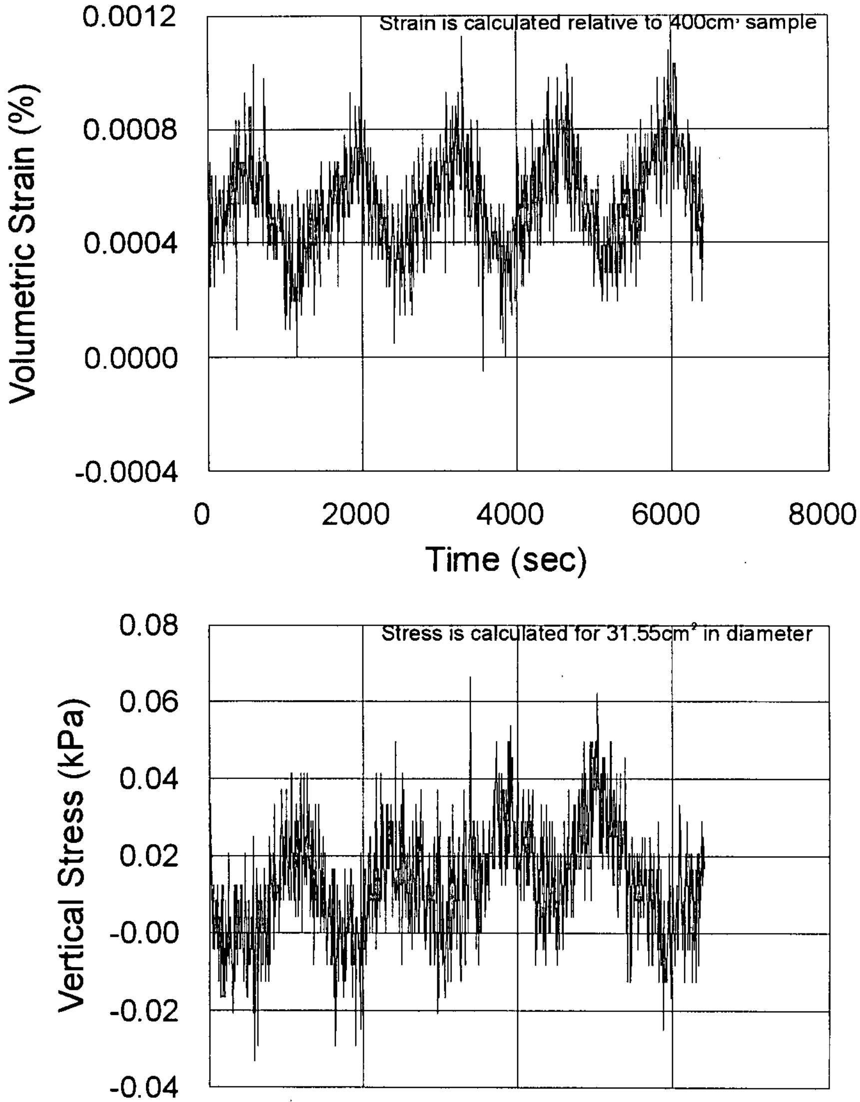

Figure 3.4 Resolution for Volume and Loading Transducers

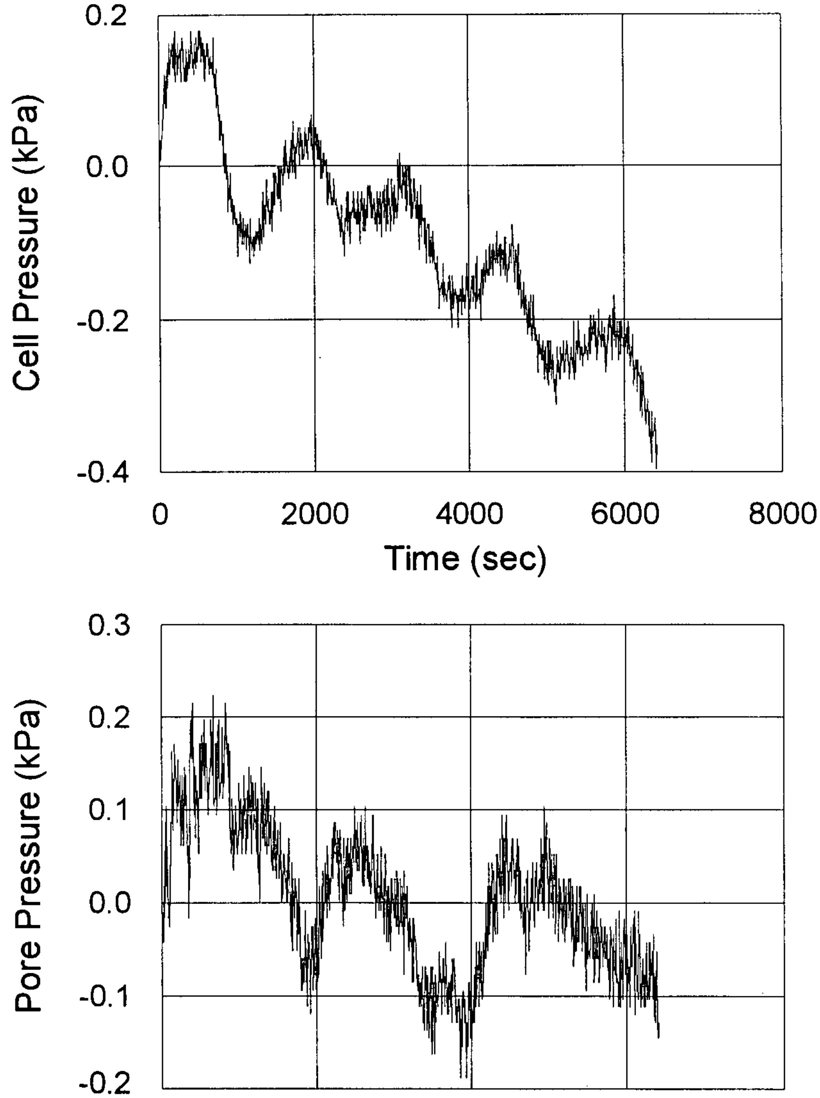

Figure 3.5 Resolution for Cell and Pore Pressure Transducers

considered to be 0.25kPa.

The data were recorded for every 2kPa increase in axial stress for the consolidation stage. During the holding duration to observe deformation by ageing, 50 data points are recorded regardless of its length. In shearing tests, data was recorded every 15 seconds which is right before the next loading application.

Table 1 Typical Measurement Resolution

Parameter	Instrument	Resolution	Notes
Axial Strain, ε_a	LVDT	0.002-0.004% or 0.0025-0.005mm	Sample Height=130mm
Volumetric Strain, ε_v	Differential pressure transducer connected to small bore burette	0.001%	Sample Volume=400cm^3
Radial Strain	Calculated		
$\varepsilon_r=1/2(\varepsilon_v-\varepsilon_a)$		Assumes sample deform as a right cylinder	
Axial Stress	Load Cell	0.1 kPa	Vertical load corrected for membrane force, ram friction and uplift force
Cell pressure	Pressure transducer	0.25 kPa	
Pore pressure	Pressure transducer	0.25 kPa	

3.4 Special consideration of limitations of test

3.4.1 Ram Friction

Friction between the loading ram and triaxial cell can be measured and the applied load can be corrected. If this friction is not considered, measured load differs from the actual load applied to the samples. Ram friction was measured by applying pressure to a triaxial cell filled with water and then applying an axial strain with the ram moving through the water. The reading of the load cell indicated the value of the up-lift force created by cell pressure. When a loading ram was moved down slowly, the reading of the loading cell became smaller due to the force created by ram friction, which was subtracted from the value of up-lifting force. The triaxial cell, which was used in these series of tests, was called "a Frictionless Cell." Pressure is applied between a loading ram and a triaxial cell cap and creates the air cushion, which will minimize friction. Friction, however, was still observed. The measured friction force was about 20gf (0.196N), which is equivalent to 0.06kPa in the axial loading.

3.4.2 Membrane Penetration

In order to perform the triaxial test, samples are covered by a thin membrane. When the confining pressure changes, a membrane will deform into or out of the pores of the sample surface. In the case of the drained test, this creates an error in the volume change and in the case of the undrained test, it creates an error in pore pressure readings. To estimate the error caused by the membrane penetration, there are a couple of methods available from previous studies. The method used here is based on the assumption that the volumetric strain is the same as three times the axial strain under the isotropic unloading condition. If the volume change is observed to be more than three times the axial strain change, the difference is created by the membrane penetration. This unloading curve in the unit membrane penetration volume and log σ_3' space has a linear relationship (Vaid and Negussey, 1984). The membrane penetration is usually measured by reducing the confining stress in steps, e.g. reducing 50kPa and waiting for few minutes. During a triaxial test, the confining stress will, however, be applied to the specimen in the continuous manner. So for the work presented in this thesis, the membrane penetration effects were measured in both steps and continuous confining stress reduction. Regardless of whether the stress reduction was applied in steps or continuously, the relationship between the volume change by membrane correction and the confining pressure was linear and the magnitudes of slopes in both cases were identical. The value applied for this test was 0.0021, which is ε_m in the equation below. The corrected amount is about 0.1% of the sample volume for the lateral stress from 20kPa to 100kPa. Figures for membrane volume and confining stress can be seen in Appendix A1, A2 and A3.

$$\Delta V_m = \varepsilon_m \times A_m \times \log\left(\frac{\sigma'_{current}}{\sigma'_{initial}}\right)$$

ΔV_m : Recoverable volume change on hydrostatic unloading

A_m: Specimen surface area covered by membrane

ε_m : Unit membrane penetration

$\sigma'_{current}$: Current confining stress

$\sigma'_{initial}$: Initial confining stress

3.4.3 End Restraint

Friction between the ends of the specimen and the rigid end caps may create the inaccurate response in the specimens due to stress inhomogeneity. This problem becomes more significant if the specimens are deformed to large strain. However, if the height of specimens is more than twice the diameter of specimens, there is no significant error in the strength measurement (Bishop and Henkel, 1957). The specimen size in this series of tests was about 130 mm in the height and 64 mm in diameter, which satisfied the condition to avoid a significant error due to end-restraint. In addition, due to the purpose of these series of tests, most of the specimens were required to be deformed only to less than 5% axial strain including the strain developed in the consolidation phase. So, the influence of the end restraint would not cause significant error to results. The practical application of deformation characteristics measured in a drained test is generally limited to small strains where end restraint is not of importance (Bishop and Henkel, 1957).

3.4.4 Membrane Force

For the triaxial test, the specimens are covered by the thin rubber membrane. This thin membrane is also carrying part of the axial load applied to the specimens, which creates error between the reading and the actual load application. Membrane force can become a significant fraction of the overall applied stresses, particularly in tests on soft materials. In these series of tests, axial membrane load is calculated assuming that elastic thin shell compression theory can be applied (i.e. the membrane is assumed to maintain the shape of a thin wall cylindrical shell.) This elastic thin shell compression theory is valid as long as no buckling is observed in the specimens (Kuerbis and Vaid, 1990). The results considered in this thesis consider the response of the specimens within the small strain range. In this magnitude of the axial strain, the specimens sustained a cylindrical shape without any buckling observed. The adjustment in σ'_1 is about 0.4kPa and σ'_3 is about 0.15kPa with the condition of R=2.8 and confining stress 100kPa at the end of consolidation. The equation used for the correction is given below.

$$\sigma_{am}' = \sigma_a' - \frac{4E_M t_0 (2+\varepsilon_v + \varepsilon_{Ma})(3\varepsilon_{Ma} + \varepsilon_v)}{3D_0(2-\varepsilon_v + \varepsilon_{Ma})}$$

$$\sigma_{rm}' = \sigma_r' - \frac{4E_M t_0 (2+\varepsilon_v + \varepsilon_{Ma})\varepsilon_v}{3D_0(2-\varepsilon_v + \varepsilon_{Ma})}$$

ε_{Ma} : Axial strain in the rubber of a cylindrical membrane shell

ε_v : Volumetric strains of the cylindrical membrane cavity

E_M : Young's Modulus of rubber

D_0 : Initial unstretched diameter of cylindrical membrane shell

t_0 : Initial unstretched thickness of cylindrical membrane shell

σ_a',σ_r' : Measured axial and radial effective stress on a cylindrical soil specimen

σ_{am}',σ_{rm}' : Corrected axial and radial effective stress on a cylindrical soil specimen

(Kuerbis and Vaid, 1990)

3.5 Material tested

3.5.1 General Description

The material tested in this series of tests is Fraser River Sand. This sand was deposited in the Fraser River Delta in the Lower Mainland of British Columbia. Normally Fraser River Sand contains 1% of Clay but for the test purposes, this clay content was removed by washing the sand through a 0.106mm sieve (No. 140-sieve). Fraser River Sand is a grey, uniform, semi-angular medium grained sand. The average mineral composition is 40%

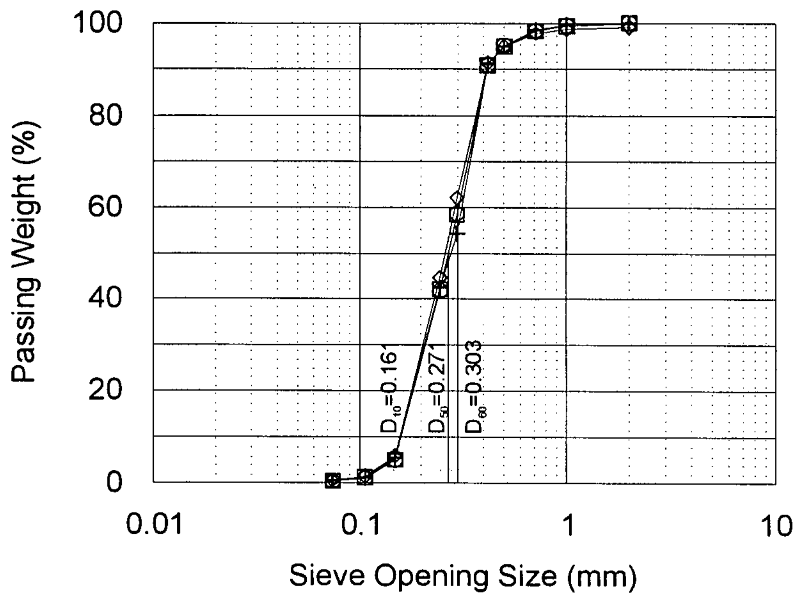

Figure 3.6 Gradation Curve for Fraser River Sand

quartz, quartzite and chert, 11% felspar, 45% unstable rock fragments (mainly volcanic) and 4% miscellaneous detritus (Garrison et. al., 1969). Figure 3.6 shows the gradation curve of material tested. D_{50} and D_{10} are 0.271 and 0.161 respectively and the uniformity coefficient is 1.88. These values were measured after removing clay particles which are smaller than 0.10mm. Also, the maximum and minimum void ratio were 0.989 and 0.627 respectively. The maximum void ratio was measured from the sample volume and sample weight before placing the loading cap on which gave an identical value each time. Several attempts were made to measure the maximum void ratio according to ASTM (D2049). The value of a maximum void ratio was very different from what was expected from the previous research with the same sample. From this fact, we applied the initial deposition void ratio in the loosest state as the maximum void ratio. The minimum void ratio was measured by accordance with ASTM D2049. The specific gravity was determined to be 2.719. The index properties are shown in Table 2.

Table 2 Property of tested Material

Specific gravity	2.72
e_{max}	0.989
e_{min}	0.627
D_{50}	0.27 mm
D_{10}	0.16 mm
Coefficient of uniformity, C_u	1.9

3.6 Test procedure

3.6.1 Sample preparation

All samples were prepared using the water pluviation technique. This technique simulates the deposition of alluvial sand and hydraulic fills. Sivathalayan (2000) has shown very good agreement between the stress-strain behaviour of undisturbed samples from water-deposited sands and samples prepared using water pluviation. Specimens prepared with this technique have proved to be very uniform (Vaid and Negussey 1984). This technique ensures the saturation of sand. The water pluviation technique may create segregation if the sand is silty or well graded, but this is not the case for the sand used for this series of tests.

The sand was first boiled for approximately 30 min, and was then pluviated into the sample mould filled with de-aired water. The water had been de-aired by boiling and kept under vacuum. The flask was turned upside down and sand flowed into the mould and displaced water. In order to keep the top surface approximately level, the flask had to be moved around the mould during deposition. To avoid large disturbance in samples, the excess sand was removed by a siphon with a flexible tube. The amount removed was measured in order to determine the final mass of samples. Most of the samples were prepared in a loose state. After excess sand was removed, the loading cap was placed and the membrane sealed with O-rings. A small vacuum (approximately 12-15kPa), was applied in order to allow removal of the metal form from the sample. During the sample preparation, the height change was monitored using a dial gauge with 0.01mm scale and the volume change was measured by the water height change in a pipette of 0.494cm^2 diameter. Usually the samples prepared with this technique have identical density after a small vacuum is applied. The relative density after the vacuum application was about 13 to 17%. A typical sample size ranged between 129mm and 131 mm in height and 63.5 to 64.0 mm in diameter regardless of density.

Some samples were purposely prepared with a different relative density. To control the relative density, the process was almost the same as the preparation of the loose samples. During the water pluviation, low frequency vibration was applied to the base of the triaxial cell which made the particles move to a denser arrangement. After the top cap was placed, further low frequency vibration was applied in order to achieve the desired relative density. Since the mass of sand and the dimensions of the mould were known, the adjustment of final density was controlled by observing the height reading. The densification process could be done only after the top cap was placed onto the specimen. In some cases, the height of samples became too short to clear the 2 to 1 ratio in specimens and a sample could not be used for a test. Better control was provided by using this method to reconstitute samples with desired relative density. The preparation was finished by filling the triaxial cell with de-aired water.

3.6.2 Set up of Samples

The triaxial cell was set up in the apparatus after all preparations were done. First, the loading cap was attached to the pneumatic piston and then the LVDT was set in place. Three tubes have to be attached to the apparatus in order to measure pressure. The drainage line coming from the loading cap was not used for this series of tests. This line was attached to the apparatus first. After setting the zero reading for each transducer, the other two tubes were attached to the apparatus. Each zero reading was measured relative to atmospheric pressure. After all tubes were attached to the triaxial cell, 20kPa cell pressure was applied. Since about 15kPa of vacuum was already applied to the specimen during the preparation, after the application of 20kPa, the reading of pore pressure was 5 to 7kPa which made the lateral effective pressure 13 to 15kPa. The B value was measured while increasing the cell pressure without drainage. By the end of B value measurement, the cell pressure was 220kPa and usually the B value reached 98% or more. After it was established that the B value was 98% or more, 200kPa of back pressure was applied to the specimens, resulting in an effective confining stress of 20kPa. The drainage valve was left open for a minute for specimens to adjust to the change in the lateral effective pressure. Usually the reading of the lateral effective pressure became 18kPa right after the cell pressure reached 220kPa. Since the desired initial lateral effective pressure was 20kPa, the sample experienced a change of 2kPa.

3.7 Test Procedure

After a satisfactory B value had been established, samples were consolidated. Samples

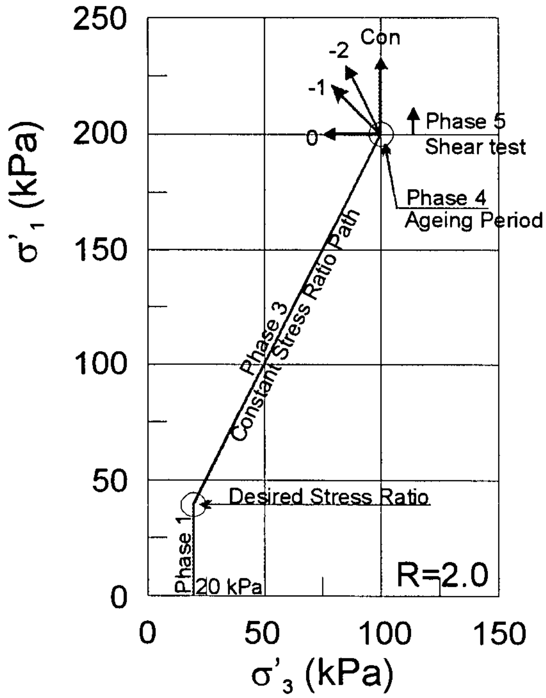

Figure 3.7 Phase Description

were consolidated to one of three stress ratios, R=1.0, 2.0 and 2.8. For R=1.0, samples were consolidated under isotropic confining stress. For R=2.0 and 2.8, the procedure illustrated in Figure 3.7 was followed. Samples were first consolidated along a conventional triaxial stress path i.e. $\Delta\sigma_{cell}$=0 (Phase 1), to the required R. Both σ_{axial} and σ_{cell} were then increased, maintaining R constant until the desired confining stress of 50, 100 or 150kPa had been reached (Phase 3). The sample was then allowed to stand at a constant stress ratio for a predetermined time (Phase 4). Phase 5 consisted of loading along one of 4 stress paths until an axial strain of about 1%. A holding duration was included at the end of Phase 1 (Phase 2) in the early tests but it was omitted in subsequent tests to avoid inconsistency in the effect of the holding duration at Phase 4. Applied stress paths were the slope of 0 which is unloading compression, the slope of -1, the slope of -2 which is the constant p' path and the conventional path in terms of $\Delta\sigma'_1/\Delta\sigma'_3$. As mentioned before, both $\Delta\sigma'_1$ and $\Delta\sigma'_3$ were

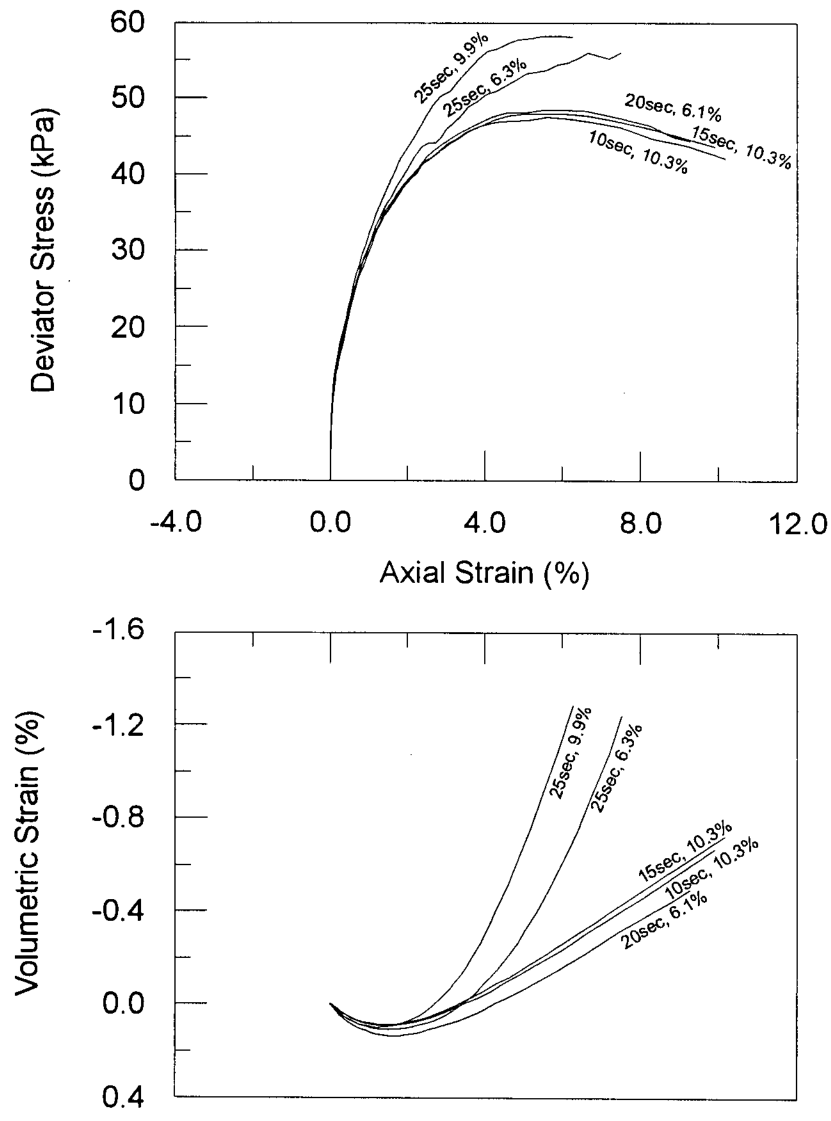

Figure 3.8 Various Length of Time for Loading Application Interval

changed simultaneously using two electric pneumatic controllers. During phases 3 and 4, the feedback-simulation was used for adjustments of both applications in $\Delta\sigma'_1$ and $\Delta\sigma'_3$ to keep the stress ratio constant. During phase 5, however, the feedback simulation was not applied in order to avoid the time lag between $\Delta\sigma'_1$ and $\Delta\sigma'_3$. Tests were stress-controlled with a small stress increment applied at 15 seconds intervals. During preliminary testing, the effect of varying the time interval between increments was investigated. Figure 3.8 shows the effect of difference in time interval for the application of the vertical and lateral stresses. The time intervals were set 10, 15, 20 and 25 seconds. It was observed that a 25 seconds interval led to a stiffer, more dilatant response at strains about 1 to 2%. For smaller time between intervals, there was no significant change in the stress-strain behaviour. All tests were fully drained. In these series of tests, 15 seconds was chosen for an interval of stress application. Also, this interval helped the applied stress path to follow the desired stress path.

Regardless of the applied stress path, the increment of stress was 1kPa in deviator stress except in the case of the stress slope of -2 where it was 1.5kPa. The rate of strain depended on the soil stiffness. It took 85 seconds or more for the first 0.1% in the axial strain which was reasonably slow for the drained condition. The rate increased at higher strains. To reach 1.0% axial strain took about 5 minutes which was about 0.2% per a minute at the fastest rate. As only the behaviour of sand at the strain of less than 1% was of interest, these rates were considered acceptable. Lastly, all tests were performed under the drained condition.

3.8 Repeatability of test

All test results must be reproducible in order to analyze the behaviour of samples. The application of stress has to be repeatable always. If two identical samples behave in different manners under the same stress application, those results will not be applicable. The results of two different samples under the same stress application can be seen in Figure 3.9. Two lines are plotted in modified Mohr space. This figure shows the stress path imposed on samples by the apparatus. The two samples shown had different relative densities. For the conventional

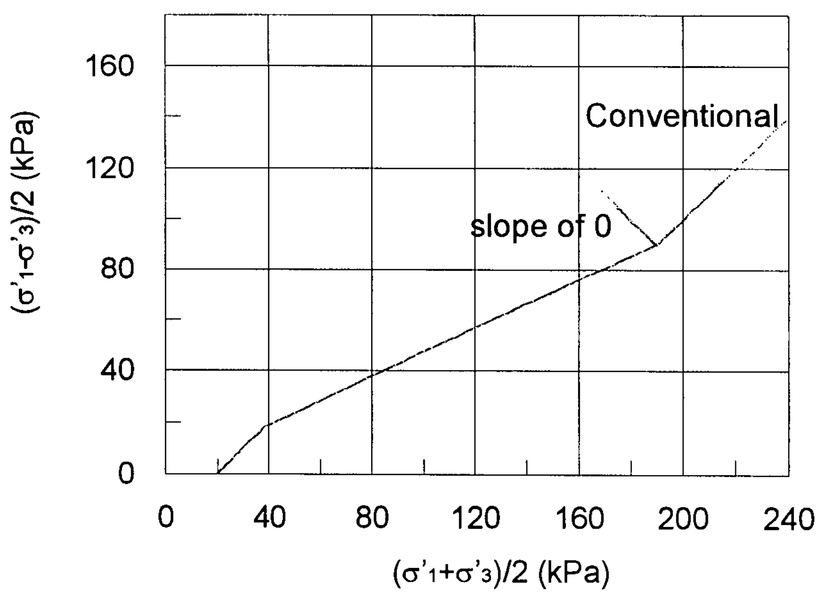

Figure 3.9 Repeatability of Stress Application

path, one was 46.4% and the other was 15.4% and for the slope of 0, one was 52.9% and the other was 14.4 % in relative density measured right after the sample preparation. Regardless of the relative density, the applications of stress increments were always the same up to phase 4 which is the end of consolidation. The figure indicates that the stress path application is repeatable.

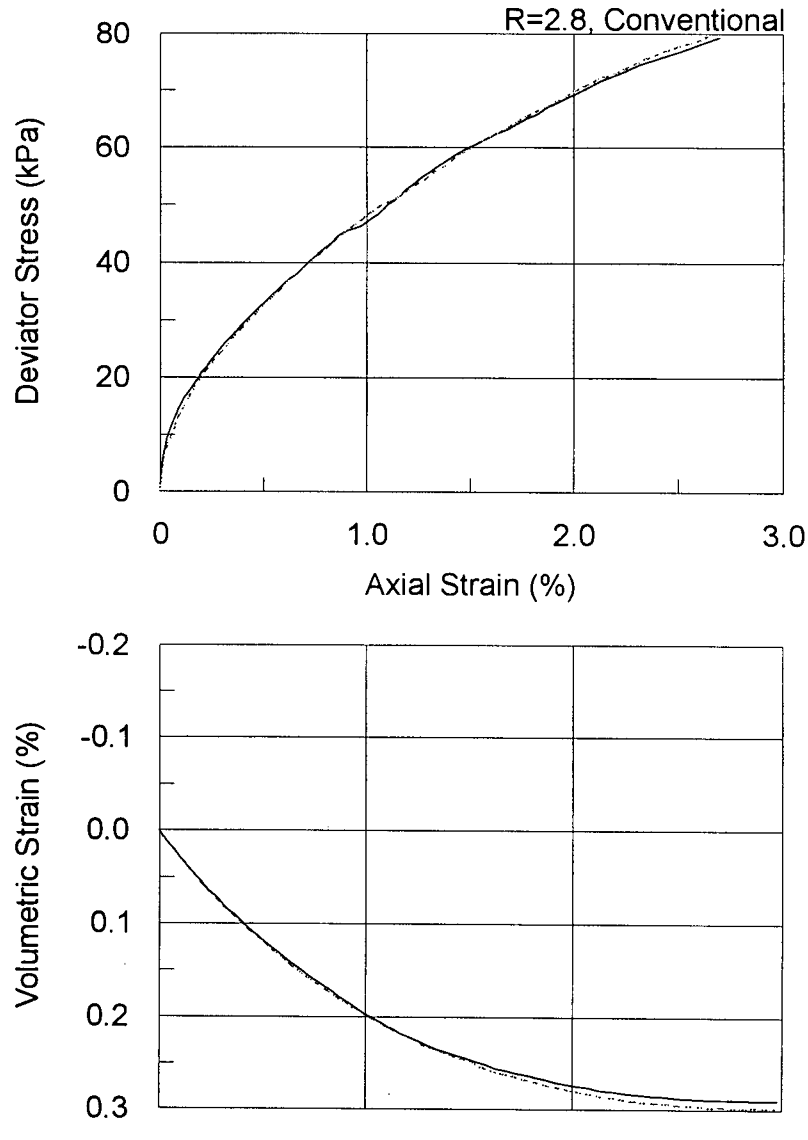

Figure 3.10 Repeatability of Shearing test on Conventional Path (R=2.8, σ'_3=100kPa)

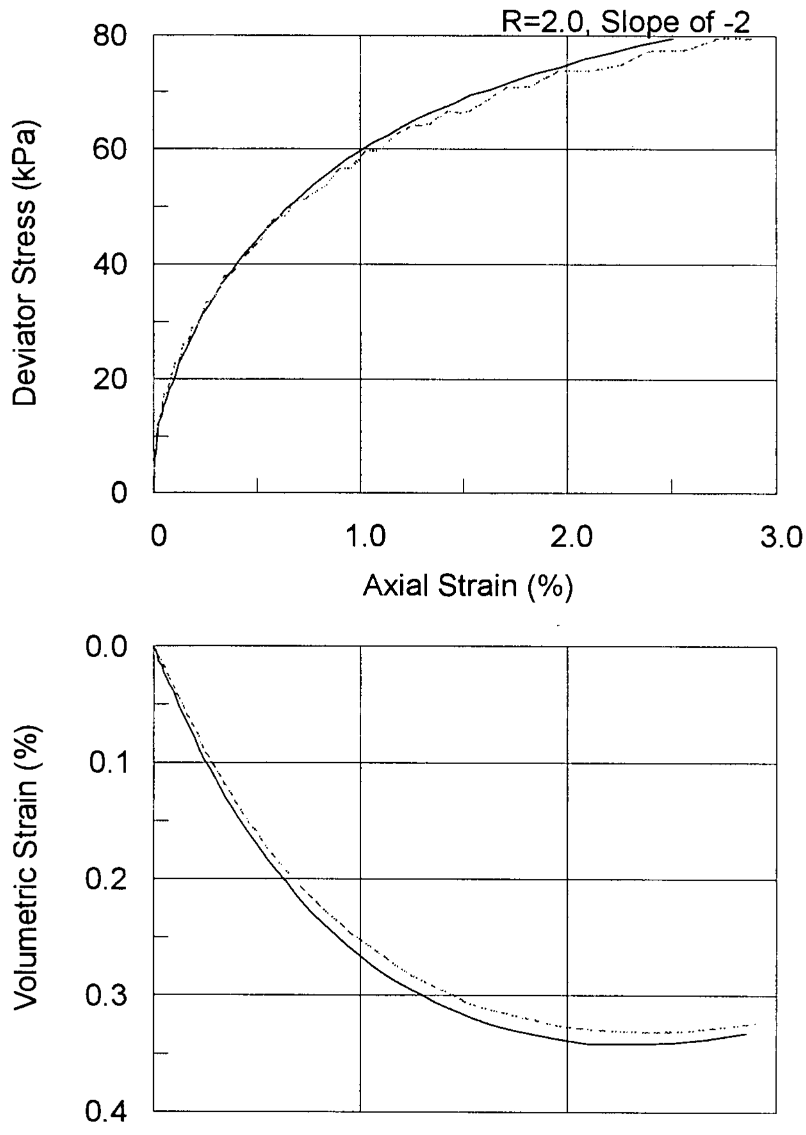

Figure 3.11 Repeatability of Shearing test on Stress-Slope of -2 (R=2.0, σ'_3=100kPa)

Figure 3.10 shows shearing tests of two samples which have the identical initial conditions. The relative density of one sample was 20.3% and the other was 21.3% at the beginning of the shearing test. The stress path applied to these samples was the conventional triaxial path at R=2.8. As seen in the figure, excellent repeatability was obtained. Figure 3.11 shows another set of two shear tests for different samples with relative density of 20.2% and 23.8%. The applied stress path was -2 in terms of $\Delta\sigma'_1/\Delta\sigma'_3$ at R=2.0. Excellent repeatability is also recognized in the figure. The slight waving in one test was due to use of the longer LVDT. From these figures, it can be seen that as long as identical samples under the same stress condition are used, samples show similar response. These results indicate acceptable repeatability for these series of tests.

3.9 Summary and Conclusion

There are several factors that have to be considered for tests in the triaxial apparatus. Since the triaxial testing apparatus has been used for a long time to study fundamental soil properties, these factors are well recognized and the methods of data correction have been previously suggested by many researchers. All adjustments presented here were applied for all tests throughout the test procedure. The apparatus used in these tests is capable of imposing the desired stress state and the resolution of transducers attached to apparatus are accurate enough to measure sample deformation and stress-state changes for the range focused on in this research. The resolution of each transducer and a brief description of material tested can be seen in Tables 1 and 2.

CHAPTER 4

Test Results

4.1 Introduction

In this chapter, test results are presented. The samples were consolidated to one of three stress ratios, R=1.0 (isotropic), R=2.0 and R=2.8. The test procedure is divided into 5 phases which consist of 3 sections; Consolidation (Phase1-3), ageing (Phase 4) and shearing test (Phase 5). Consolidation consisted of two phases: bringing the stress state up to a desired stress ratio, R (Phase 1) and following the constant stress path ratio up to a desired lateral effective pressure at constant R (Phase 3). Phase 2 was originally set as a holding phase at the desired stress ratio with confining stress of 20kPa. However, it was considered that having two holding phases in one procedure may have an unknown influence on the result of other phases. Therefore, this phase was omitted after the early stage of this research. Ageing is allowed in Phase 4, when drained creep is allowed at the desired constant stress ratio state. The shearing phase is Phase 5. The definition of the phases can be seen in Figure 4.1.

All specimens were prepared by the water pluviation technique, which simulates the in-situ deposition of Fraser River Sand. Most specimens were loose. The void ratio measured after applying the confining stress of 20kPa was about 0.93 to 0.94, which represents a range of between 13.5 and 16.5% in relative density. The majority of tests were performed under σ'_3=100kPa at R=2.8. Most figures show variables actually measured with transducers such as axial, and volumetric strain and deviator stress. All stresses are effective.

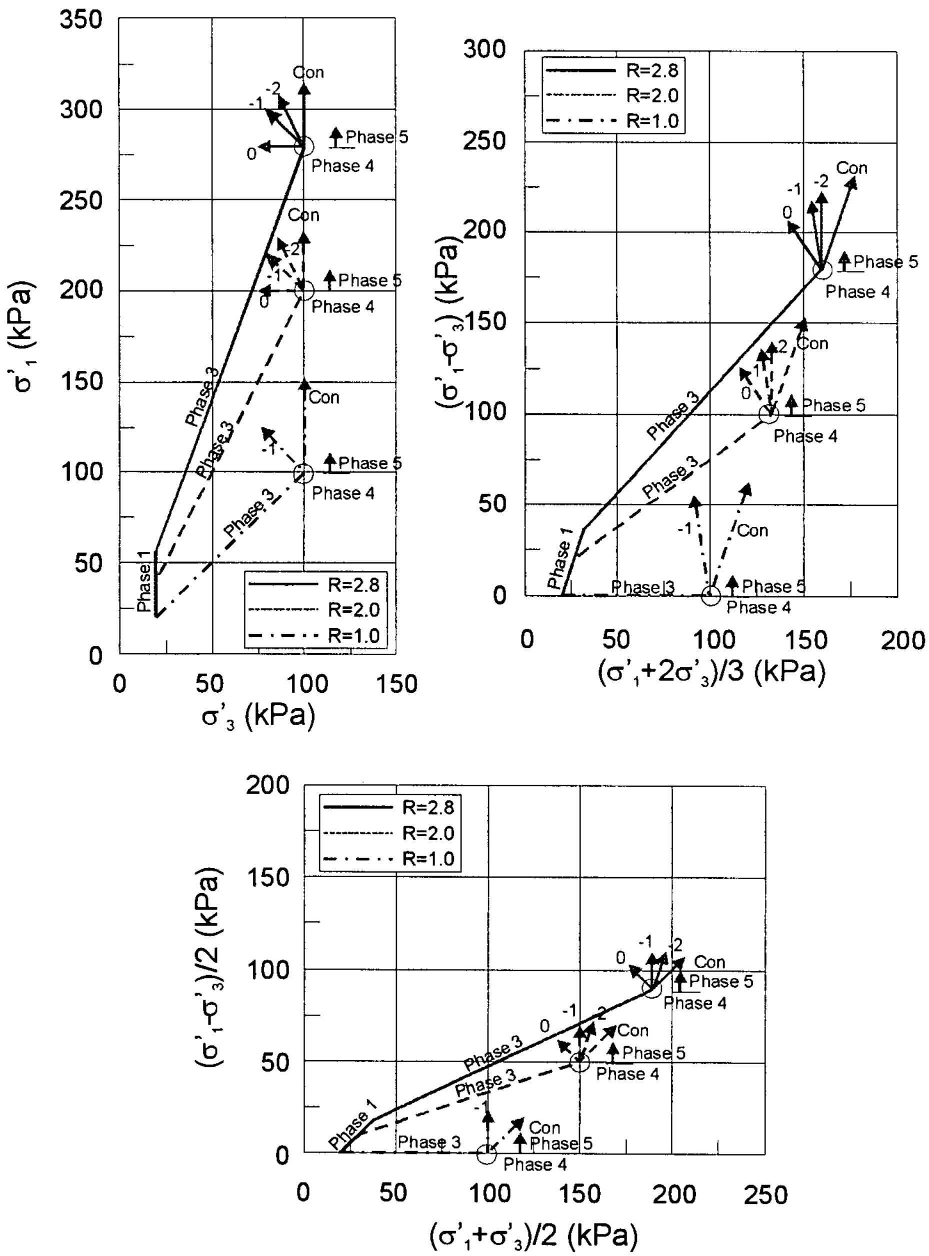

Figure 4.1 Applied Stress Paths in Different Stress spaces

4.2 Consolidation (Phases 1 and 3)

4.2.1 General

Samples are consolidated to the desired stress ratios of R=1.0, 2.0 or 2.8 until σ'_3 reached the desired value of 50, 100 or 150kPa. In order to follow the path with a desired stress ratio, application of both vertical and horizontal stresses has to take place at the same time. The vertical and horizontal stresses will, however, vary slightly depending on the sample stiffness. To keep the stress ratio constant, stress changes are monitored by the acquisition system and vertical stress is adjusted by using the feedback system. Most samples were tested under a confining pressure of 100kPa. In these phases, strain is calculated relative to the dimension of the specimens at the beginning of Phase 1.

4.2.2 Rate of stress increment in Phase 1

The vertical stress was increased under a constant horizontal stress of 20kPa, until the desired stress ratio was reached. The rate of the stress increase was about 0.12kPa/sec. It took about 3 minutes to reach R=2.0 and 5 minutes to reach R=2.8. Since the load application was at a constant rate, the rate of strain varied depending on the current stress state and relative density of the sample. For example, this rate of stress increase resulted in an average axial strain rate of 0.06%/min for R=2.0 and 0.13%/min for R=2.8 for a loose sample. Figure 4.2 shows typical strain development in Phase 1. Unlike a strain controlled test, the rate of the axial strain development depends on the stress ratio and the density of samples. As seen in Table 3, the rate of strain development is higher for higher stress ratios. For denser samples, the rate of the axial strain is lower than for loose samples. This particular

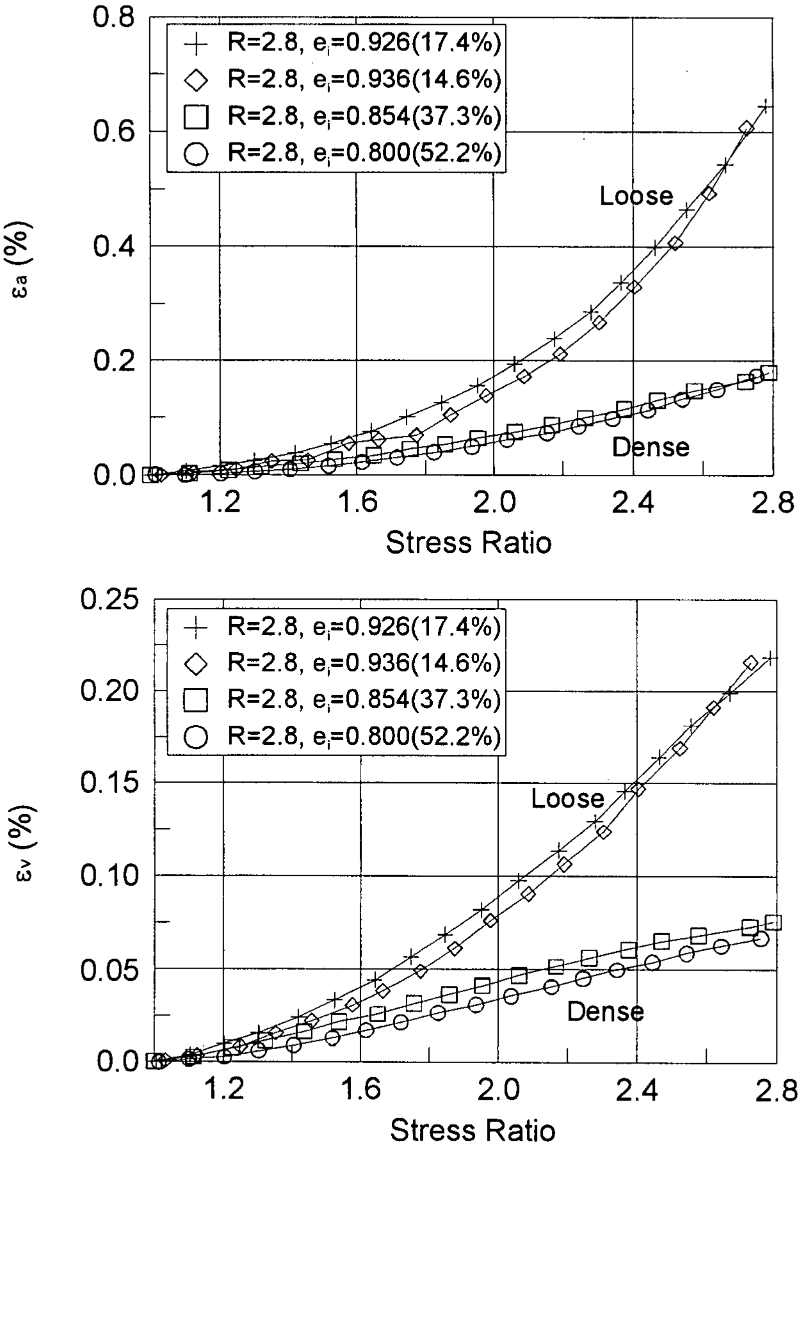

Figure 4.2 Axial and Volumetric Strains Development in Phase1

sample has a relative density of 37.3% at the beginning of Phase 1. The rate of strain is less sensitive to stress ratio in the dense sample. Figure 4.2 also shows the volumetric strain development in Phase 1. The samples in the figure are two loose samples and two dense samples. The rate of development of ε_v also depends on the current stress state but the effect is smaller than for axial strain. The ratio $\varepsilon_v/\varepsilon_a$ is plotted against stress ratio in Figure 4.3.

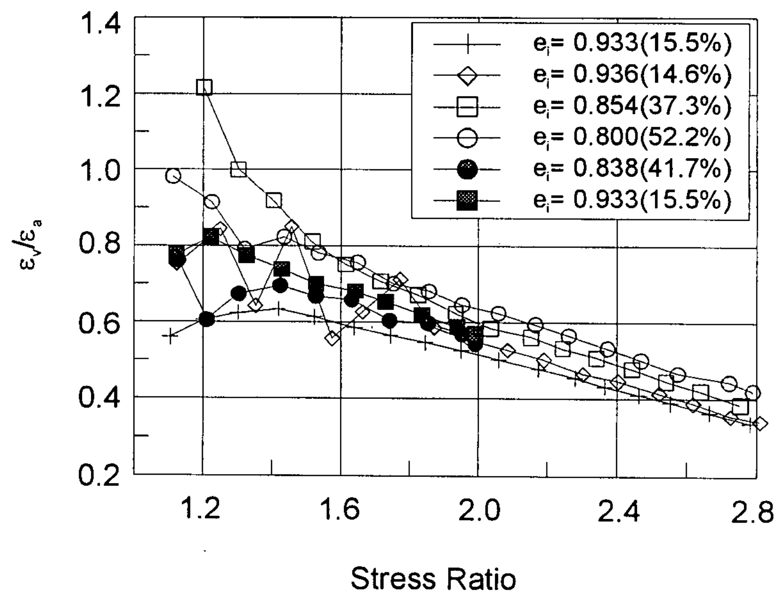

Figure 4.3 $\varepsilon_v/\varepsilon_a$ for Stress Ratio in Phase 1

Results for both loose and dense samples were included. In general, $\varepsilon_v/\varepsilon_a$ reduces with increasing stress ratio and the range of $\varepsilon_v/\varepsilon_a$ with D_r reduces with increasing stress ratio.

Table 3 Typical Average Strain Rate during Phase 1 (%/min.)

	R=2.0		R=2.8	
	Loose	Dense	Loose	Dense
ε_a	0.06	0.025	0.13	0.035
ε_v	0.035	0.015	0.045	0.015

4.2.3 The rate of stress and strain increments in Phase 3

In Phase 3, the rate of change of confining stress was kept constant for all tests at 0.16kPa/sec. Consequently, it took about 8 to 9 min to increase σ'_3 from 20kPa to 100kPa. The rate of change of vertical stress varied depending on the stress ratio resulting in rates of

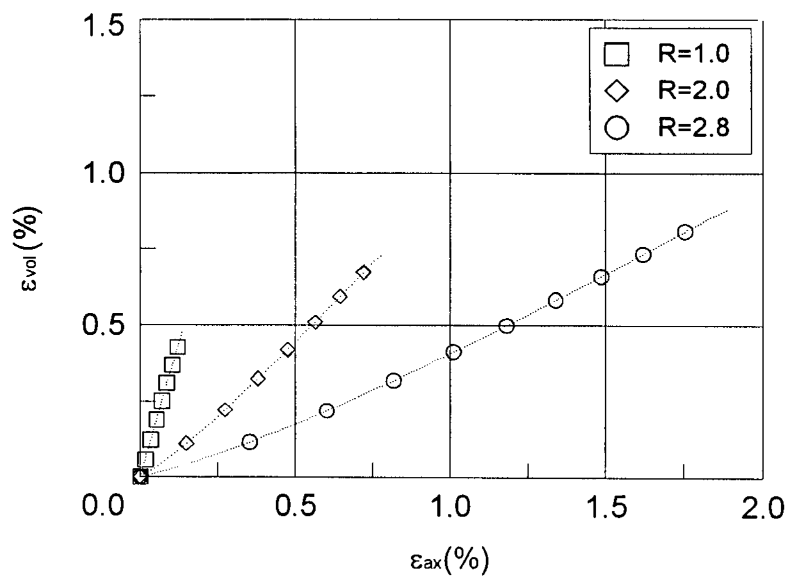

Figure 4.4 Strain Path at Phase 3

change in deviator stress of 0.288kPa/sec for R=2.8 path, 0.16kPa/sec for R=2.0 path. With this rate of stress increase, the maximum axial and volumetric strains observed during consolidation were for R=2.8 and equalled 1.8% and 0.9%, respectively. The maximum instantaneous strain rate observed was 0.440%/min for the R=2.8 tests on a loose sample.

Table 4 Typical Average Strain and Average Rate during Phase 3

	R=1.0				R=2.0				R=2.8			
$\Delta\sigma_d$	0.00kPa/sec				0.160kPa/sec				0.288kPa/sec			
	Loose		Dense		Loose		Dense		Loose		Dense	
	total (%)	average (%/min)	total (%)	average (%/min)	total (%)	average (%/min)	total (%)	average (%/min)	total (%)	average (%/min)	total (%)	average (%/min)
ε_a	0.15	0.02	0.1	0.01	0.73	0.09	0.34	0.04	1.8	0.22	0.55	0.07
ε_v	0.55	0.065	0.3	0.03	0.7	0.08	0.34	0.04	0.9	0.1	0.34	0.04

The resulting average strain rates are given in Table 4.

Figure 4.4 shows the typical strain development in Phase 3. Regardless of the stress ratio path followed, the ratio between axial strain and volumetric strain ultimately reaches a constant value, i.e. becomes linear. For R=1.0 path, the strain path appears linear over the

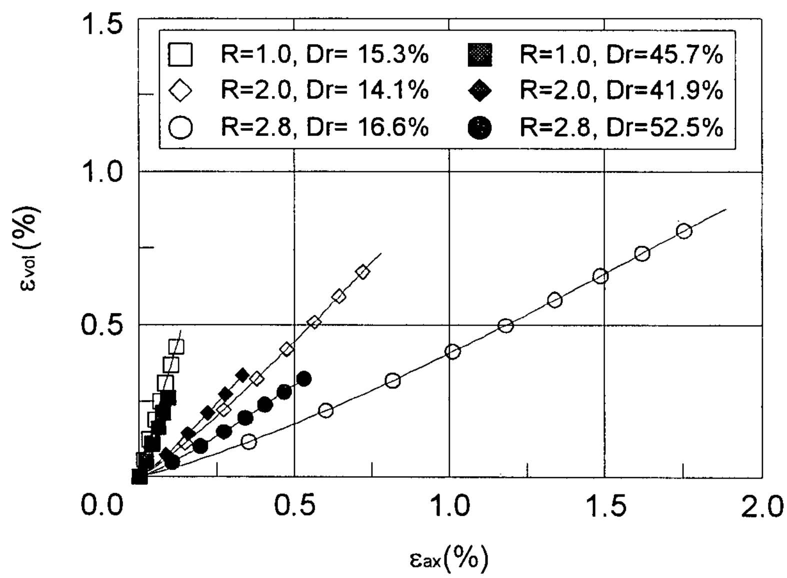

Figure 4.5 Strain Path for Different Relative Density in Phase3

complete range of consolidation. For the very loose sand, the slope of the strain path is about 3.5, ie. $\varepsilon_v/\varepsilon_a$=3.5. For other stress ratios, the strain path is initially convex downwards, but appears to become linear towards the end of consolidation. The value of $\varepsilon_v/\varepsilon_a$ ultimately reaches about 1.02 for R=2.0 and 0.55 for R=2.8.

The effect of relative density on the observed strain paths is shown in Figure 4.5. Relative densities are 45.1% and 15.3% for R=1.0, 41.5% and 16.0% for R=2.0, and 52.5% and 16.6% for R=2.8. All relative densities are measured at the beginning of Phase 3. For isotropic consolidation, the strain path on plot of ε_v vs. ε_a rotates in the clockwise direction as density increase. For D_r=15%, $\varepsilon_v/\varepsilon_a$=3.5, and at D_r=45%, $\varepsilon_v/\varepsilon_a$=3.0. On the contrary, for R=2.0 and 2.8, strain paths rotate anticlockwise as density increase. For both stress ratios, $\varepsilon_v/\varepsilon_a$ is measured after the value of $\varepsilon_v/\varepsilon_a$ becomes constant. This is consistent with the finding

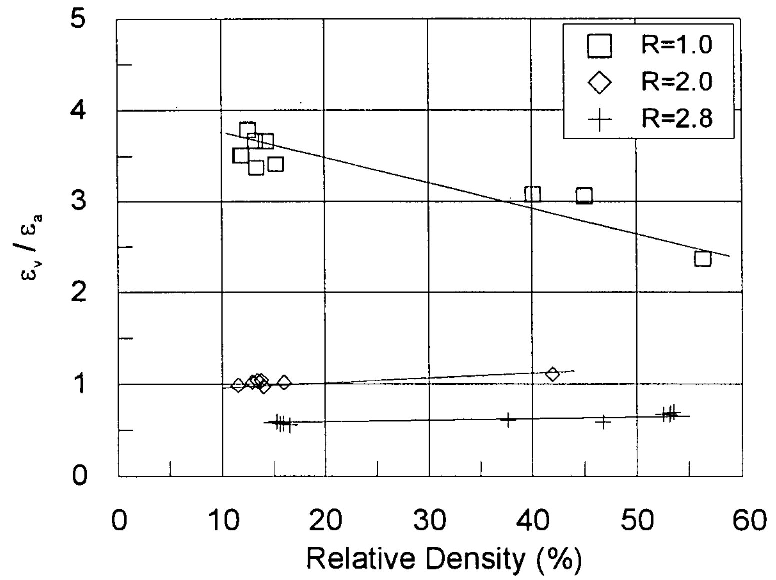

Figure 4.6 $\varepsilon_v/\varepsilon_a$ for Different Relative Density

of Eliadorani (2000) and Sivathayalan (2000). The data are plotted in Figure 4.6 with the relative density on the x-axis and $\varepsilon_v/\varepsilon_{ax}$ in the y-axis. These data suggests that:

(a) The very loose sand deforms isotropically at about D_r=45%.

(b) For D_r=15 to 42%, K_0 increases slowly from 0.5 to slightly less than 0.5 as D_r increase.

(c) Anisotropy of deformation is very sensitive to density under isotropic stress state and is less sensitive at higher stress ratios. i.e. stress ratio dominates.

Figure 4.7 shows the total axial and volume strain changes during Phase 3 for very loose sample (D_r=14%) at different confining stresses, σ'_3=50, 100 and 150kPa. The strain path is identical for all confining stresses. During Phase 3, it requires a longer duration to reach a higher confining stress and more strain is generated. In this series of tests, the value of $\varepsilon_v/\varepsilon_a$ for σ'_3=50kPa is only 0.45, which is smaller than 0.55 in other confining stresses, since a strain path for higher stress ratios initially has a convex downwards shape. However,

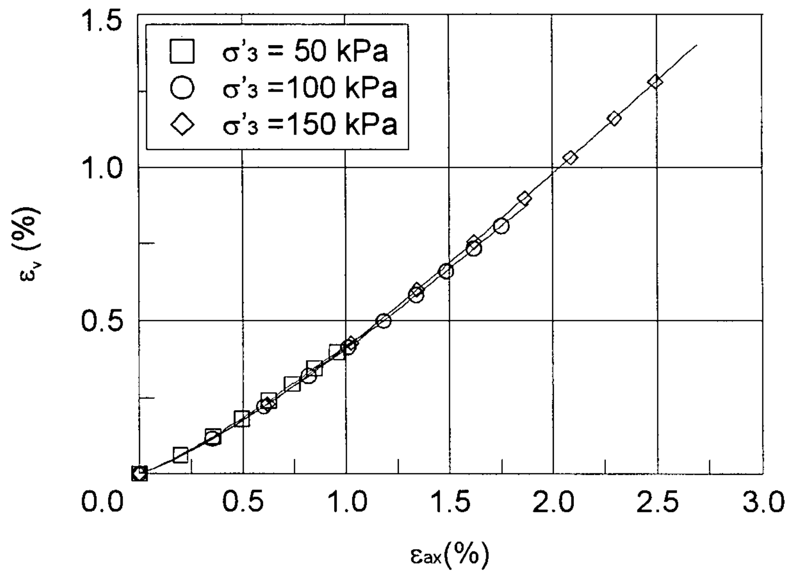

Figure 4.7 Strain Development for Different Confining Stress

no significant pore pressure rise is observed and small adjustments on pore pressure were made by open or close pressure line slightly, if necessary throughout this phase. At the point that σ'_3= 50kPa, the ε_v vs. ε_a curve is still in the convex upwards shape and the value of $\varepsilon_v/\varepsilon_a$ has not reached a constant value. The ratio stays constant and the slope is not affected by the confining stress difference, once σ'_3 reaches to 100kPa.

4.2.4 Load application for the consolidation

As described in the previous section, $\varepsilon_v/\varepsilon_a$ during hydrostatic consolidation is 3.5 which is observed to be lower than other researchers found. Previous studies suggest the ratio should be around 4 to 5. This difference may be explained by the difference in the method of application of loading for the tests in this thesis.

Usually, consolidation is achieved by increasing the confining stress in steps. For example, the confining stress is increased by 50kPa and held for a certain length of time before the next increment. This is continued until the confining stress reaches the desired value. In tests reported here, the increment of confining stress is applied in a continuous manner up to the desired value. The length of time to reach the desired value is about 8 minutes. The results with the two approaches to loading application are seen in Figure 4.8; in one, the stress is applied continuously and in the other, it is applied in steps. Consolidation of both samples is completed in about 8 to 10 minutes. During consolidation, there is no excess pore pressure observed in either method. Despite the similar length of time for application of the consolidation stress, the sample with step load application has a higher value of $\varepsilon_v/\varepsilon_a$ than the continuous load application (4.2 vs. 3.5). The value of 4.2 is comparable to the findings of other researchers. This indicated that consolidation under isotropic loading is rate dependent.

This is also an issue regarding the idea of the end of consolidation. Consolidation for granular soil has been accepted to be completed within a very short time. However, from the two tests presented above, different procedure and times create a difference in the consolidation of samples. During the consolidation phases, no excess pore pressure was measured in either method. In this thesis, completion of consolidation is considered to be when the stress state has traveled to the desired stress state with no excess pore pressure.

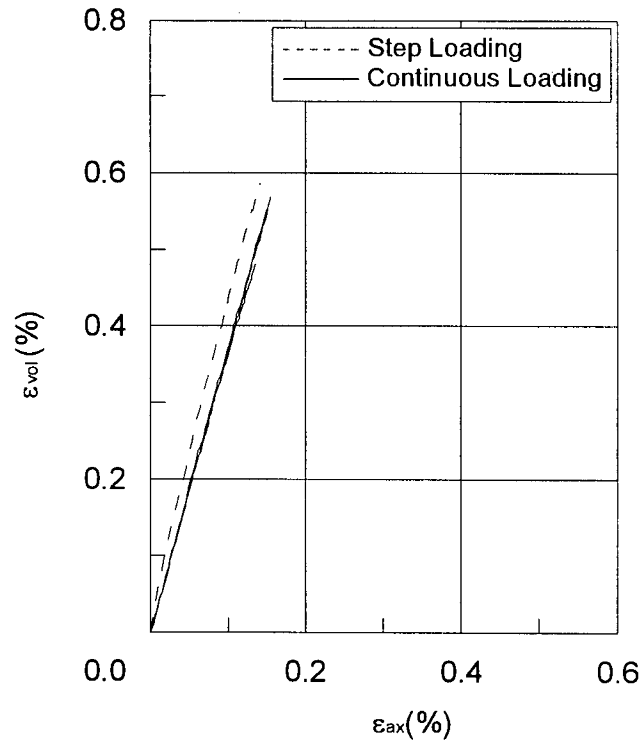

Figure 4.8 Strain Development for Different Loading Application

4.3 Creep behaviour (Phase 4)

4.3.1 General

In Phase 4, the samples were left at a constant stress ratio for holding durations of varying length. Stress ratio of 1.0, 2.0 and 2.8 were maintained for periods of 1, 10, 100, 1,000 and, in one case, 10,000 minutes. Most tests were conducted at a confining stress of 100kPa with some tests conducted with σ'_3=50kPa and 150kPa for comparison purposes. All strains in this section on Phase 4 are calculated relative to the dimensions of the sample at the beginning of Phase 1. As the total strain at the end of Phase 4 is less than 10% in all cases, this should not introduce any large errors.

4.3.2 Strain development with time

Figure 4.9 shows the development of axial and volumetric strain with time during Phase 4. This figure is a typical result of a test for each stress ratio at 100kPa confining stress. Table 5 shows axial and volumetric strain development for each stress ratio.

As seen in the figure, initial strain rates are much higher for R=2.8 than for R=1.0.

Table 5 Strain Development at Phase4 (%)

t	1.0		2.0		2.8	
(min)	ε_a	ε_v	ε_a	ε_v	ε_a	ε_v
1	0.002	0.008	0.013	0.011	0.03	0.015
10	0.007	0.025	0.04	0.035	0.1	0.05
100	0.015	0.047	0.08	0.07	0.19	0.11
1,000	0.027	0.09	0.115	0.085	0.27	0.14

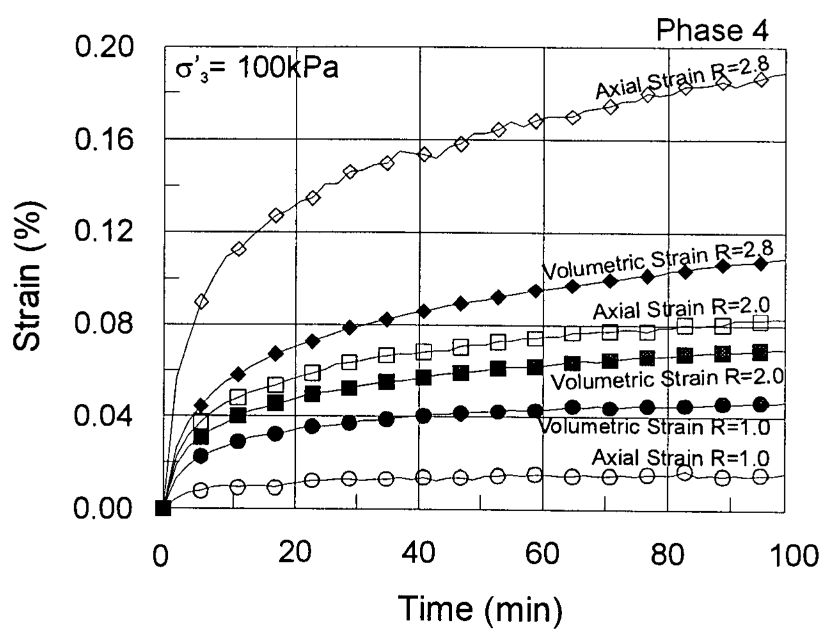

Figure 4.9 Strain Development against Time

The rate of strain gradually reduces to a slower rate with time. Axial strain develops faster than volumetric strain for R= 2.0 and 2.8. On the contrary, axial strain develops slower than volumetric strain for R=1.0. Lade (1998) presented the results of his tests for creep on Antelope Valley Sand under triaxial compression. Tests were performed on Antelope Valley Sand with 5 periods of holding at different stress ratios. The development in axial strain became faster with increasing stress ratio, whereas the rate of development of volumetric strain only increased slightly. The relationship between axial and volumetric strain reversed at a stress ratio close to $R=1/K_0$ which is slightly below 2.0.

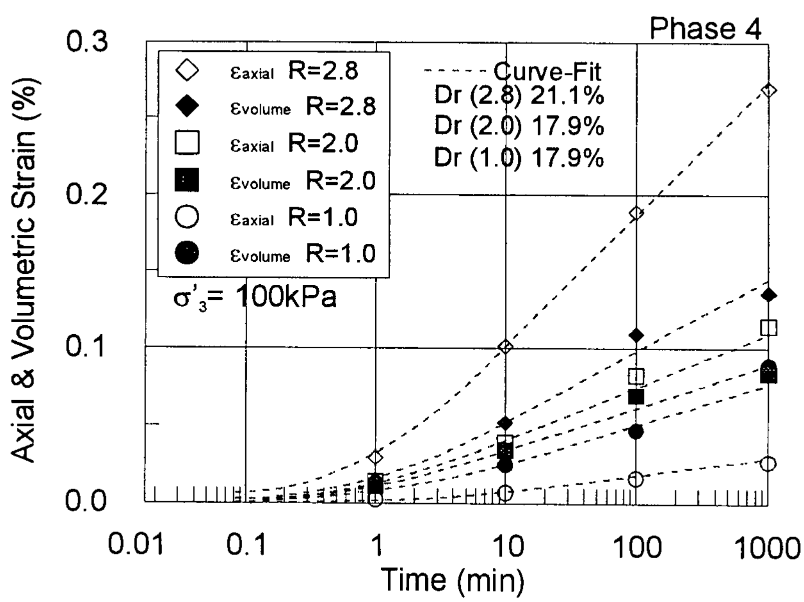

Figure 4.10 Strain Development for Different Duration

Figure 4.10 shows the strain development in Phase 4 against the logarithm of holding duration for each stress ratio. Samples are in the loose state with a slight difference in relative density between them. For holding duration greater than 10 minutes, the development of both axial and volumetric strains becomes approximately linear against the logarithm of holding duration.

4.3.3 Relationship between axial and volumetric strain during creep

Figure 4.11 shows the relationship between axial and volumetric strains in Phase 4. Specimens were all prepared in a loose state. Regardless of the magnitude of the stress ratio, the relationship between axial strain and volumetric strain developments is approximately linear. The difference in length of duration does not affect the direction of the strain path. The value of $\varepsilon_v/\varepsilon_a$ depends primarily on the stress ratio. Mejia et al (1991) showed that a

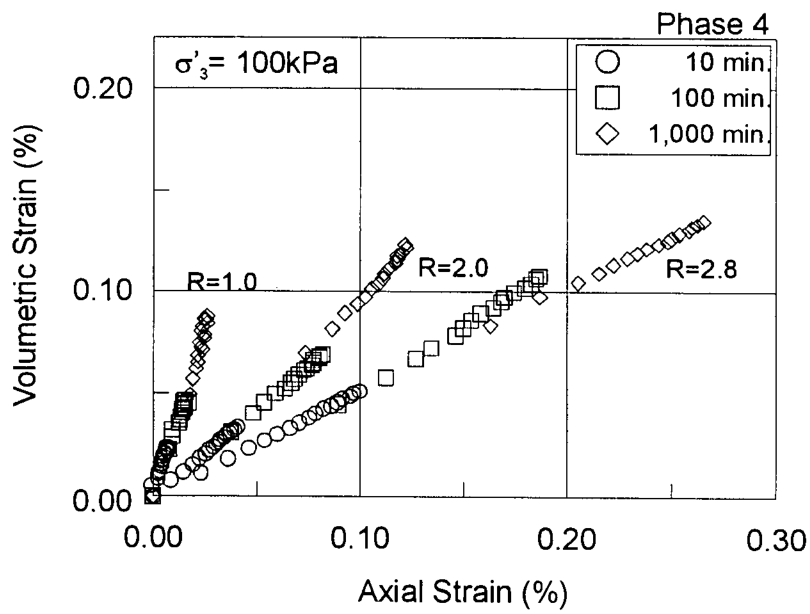

Figure 4.11 Relationship Between ε_a and ε_v in Phase 4

linear relationship existed between the logarithm of strain rate and the logarithm of holding time. In addition, the log strain rate vs. log time relationship is shifted parallel as the stress ratio increases. The suggestion was made that creep strain increments follow an approximately fixed direction during creep deformation at R states of up to about 2.8. i.e. $\varepsilon_v/\varepsilon_a$=f(R)

The value of $\varepsilon_v/\varepsilon_a$ is 0.55 for R=2.8, about 1.0 for R=2.0 and about 3.0 to 3.5 for

R=1.0. These are similar values to those observed at the end of consolidation. In the case of R=1.0, the variability in strain ratio is larger than for the other stress ratios. This is because the strain magnitude during creep under isotropic stresses is small and close to the resolution of the measurements.

In Phase 3, two load applications were attempted and $\varepsilon_v/\varepsilon_a$ was affected by the method of load application as show in section 4.2.4. However, the method of loading application in the previous phase does not seem to affect the strain path direction during a holding phase under the isotropic loading. This may imply that, regardless of the method of loading application, the strain path direction is identical. i.e. $\varepsilon_a/\varepsilon_v$=3.37 at R=1.0 for both methods.

4.3.4 Effect of relative density on strain development during creep

Strain develops in a similar manner in denser samples and in loose samples but the amount of strain is smaller for denser samples. Figure 4.12 shows that the $\varepsilon_v/\varepsilon_a$ ratio is largely independent of D_r over the range of 10% to 50% relative density for creep at constant stress ratio. The total strain during ageing is less for denser samples. Again the magnitude of the stress ratio controls $\varepsilon_v/\varepsilon_a$.

4.3.5 Effect of the confining stress

In addition to σ'_3=100kPa, several samples were tested under σ'_3=50kPa and 150kPa. All samples were prepared in a loose state and consolidated at R=2.8. Figure 4.13 shows the

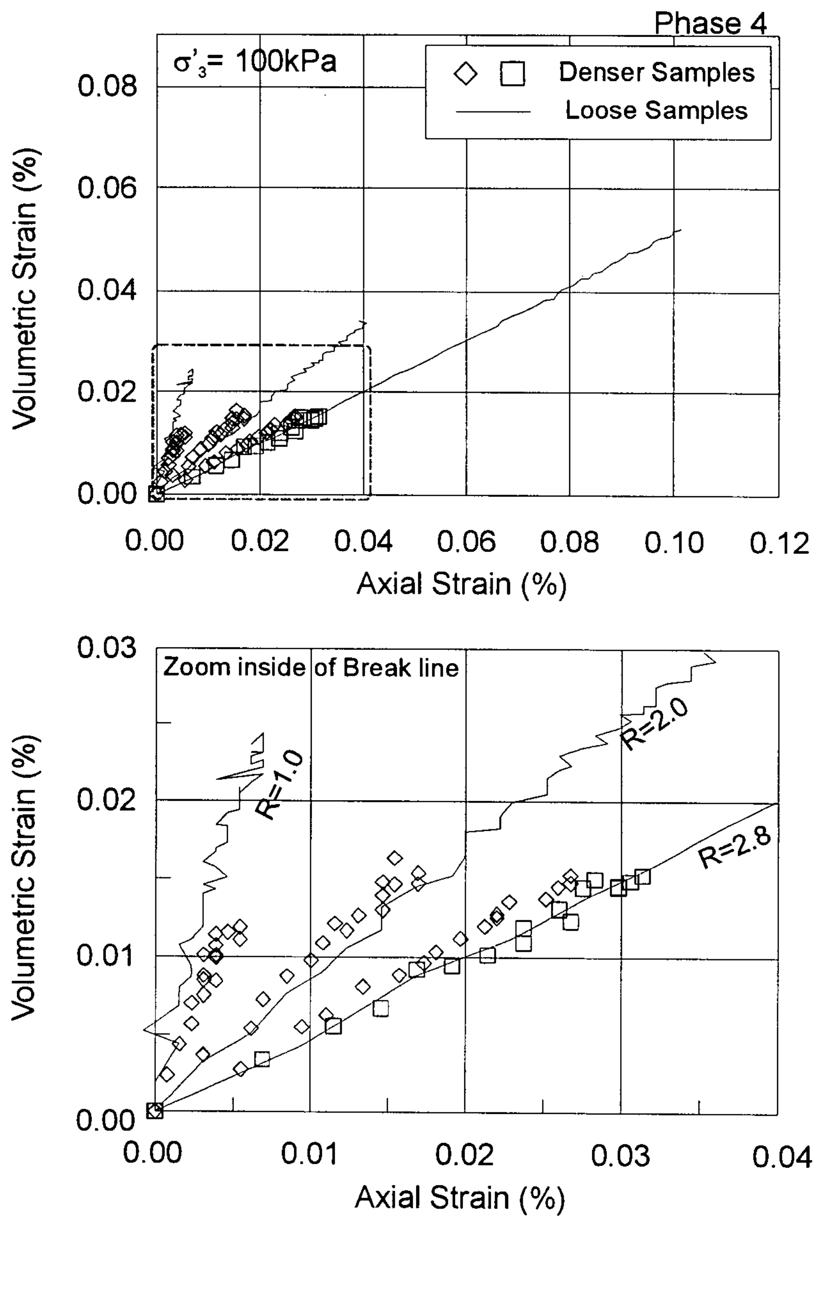

Figure 4.12 Relationship between ε_a and ε_v for Different Relative Densities

development of strain with time for 3 samples at D_r=18.2%, 20.2% and 22.0% for σ'_3=50kPa, 100kPa and 150kPa, respectively. The initial strain rates are higher for higher confining stresses. The rates decay with time. Figure 4.14 shows that $\varepsilon_v/\varepsilon_a$ is independent of confining stress up to an ageing time of 1,000 minutes.

Figure 4.15 shows the development of axial and volumetric strain against the logarithm of time. Both strains develop in a similar manner regardless of the level of confining stress. Once a holding duration exceeds 10 minutes, the relationship between strain and the logarithm of holding duration remains linear up to 1,000 minutes. Lade (1998) carried out similar tests on very dense granular samples. The applied stress ratio was 2.0 and

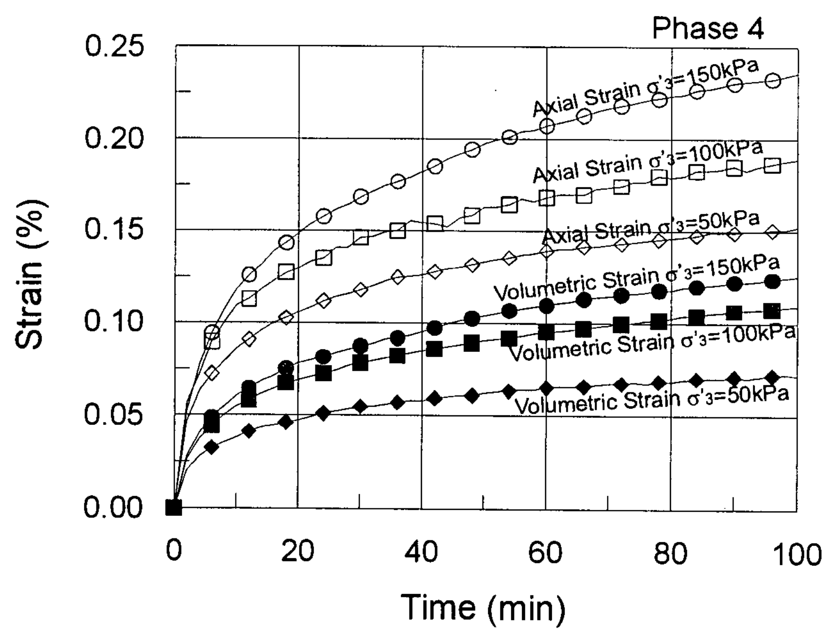

Figure 4.13 Strain Development in Different Confining Stresses

confining stresses were 192kPa, 392kPa and 785kPa. He showed that both strains developed linearly against the logarithm of time regardless of the magnitude of confining stress. On the contrary, the manner of strain development did not seem to be affected by the observed magnitude of confining stress, which is different in this experiment. Assuming samples were prepared in the same relative density, the average void ratio in Lade's tests was 0.96, whereas the minimum void ratio was 0.98. Samples were prepared in a very dense state. The strains developed in dense samples are very small and are too small for observation of a strain development. In loose samples, both strains develop faster and more under higher confining stress.

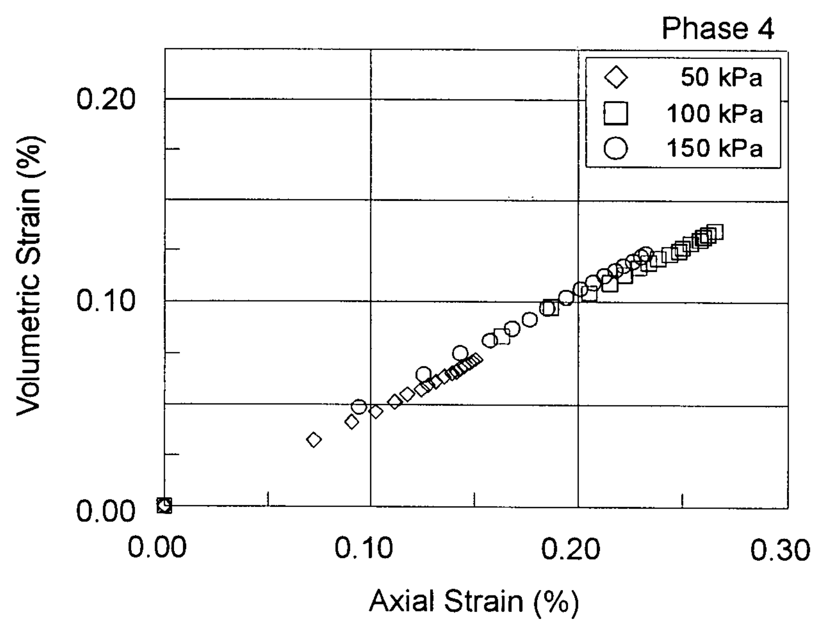

Figure 4.14 Effect of Confining Stress on Strain Development, R=2.8

4.3.6 Conclusion on Phase 4

From the results presented in this section, axial and volumetric strains develop linearly against the logarithm of holding duration, as has been presented in previous studies. The quantity of strains under the constant stress state is increased at higher stress ratios. In addition, strains develop faster at higher confining stresses. Axial strain is more affected by the difference in stress ratio than is volumetric strain. The ratio $\varepsilon_v/\varepsilon_a$ is approximately constant for a given stress ratio over D_r=10 to 50% and confining stresses 50 to 150kPa.

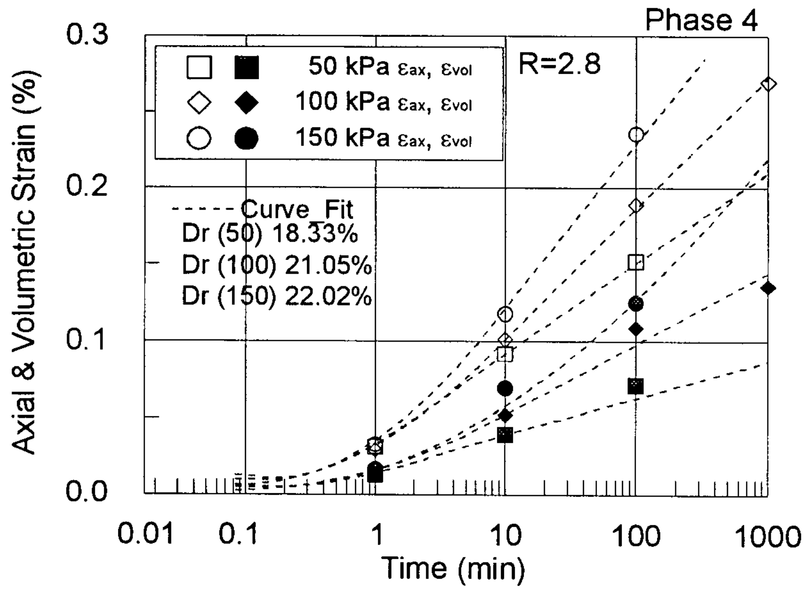

Figure 4.15 Total Strain Development for Different Duration under Different Confining Stresses.

4.4 Shearing test (Phase 5)

4.4.1 General

After the ageing phase (Phase 4), all specimens were tested for shear response. One of four different stress paths was applied to the specimens as shown in Figure 4.1. These stress paths were shows in below

- Conventional path
- Stress-slope of -2 path (P'-constant path or $\Delta\sigma'_1=-2\Delta\sigma'_3$)
- Stress-slope of -1 path ($(\sigma'_1+\sigma'_3)/2$ constant, or $\Delta\sigma'_1=-\Delta\sigma'_3$)
- Stress-slope of 0 path (unloading compression path, or $\Delta\sigma'_1=0$)

All stress slopes are described in terms of $\Delta\sigma'_1/\Delta\sigma'_3$. The stress was applied at a rate of 1kPa change in σ_d for every 15 seconds except the stress slope of -2, on which increment of σ_d was about 1.5kPa for every 15 seconds. As previously stated in Section 3.7, several different intervals were tried. Up to 25 seconds, there was no effect on the reading in the strain development in the case of a 15sec or lower interval (ref. Figure 3.11). This interval makes the stress state inside the sample stable and avoids a possibility of generating excess pore pressure. In addition, since both stresses must be adjusted to allow application of stress paths other than the conventional triaxial path, having an interval between each stress application is necessary in order to maintain a current stress state on the desired stress path. Transducer readings were recorded immediately before the next stress application took place. Therefore, the excess pore pressure, if generated, will disappear and unexpected effects from stress application were allowed to stabilize within each interval.

Under stress-controlled loading, the resulting strain rate is strongly dependent on the relative density, the desired stress ratio and the applied stress paths.The fastest strain development, occurred for R=2.8, 1 minute holding duration and a stress-slope of -2. In that case, it took about 1.5 minutes to reach 0.1% axial strain which results in a strain rate of about 0.07%/min. It can be considered as a slow rate for the strain development and ensured that no excess pore pressures were generated. In the case of the strain controlled test, the rate is conventionally set based on the time to failure. For saturated sand, as sands are free draining, the duration of the test is governed by the necessity of being able to take accurate readings of loading and volume change. A test time of about 1 hour is suitable (Bishop and Henkel, 1957). In this material, the failure can be reached after about 5% axial strain developed. If it is an hour to reach the failure, the imposed rate of strain is about 0.08%/min in the axial strain. All strains in Phase 5 are calculated relative to the dimension at the beginning of Phase 5.

Table 6 shows the calculated strain rate attained at an axial strain of 0.1% and 1% on a sample aged for only 1 minute after completion of consolidation. The strain rate is calculated by dividing the observed strain by the elapsed time to reach that strain. Under the stress controlled test, the rate of strain tends to increase as the strain increases. The calculated fastest strain rate in this study is slower than the suggested strain rate by Bishop and Henkel in ε_a<0.1%, which is the range of interest in this study. Since the application of a load is faster in stress-slope of -2, the resulting strain rate is faster in that stress path. If the loading application is the same on every stress paths, the strain rate is faster as stress path is vertical. The larger the path direction change, the faster the strain rate at R=2.0 or more. At

R=1.0, a large change of path direction resulted in a lower strain rate.

The effect of ageing on the stress-strain response will be discussed first with respect to the conventional stress path. The effect of variation in stress paths on that typical response will then be considered.

Table 6 Strain Rate with 1 minute duration (%/min.)

Stress Ratio	Stress Path	ε_a=0.1%	ε_a=1.0%
2.8	Con	0.039	0.08
	-2*	0.071	0.2
	-1	0.049	0.157
	0	0.061	0.226
2.0	Con	0.022	0.049
	-2*	0.036	0.105
	-1	0.024	0.077
	0	0.029	0.112
1.0	Con	0.013	--
	-1	0.009	0.042

Load Application 1.0kPa/15sec in σ_d

*Load Application 1.5kPa/15sec in σ_d

4.4.2 Stress Strain response for conventional path

Figure 4.16 shows the effect of ageing at R=2.8 on the stress-strain curve obtained in a conventional triaxial compression test. The specimens were at relative densities of 21% for holding times of 1, 10, 100 and 1,000 minutes. For longer ageing times, the initial part of the stress-strain curve becomes steeper, i.e. the stiffness increases. Longer ageing times result in less volumetric strain during the early part of subsequent shearing. The ε_v vs ε_a curve is poorly defined for $\varepsilon_v < 0.002\%$.

Figure 4.17 shows that although the initial part of the stress-strain curve is strongly affected by ageing, the effect disappears at an incremental axial strain of less than 0.1%. The

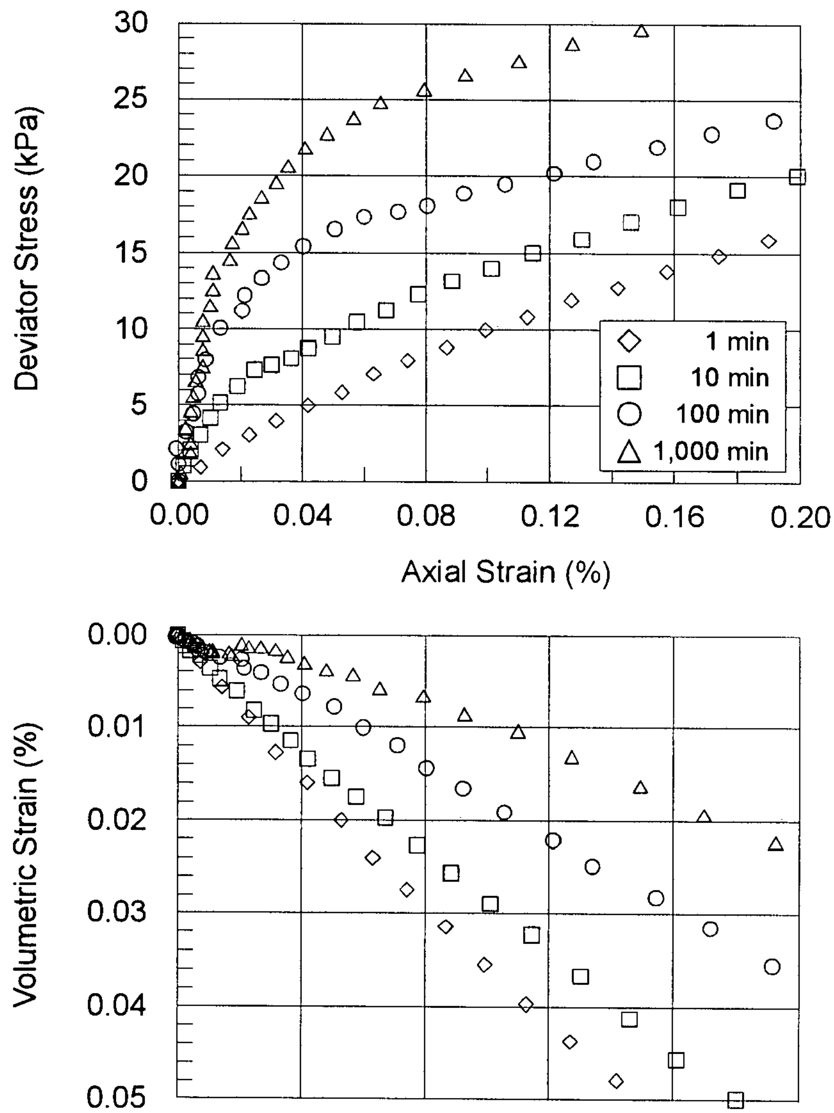

Figure 4.16 Stress-Strain Response on Conventional Path, R=2.8

test at 1,000 minutes plots above other curves because it is slightly denser (D_r=24% vs. 21%). The same effects were noted for ageing at R=2.0 and R=1.0 as shown in Appendix A13 and A17.

The general trend can be summarize as shown in Figure 4.17, which shows data from samples consolidated to stress ratios of R=1.0, 2.0 and 2.8 and aged for a variety of times.

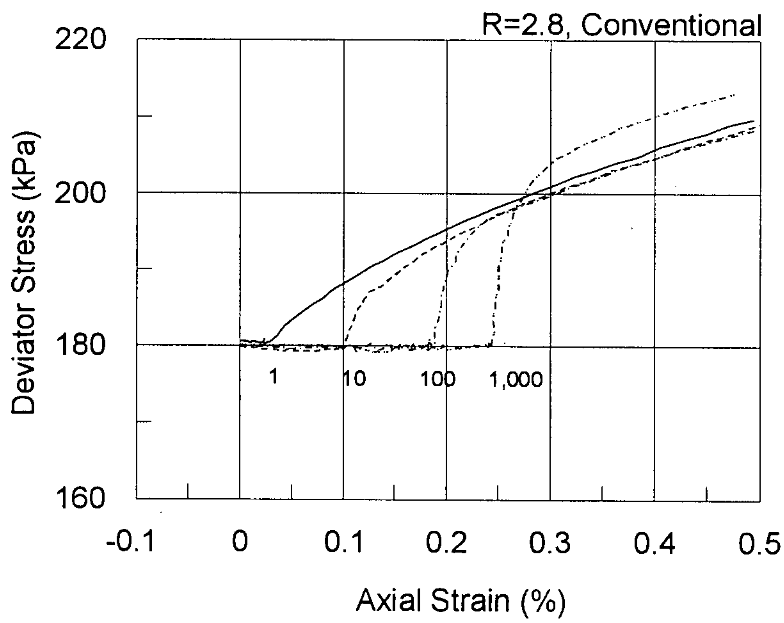

Figure 4.17 Stress Strain Curve during Phase 4 and 5

Zero strain is taken to be the start of Phase 4. All tests follow approximately the same overall deviator stress vs. axial strain curve. The initial stiffness of each individual curve is affected by the consolidation path and the holding time, but at large strain, the curves tend to fall on top of each other. The overall curves are softer at higher stress ratios.

4.4.3 Residual strain in Shearing Phase

It is clear from Figure 4.11 that during each period of ageing at R=2.8, strain will continue to occur without any change in deviator stress. As the ageing period increases, the

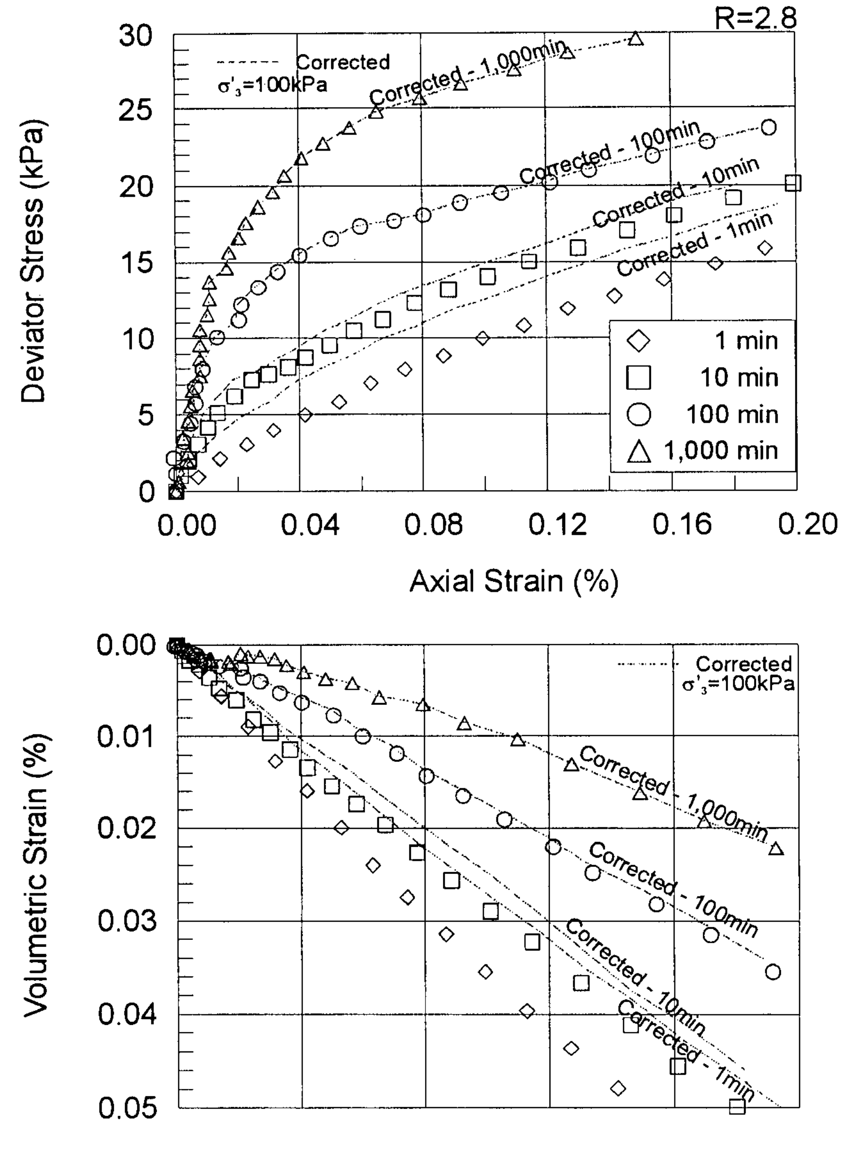

Figure 4.18 Stress-Strain Response with Residual Creep Correction

potential residual creep reduces. In order to estimate the effect of ageing on the stress strain response of the sample, it is necessary to correct the stress-strain curve obtained during the shearing phase by the amount of strain which would have occurred with no stress changes. Figure 4.18 shows the effect of removing the residual strain on an assumption that creep will continue to be generated in the same quantity as one generated under the constant stress state. Based on the data in Phase 4, the residual strain will be significant if the holding duration is short. The stress-strain curve for samples aged for 1 minute and 10 minutes are changed significantly by the correction but the changes are small for samples aged for 100 minutes and longer. Corrected curves for R=1.0 and 2.0 are shown in Appendix A13 to A17. The trend observed in all tests was for the volumetric strain in the early stage of shearing to be reduced by the ageing effects.

4.4.4 Effect of the stress path on stress-strain behaviour

The effect of ageing time on the stress-strain response was also studied for stress paths other than the conventional triaxial path. The applied stress paths were the conventional, the slope of -2, the slope of -1 and the slope of 0 in terms of $\Delta\sigma'_1/\Delta\sigma'_3$ as shown in Figure 4.1. These stress paths are applied to samples at R=2.8, 2.0 and 1.0. Figure 4.19 illustrates the effect of imposed stress path on the stress-strain response for a holding time of 10 minutes at R=2.8. The relative density of the samples ranged from 21% to 27% as shown on the figure. The initial slopes of the stress-strain curves do not vary greatly in the very early part of the curve but the curves begin to diverge at about ε_a=0.015%. The highest shear resistance is mobilized for the stress path with increasing mean normal stress (a

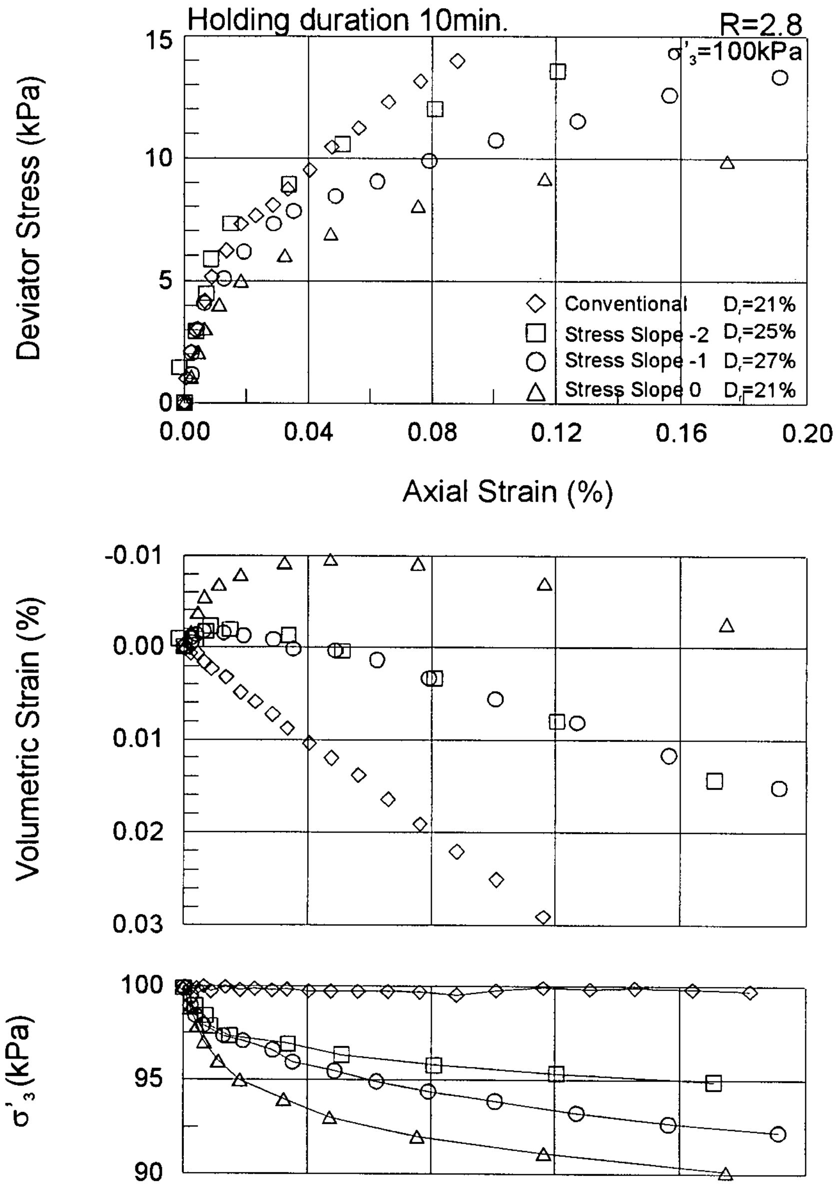

Figure 4.19 Stress-Strain Curve at R=2.8 with Holding Duration of 10 min on Various Stress Paths

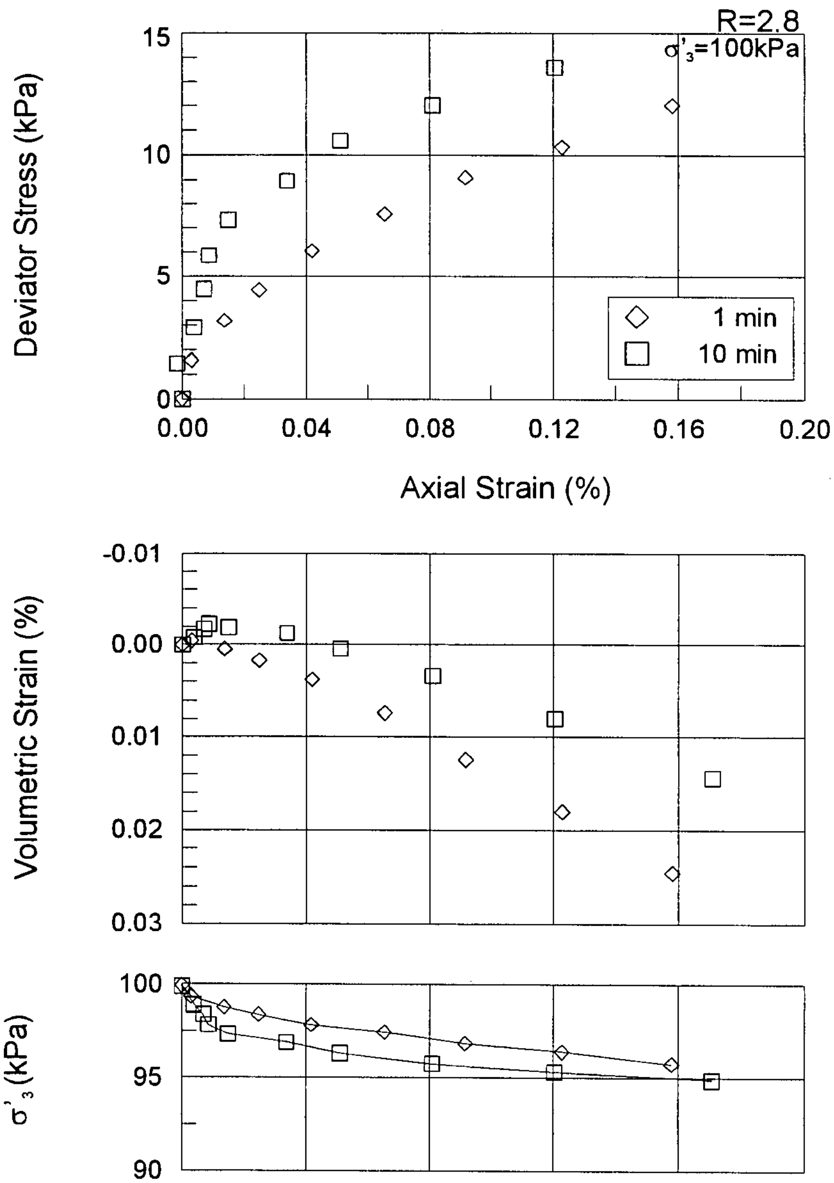

Figure 4.20 Stress-Strain Curve for Stress-Slope of -2 at R=2.8

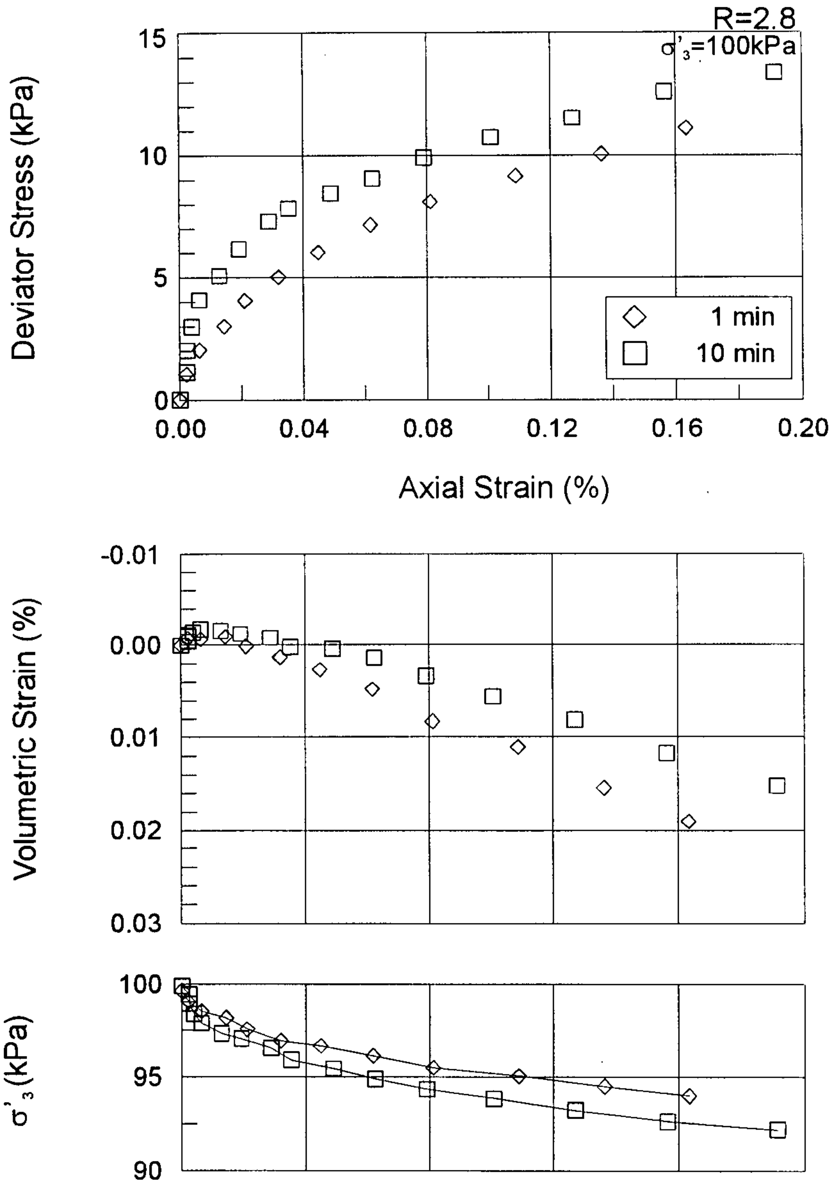

Figure 4.21 Stress-Strain Curve for Stress-Slope of -1 at R=2.8

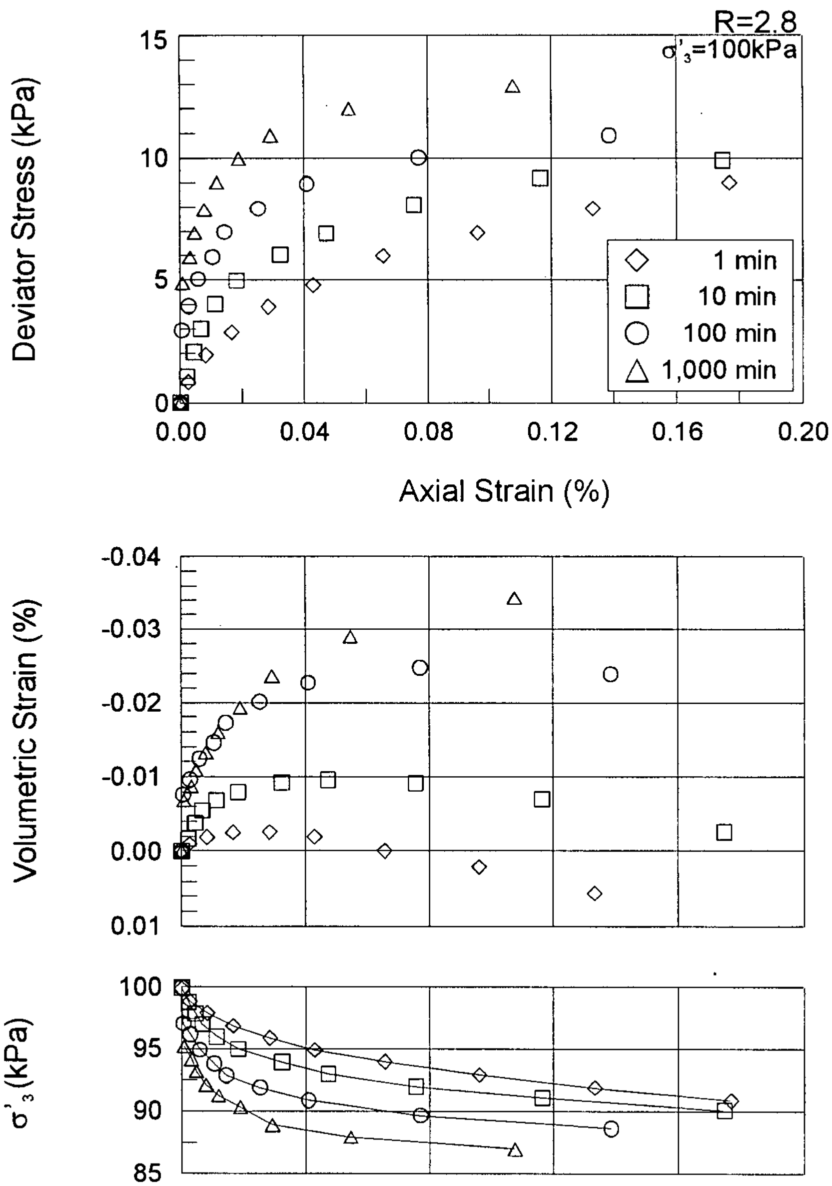

Figure 4.22 Stress-Strain Curve for Stress-Slope of 0 at R=2.8

conventional path) and the least resistance is mobilized in the test where mean normal stress decreases the most ($\Delta\sigma'_1$=0). It can be seen in Figure 4.1 that the stress ratio R increases fastest for $\Delta\sigma'_1$=0. The major difference between the curves as a consequence of stress path is the development of volumetric strain. For $\Delta\sigma'_1/\Delta\sigma'_3$=-2 and -1, very little volumetric strain occurs until an axial strain of about 0.05% has occurred (R=2.98). Contractive volumetric strain then occurs. For the stress slope of 0, the sample dilates initially but begins to contract beyond about ε_a=0.07% (R=3.04). The effect of ageing time on the stress-strain curve response under each of the applied stress path $\Delta\sigma'_1/\Delta\sigma'_3$=-2, -1 and 0 are shown in Figure 4.20, 4.21 and 4.22 respectively. In general, longer ageing times result in stiffer response along the stress path although at least some of the increased stiffness for stress slope of -2 and -1 can be explained by difference in D_r. The effect of ageing is clear in Figure 4.22 for $\Delta\sigma'_1$=0. For D_r=24%, ageing for 1,000 minutes results in a very stiff initial response compared to the sample aged for 1 minute. The 1,000 minutes samples dilates strongly up to a stress ratio of 3.2 while the 1 minute sample begins contracting at ε_a=0.11% about R=2.95 (ϕ_{mob}=29.5°). The exact onset of contraction is difficult to define accurately due to the effect of the correction for residual creep but the trend is clear.

The effect of stress path on stress-strain behaviour for consolidation to R=2.0 and 1.0 is shown in Figure 4.23 and 4.24 respectively. For R=2.0, the initial part of the stress-strain curve is again very similar for all stress paths but the curves again diverge as stress increases. For ageing times of 10 minutes, only the stress-slope=0 shows any tendency to dilate during the very early stages of shearing. Figure 4.24 shows that longer periods of ageing results in

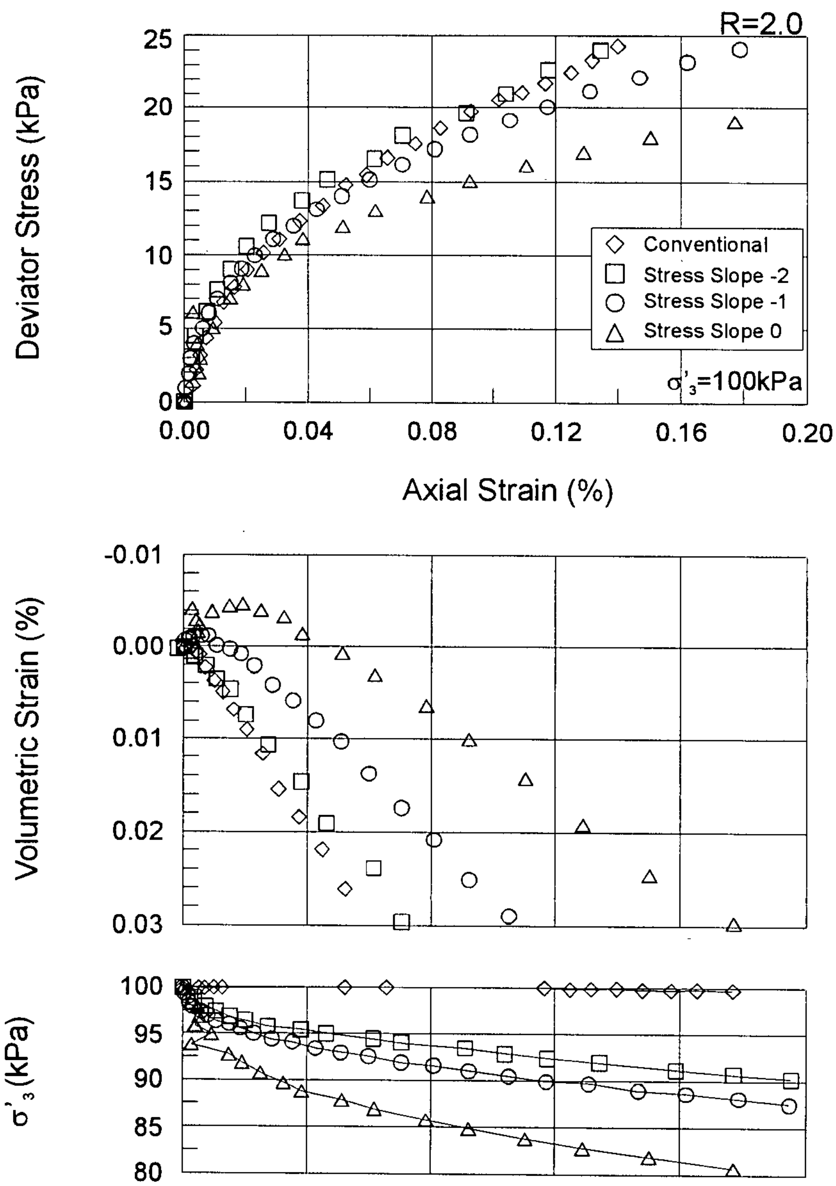

Figure 4.23 Stress-Strain Curves for R=2.0 on Various Stress Paths with 10 min. Holding Duration

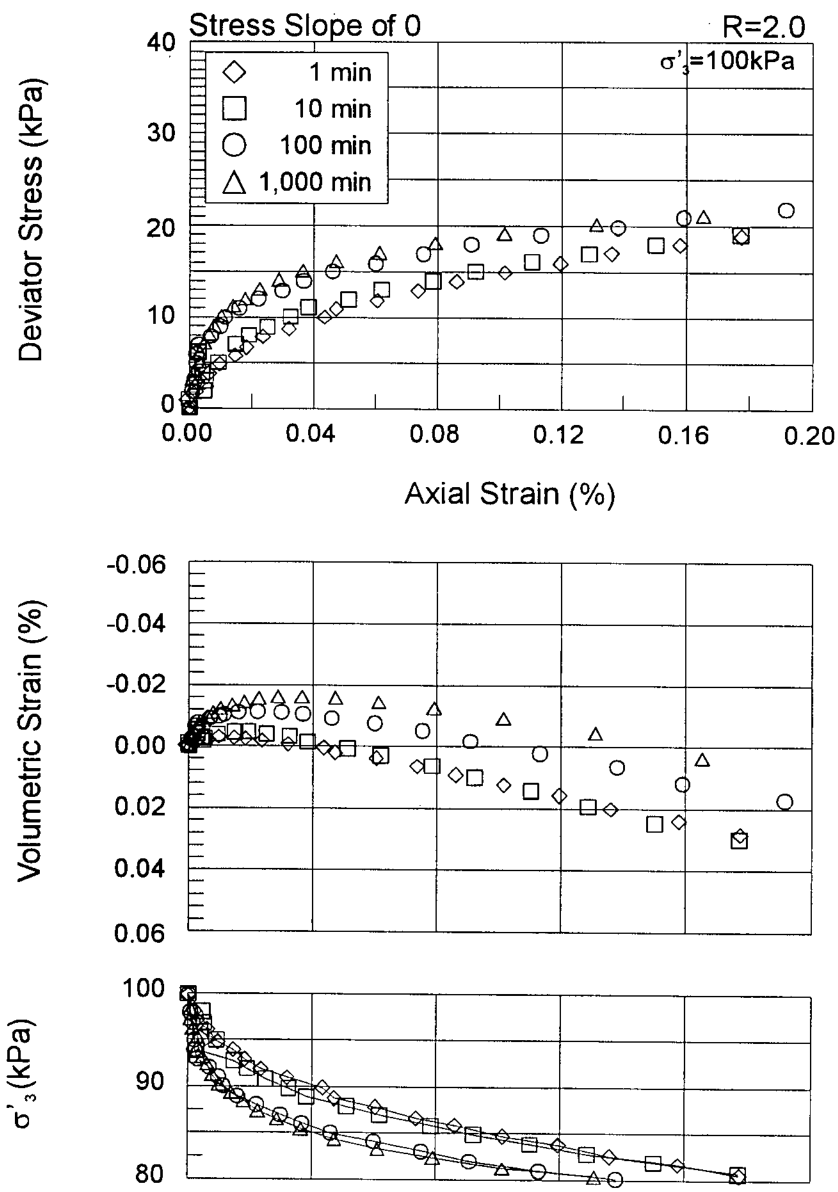

Figure 4.24 Stress-Strain Curve for R=2.0 on Stress Slope of 0 Path with Various Holding Duration

stronger dilation in the very early stages of shear for a stress-slope of 0. The tendency for dilation is only seen in the stress-strain curves for R=2.0 or higher with stress paths accompanied by lateral stress reduction. It becomes more significant when a stress ratio is higher or stress-slope is close to horizontal.

For R=1.0, i.e. isotropic consolidation, the trend observed for R=2.8 and 2.0 are reversed in the range of small strain (ref. Figure A20 in Appendix). Shearing along a path with a stress-slope of -1 results in a stiffer response than for the conventional triaxial path. This is despite the fact that the former path results in a reduction in mean normal stress and a more rapid increase in stress ratio than occurs in a triaxial path. The $\Delta\sigma_1/\Delta\sigma_3$=-1 path still shows a greater tendency to expand more than the conventional test.

4.4.5 Effect of confining stress

Figure 4.25 and 4.26 show the effect of confining stress on the triaxial compression stress-strain curves on ageing at R=2.8 for 10 minutes and 100 minutes. In each case, an increased confining stress results in a stiffer response and more contractive volumetric strain at a given axial strain, i.e. $d\varepsilon_v/d\varepsilon_a$ increases with confining stress. Again, an increase in ageing results in less tendency to contract during shear, i.e $d\varepsilon_v/d\varepsilon_a$ at a particular confining stress is smaller for a longer period of ageing.

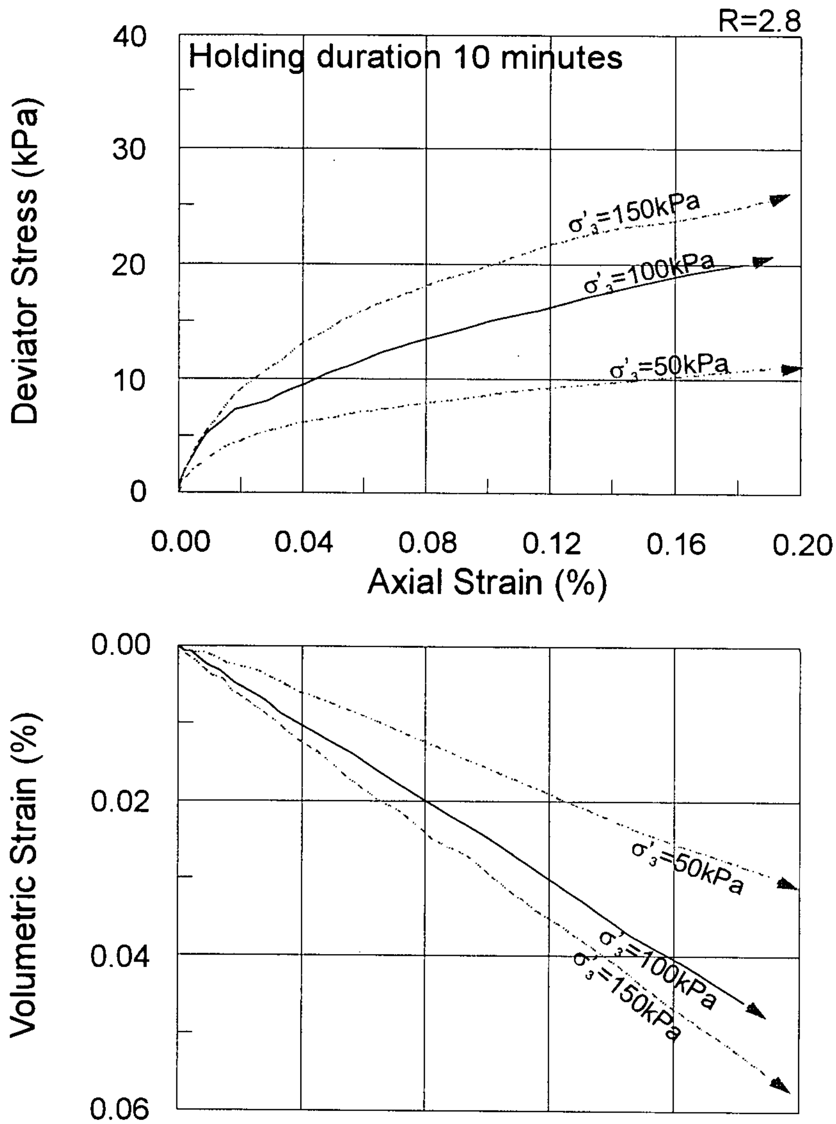

Figure 4.25 Stress-Strain Curves for Various Confining Stresses, R=2.8, 10min.

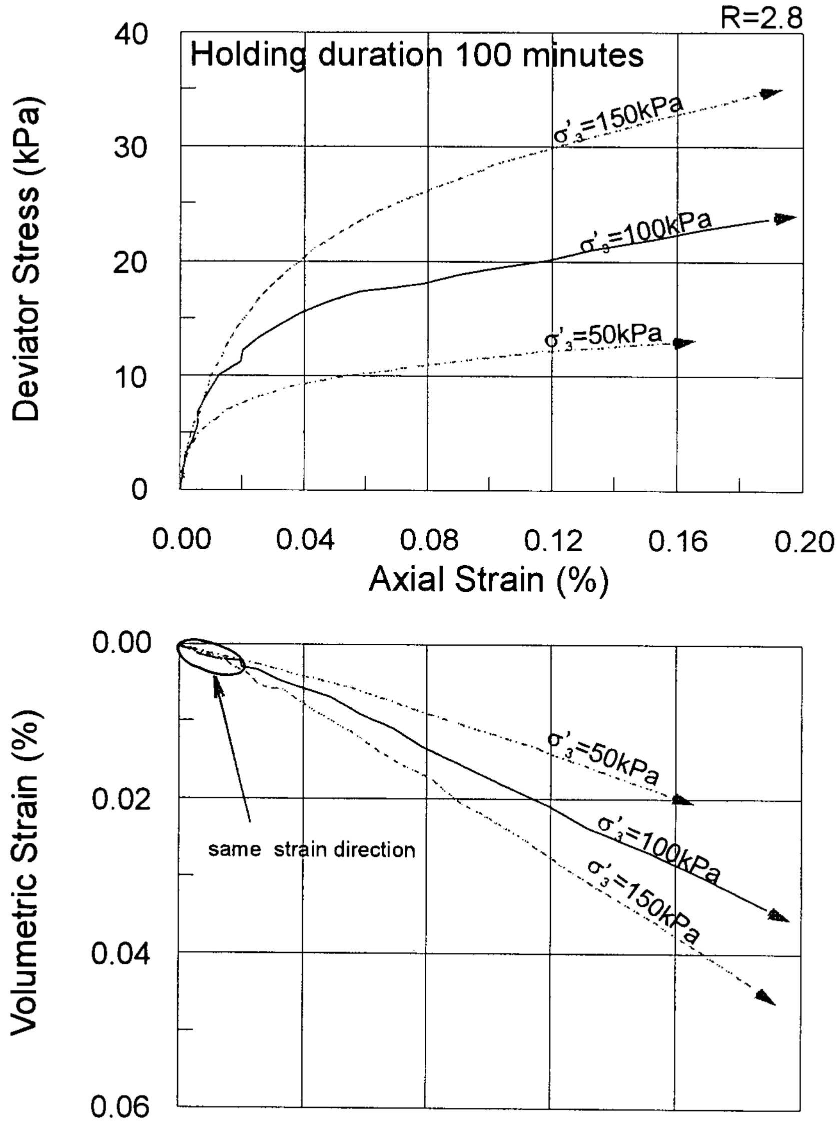

Figure 4.26 Stress-Strain Curve for Various Confining Stresses, R=2.8, 100min.

4.4.6 Summary of general behaviour

The effect of ageing on the stress-strain response of a very loose Fraser River Sand may be summarized as follows

Consolidation and ageing

- Consolidation along constant R paths result in an unique value of $d\varepsilon_v/d\varepsilon_a$ for a given D_r
- $d\varepsilon_v/d\varepsilon_a$ during consolidation is very sensitive to D_r and to the method of loading application for R=1.0, i.e. isotropic loading.
- Deformation is not isotropic under isotropic loading.
- K_0 consolidation (K_0=0.5) occurs at around R=2.0 for very loose sand and at R=2.2 for medium dense sand (K_0=0.45) - largely independent of ageing time.
- $\Delta\varepsilon_v/\Delta\varepsilon_a$ largely constant for a given stress ratio and independent of time.
- $\Delta\varepsilon_v/\Delta\varepsilon_a$ decreases as R increases
- $\Delta\varepsilon_v/\Delta\varepsilon_a$ is largely independent of density for Dr=20% to 50%, governed by R
- $\Delta\varepsilon_v/\Delta\varepsilon_a$ independent of confining stress level, governed by R.
- Strain development linear against log time.

Shear

- On any stress paths, an increase in ageing time results in a stiffer initial stress-strain response.

- Increased ageing time results in a reduced tendency for contractive volume change, during the early stages of shearing for all consolidation stress ratios.
- Higher confining stress results in stiffer and more contractive response at R=2.8.

4.5 Effect of Time and Stress Path on Stiffness

4.5.1 Definition

Due to recent rapid improvement in the capability for measurement of small strains, soil behaviour is now commonly understood to be highly non-linear. Nevertheless, for purposes of calculating deformation in engineering practice, it is conventional to idealize the soil as a linear elastic isotropic material under increments of stress and strain. Over the strain range of interest, the relationship between stress and strain for such a material can be completely defined by two elastic parameters commonly taken to be Young's Modulus, E, and Poisson's Ratio, ν, or shear modulus, G, and bulk modulus, K. Non-linearity is accommodated by using secant or tangent elastic parameters over the strain range of interest. In the case of triaxial tests, E and ν are widely used for presentation of results. Mostly tests are performed on the conventional triaxial path i.e. $\Delta\sigma'_3=0$ and E is simply calculated from the slope of σ_d vs. ε_a curve. In order to derive Young's Modulus under non-conventional stress paths accompanied by changes in lateral effective stress, Young's Modulus can be calculated from the slope of the stress-strain curve using the applicable value of ν. Young's modulus can be derived by the equation:

$$E = \frac{\Delta\sigma_1'}{\Delta\varepsilon_1} + 2\times\left(\frac{-\nu\Delta\sigma_3'}{\Delta\varepsilon_1}\right)$$

$$E = \frac{\Delta\sigma_d}{\Delta\varepsilon_1} + \frac{\Delta\sigma_3'}{\Delta\varepsilon_1}(1-2\nu)$$

Where E_v: Young's Modulus

$\Delta\sigma_1'$,$\Delta\sigma_3'$, $\Delta\sigma_d$: Effective axial, lateral and deviator stresses

$\Delta\varepsilon_1$, $\Delta\varepsilon_3$: Axial and Lateral strain

ν: Poisson's Ratio (= $-\Delta\varepsilon_3/\Delta\varepsilon_1$)

This equation is established based on an assumption that a soil behaves incrementally as a linear elastic isotropic material. If soil behaves in an isotropic manner, the volumetric strain should stay zero under the constant P'-path (Atkinson, 1991), which is the stress slope of -2 in terms of $\Delta\sigma'_1/\Delta\sigma'_3$. However, as shown later, in the stress strain curve on constant P'-path, the volume change is still observed. It is obvious that the behaviour of soil is not isotropic elastic and the equation above may not be applicable. In addition, it is common practice to assume a constant value of Poisson's ratio regardless of the current condition. However, ν depends on the current stress state. In order to ensure consistency in interpretation of stiffness along the different stress paths, shear modulus will be used in this thesis. The shear modulus can be calculated from plots of the shear stress vs. shear strain applied to a specimen without the need to invoke the use of Poisson's ratio. Shear stress is defined to be $(\sigma_1-\sigma_3)/2=\sigma_d/2$ and shear strain is taken to be $(\varepsilon_1-\varepsilon_3)=\gamma$.

4.5.2 Poisson's Ratio

Figure 4.27 shows Poisson's ratio development for the shearing phase on a loose sample. The sample is sheared along the conventional path with a holding duration of 10 minutes at each stress ratio. For each stress ratio, the instantaneous measured value and a smoothed line are plotted. The tangent Poisson's ratio changes depending on the magnitude of the stress ratio and it continues to increase as the loading applications proceed. The initial value of Poisson's ratio is 0.1 for R=1.0, 0.2 for R=2.0 and 0.32 for R=2.8. Regardless of initial stress condition, Poisson's ratio data are very scattered at the beginning. This is because the strain development is very small for the first couple of load applications. This becomes more obvious for samples with longer holding durations. The scatter disappears

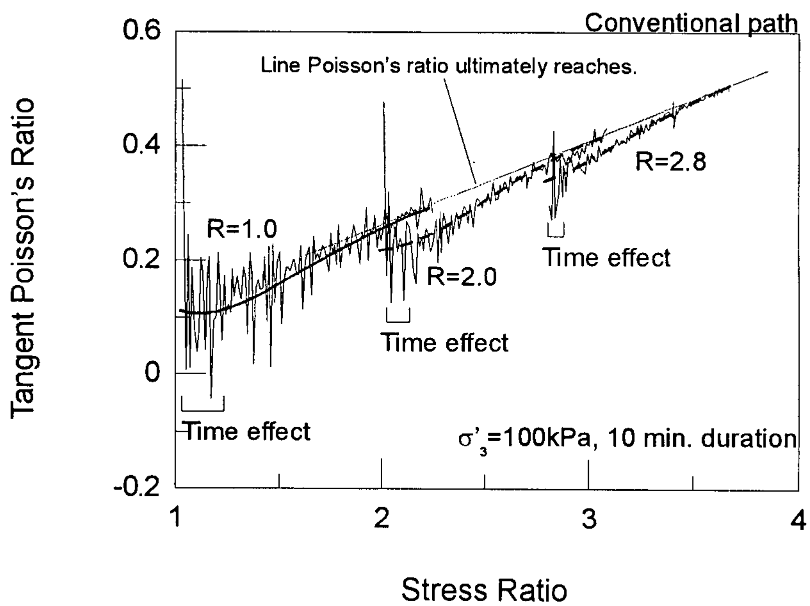

Figure 4.27 Poisson's Ratio for Different Stress Ratios

gradually as additional loading is applied. If the applied stress path is conventional, the tangent Poisson's ratio reaches the same curve regardless of the initial condition. To reach this line, it requires an increase in stress ratio of 1.0, regardless of magnitude of initial stress ratio.

The magnitude of Poisson's ratio is quite different depending on the stress state. For the early stages of a first loading of sand, when particle rearrangements are important, ν typically has values of about 0.1 to 0.2 (Lambe and Whitman, 1968). This value is close to the results for R=1.0. However, for other stress ratios, it seems to increase by a large amount. Tangent Poisson's ratio is about 0.2 to 0.4 for R=2.0 and 0.3 to 0.5 for R=2.8. It is common in the technical literature to see a constant value of 0.1 to 0.2 used in incremental elastic analysis. However, it is clear from these results that the value may vary over a large range depending on the stress condition.

4.5.3 Strain Level

Figure 4.28 shows a typical idealization of the variation of shear modulus with strain level. Due to the improvement of measuring devices, recent studies have focused on the soil behaviour in the very small strain range, i.e. <0.001%. This study focused on the soil behaviour in the small strain range, i.e. >0.001% and <1%. This is the range which has not been studied yet by many researchers (Atkinson and Sallfors, 1991). As previously stated, the

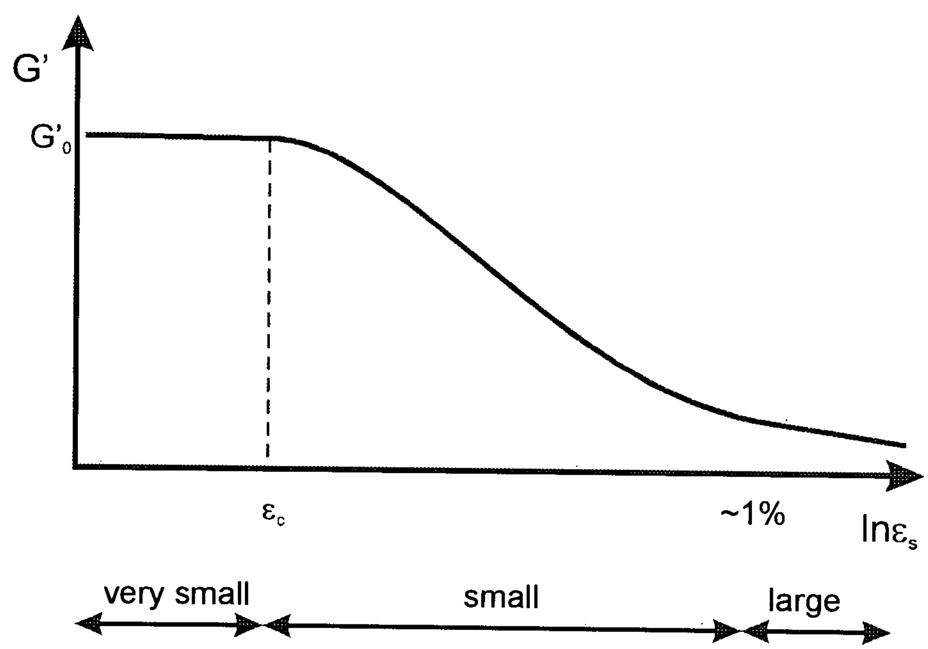

Figure 4.28 Idealization for the Variation of Stiffness with Strain for Soil (Atkinson, 1991)

axial strain is measured by a LVDT and the maximum resolution is about 0.002 - 0.004% of the height of the sample. The volumetric strain is measured by a differential transducer and the maximum resolution is about 0.001%. From both maximum resolutions, a possible maximum resolution for the shear strain may be around 0.007%. Considering this, shear modulus is calculated at 0.03% and 0.15% of the shear strain, which is about, at least, 4 times more than a possible maximum resolution level for shear strain.This strain level is selected as the minimum strain level in which we have confidence.

4.6 Effect of time on G_s

4.6.1 Conventional Path

As stated before, the secant shear modulus is calculated from a corrected stress-strain curve. Figure 4.29 shows the secant shear modulus at the shear strain of 0.03% and 0.15% ($G_{s0.03}$ and $G_{s0.15}$ respectively) for R=2.8 for loading along the conventional path under 100kPa confining stress. The uncorrected $G_{s0.03}$ is about 5.3MPa and the corrected one is

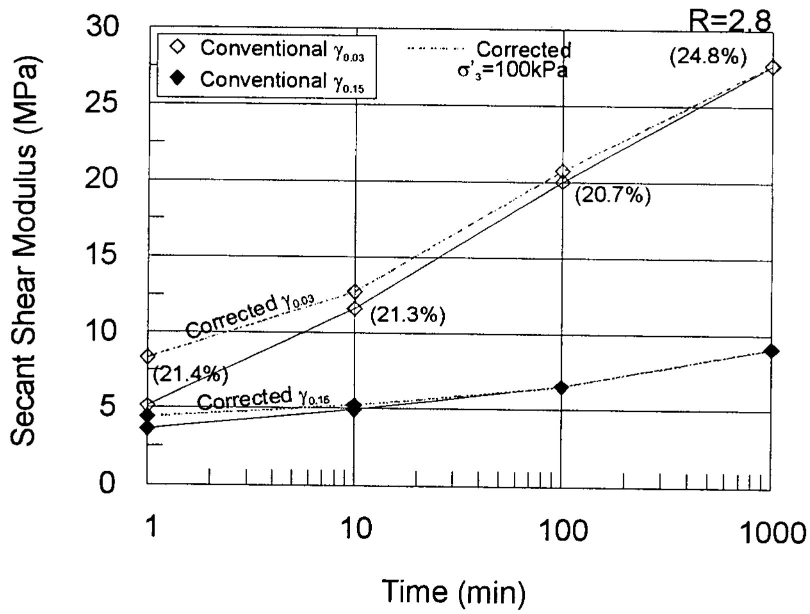

Figure 4.29 Secant Shear Modulus and after Correction

about 8.3MPa for the sample with 1 minute holding duration, i.e. a 60% increase over the uncorrected value. For $G_{s0.15}$, the increase is still 50% in reading. When the holding duration reaches 10 minutes, the uncorrected $G_{s0.03}$ is about 11.5MPa and the corrected one is about 12.7MPa, which is about 10% of an uncorrected value increase. For $G_{s0.15}$ in 10 minutes holding time, the increment becomes smaller than 7%. There is no significant correction if the duration becomes more than 10 minutes.

In the same figure, shear modulus at both strain levels increases depending on the length of holding duration. It is about a 5MPa increment observed in $G_{s0.03}$ between samples with 1 and 10minutes holding duration, and it becomes 8MPa per logarithm cycle up to 1,000 min. This effect is less visible for $G_{s0.15}$. From the holding duration 1 to 10 minutes, the increase in $G_{s0.15}$ is about 0.7MPa. The increment of $G_{s0.15}$ increases for each logarithm of time. The increase between 10 and 100minutes is about 1.3MPa, and between 100 and 1,000 minutes, it is about 2.7MPa. From these results, $G_{s0.03}$ increases to a little more than 300% of its value at 1 minute and $G_{s0.15}$ to 200% over three logarithmic cycles of time. To make this effect clear, Figure 4.30 shows the variation of G_s normalized by the value measured at 10

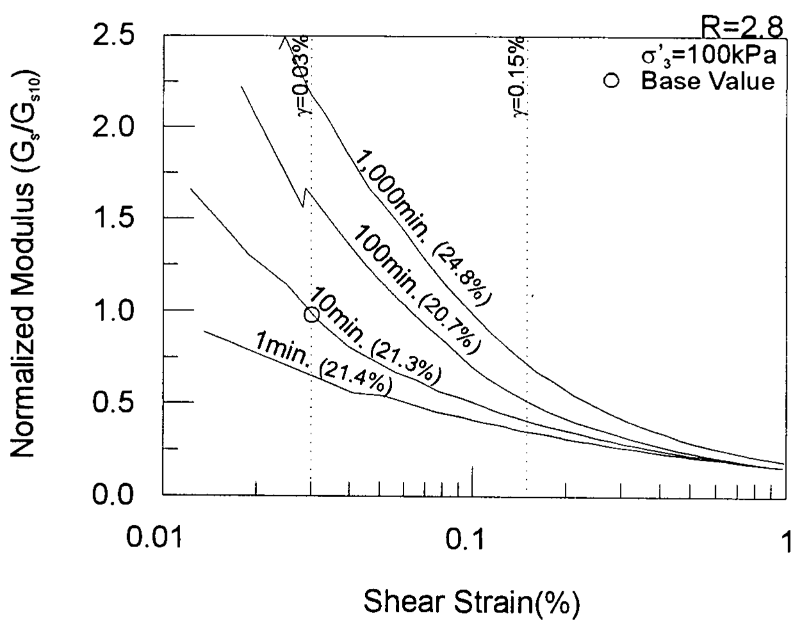

Figure 4.30 Attenuation Curve for R=2.8 on Conventional path

minutes vs. shear strain. The base value can be seen in the figure. The time effect is significant when the shear strain is in the smaller range. At a shear strain of 0.03%, the magnitude of $G_{s0.03}$ varies between 0.8 and 2.2 times the base value 12.7MPa, depending on the time of ageing. The range becomes between 0.5 and 1.0 at the shear strain 0.15%. At very small strains, the shear modulus of soil is generally relatively large but reduces by a factor of about 10 times over the first 1% strain or so (Atkinson and Sallfors, 1991). The degree of modulus attenuation with shear strain is seen to increase with the time for which the sample has been aged. If attention is not paid to consistent practices in ageing of samples, regardless of the small details, time effects could cause significant differences in the results of laboratory studies of stiffness at small strain. Even if identical samples are used with the same test procedures, the differences in holding duration could create variations in modulus of 200 to 300%. Murashev (1997) presented test data for two granular samples. Both samples had the same material with an identical density but one was an "undisturbed" sample and the other was reconstituted. The moduli of the "undisturbed" samples were higher than those for the remoulded samples. He also presented data showing that in "undisturbed" samples, negative dilatancy (contraction) was less and positive dilatancy was more than for the remoulded samples. The results presented here confirm these observations, an "undisturbed" sample being an aged sample and a remoulded sample being a freshly deposited sample. The tendency observed at R=2.8 seems to be very similar for other samples at different stress ratios, although the effect of holding duration becomes less obvious at lower stress ratios.

4.6.2 Effect of Stress Path

Figure 4.31 shows the effect of the stress path on G_s at R=2.8. Regardless of which stress path is followed, the magnitude of $G_{s0.03}$ increases with time and the increase appears approximately linear against the logarithm of holding duration. This increase develops fastest

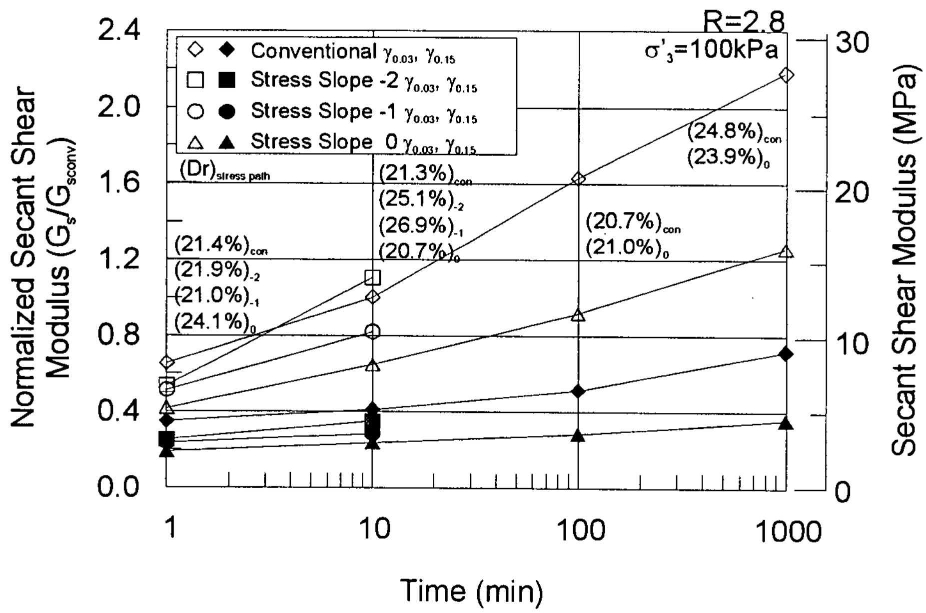

Figure 4.31 Variation of Secant Shear Modulus of Various Stress Paths with time for R=2.8

on the conventional path and it will decrease as the stress path slope goes close to horizontal. As previously stated, the increase is about 8MPa/log cycle on the conventional path. It is 7, 4 and 3MPa/log cycle for Stress-Slopes of -2, -1 and 0, respectively. The effect of time on the development of $G_{0.15}$ is also seen in the same figure. The rate of increase with ageing is much less than for $G_{s0.03}$ but follows the same pattern, i.e. $G_{0.15}$ increases about 1.3 to 1.5MPa/log cycle for the conventional path. The rate of increase reduces gradually as the stress path rotates toward the stress slope of 0 at which is about 0.6 to 0.8MPa/log cycle. The moduli in Figure 4.31 have been normalized to the value on the conventional path at 10 minutes ageing.

Figure 4.32 shows the normalized attenuation curve for each stress path for 10 minutes of ageing. $G_{s0.03}$ for a slope of -2 is slightly larger than on the conventional path and slope of -1 and 0 is slightly less than it is on the conventional path. The limited data for the stress-slope of -2 loading suggests that the initial rate of increase may be higher. Also, the

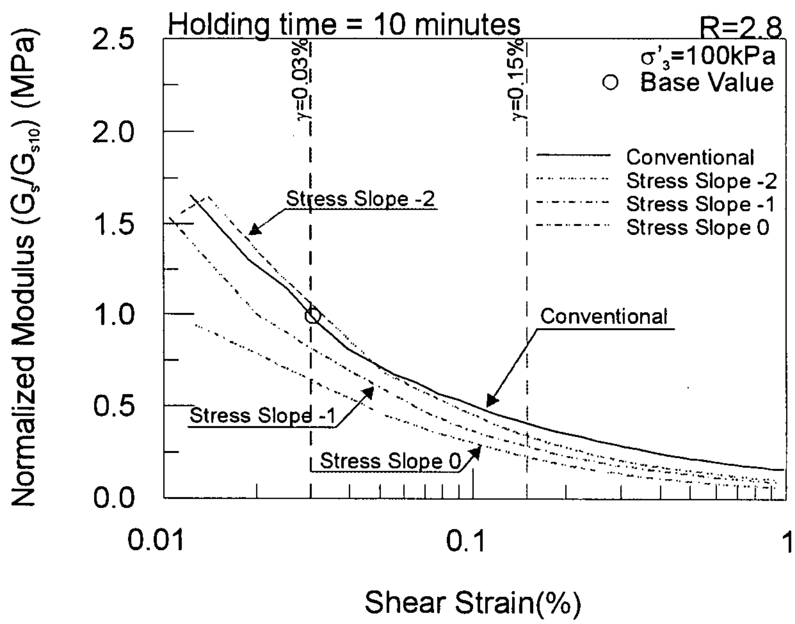

Figure 4.32 Attenuation Curves for Various Stress Paths

rate of loading is faster on stress-slope of -2, which may generate a stiffer response. The stiffness is reduced by about 40% as the stress path rotates from the conventional path to a stress-slope of 0. This is reasonable as the stress ratio rises more rapidly as the direction of

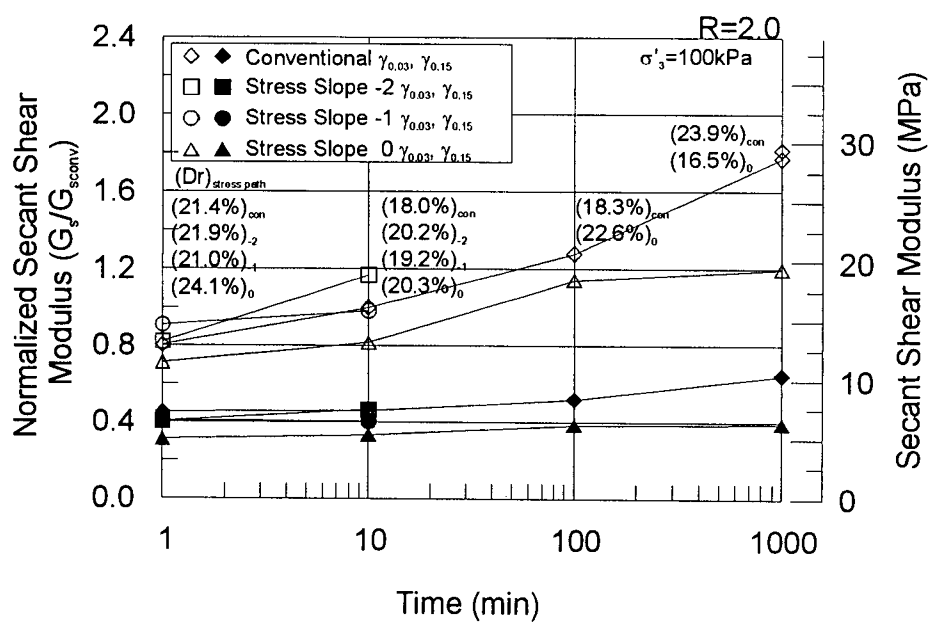

Figure 4.33 Normalized Secant Shear Modulus for various stress paths, R=2.0

the stress path rotates.

Unlike the comparison between the conventional path with different holding duration, the effect of the stress slope remains at a large shear strain range, although it becomes slightly less significant at the larger strain. The deviation between the highest and the lowest values is about 0.4 for $G_{s0.03}$ and 0.2 for $G_{s0.15}$, representing about 30% and 40% reduction of th highest value, respectively.

Figure 4.33 shows the normalized secant modulus for ageing at R=2.0. The base value is G_s for R=2.0 on the conventional path with 10 minutes holding duration. The effect

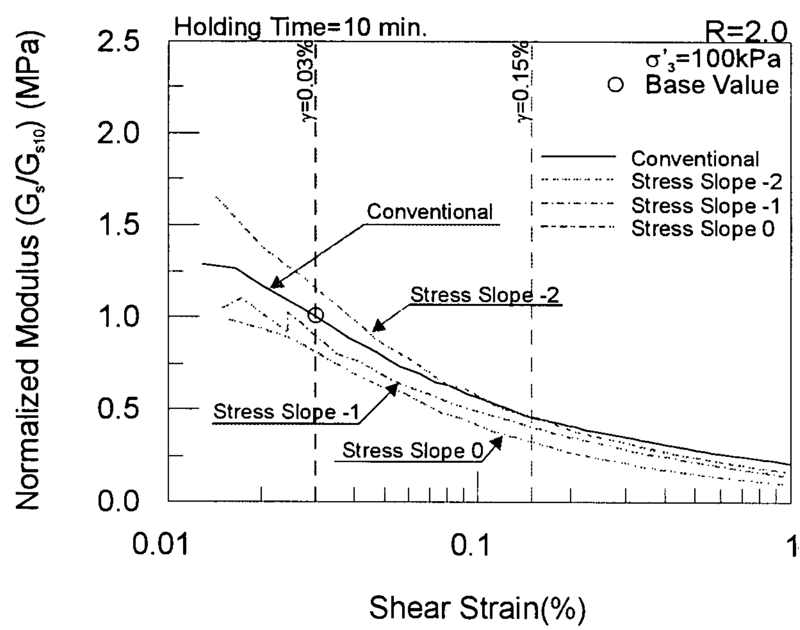

Figure 4.34 Attenuation Curves for Various Stress Paths

of stress path is much smaller than it was at R=2.8. Also, the increase/log cycle seems to stay constant regardless of holding duration length if the relative densities are identical. Figure 4.34 shows the normalized attenuation curves. The range between the largest and smallest value for $G_{s0.03}$ is 0.3 and it is smaller than ones at R=2.8. This represents 30% of the base value. In addition, it becomes more obvious that the attenuation curve for the stress slope of -2 lies above the conventional path. Since the effect of stress slope difference becomes less, the effect of the loading application rate may stand out at this stress ratio.

Figure 4.35 shows the G_s for the logarithm of holding duration for R=1.0. The shear modulus increase is still observed for the longer holding duration. Since there is only one test with another stress path performed at R=1.0, it is hard to define the effect in detail. This test

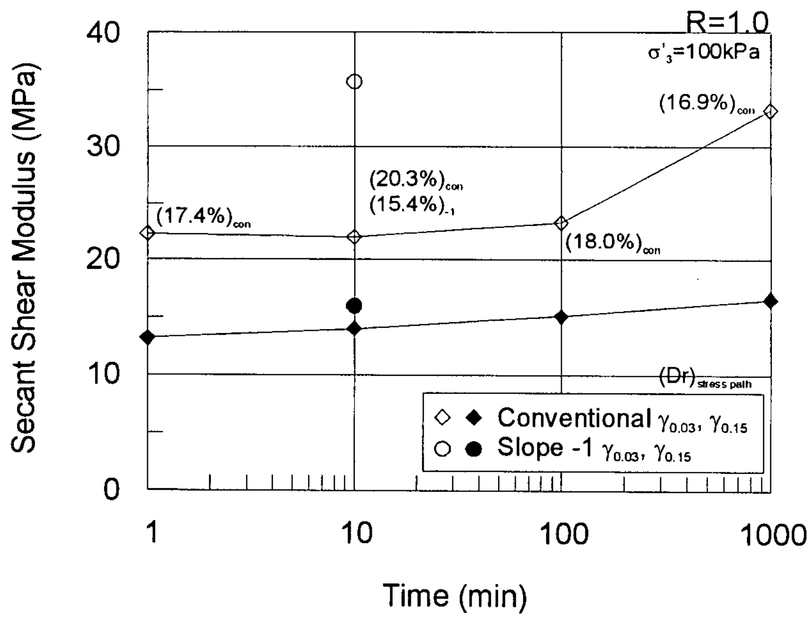

Figure 4.35 Secant Shear Modulus on Two Stress Paths for R=1.0

result is also plotted in the same figure. $G_{s0.03}$ and $G_{s0.15}$ increase significantly from the conventional path to stress slope of -1. This phenomenon is clearly seen in the normalized attenuation curve in Figure 4.36. The increase in $G_{s0.03}$ is about 1.6 of the value on the conventional path at R=1.0.

Atkinson and Richardson (1991) showed the effect of applied stress paths on clay samples. Samples were consolidated at the two different points in the p'-q space, which were q/p'=0.05 and 0.40. These correspond to R=1.05 and 1.46. Applied p' was 200kPa and the applied stress path was defined by an angle measured anti-clockwise from the consolidation stress path. From these results, the stiffness parameter ($\Delta q/\Delta\varepsilon_s$) showed a significant increase

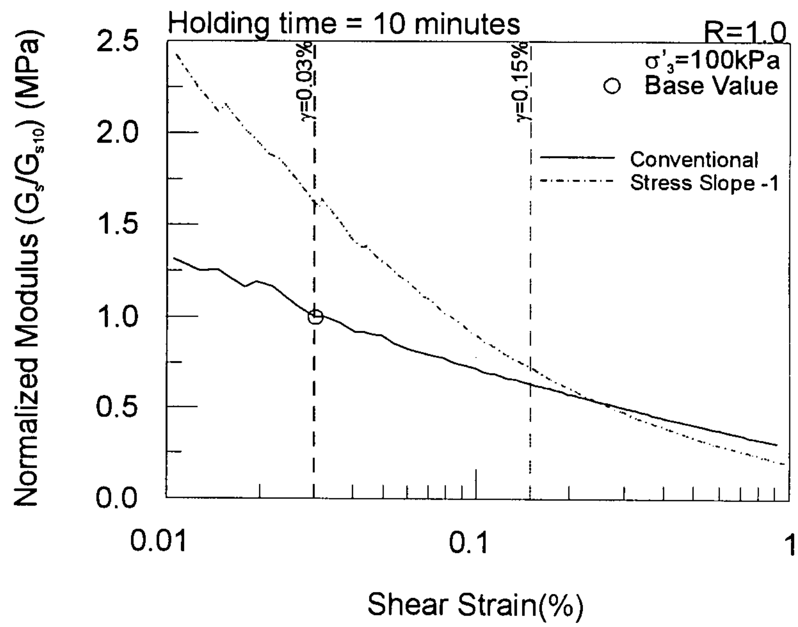

Figure 4.36 Normalized Attenuation Curves on Two Stress Paths for R=1.0

in magnitude as the angle increased an anti-clockwise direction from the conventional triaxial path at lower stress ratio (R=1.05). On the other hand, there was no increase observed at R=1.46. The identical phenomena are observed in this series of the results between R=1.0 and 2.0.

Figure 4.37 shows the effect of stress ratio during consolidation on G_s for 10 minutes holding duration. All G_s values are normalized by $G_{s0.03}$ at R=1.0 on the conventional path. The effect of stress ratio seems to be similar at R=2.0 and 2.8. If variability of factors such as a slightly higher loading rate at stress-slope of -2 and variable relative density could be

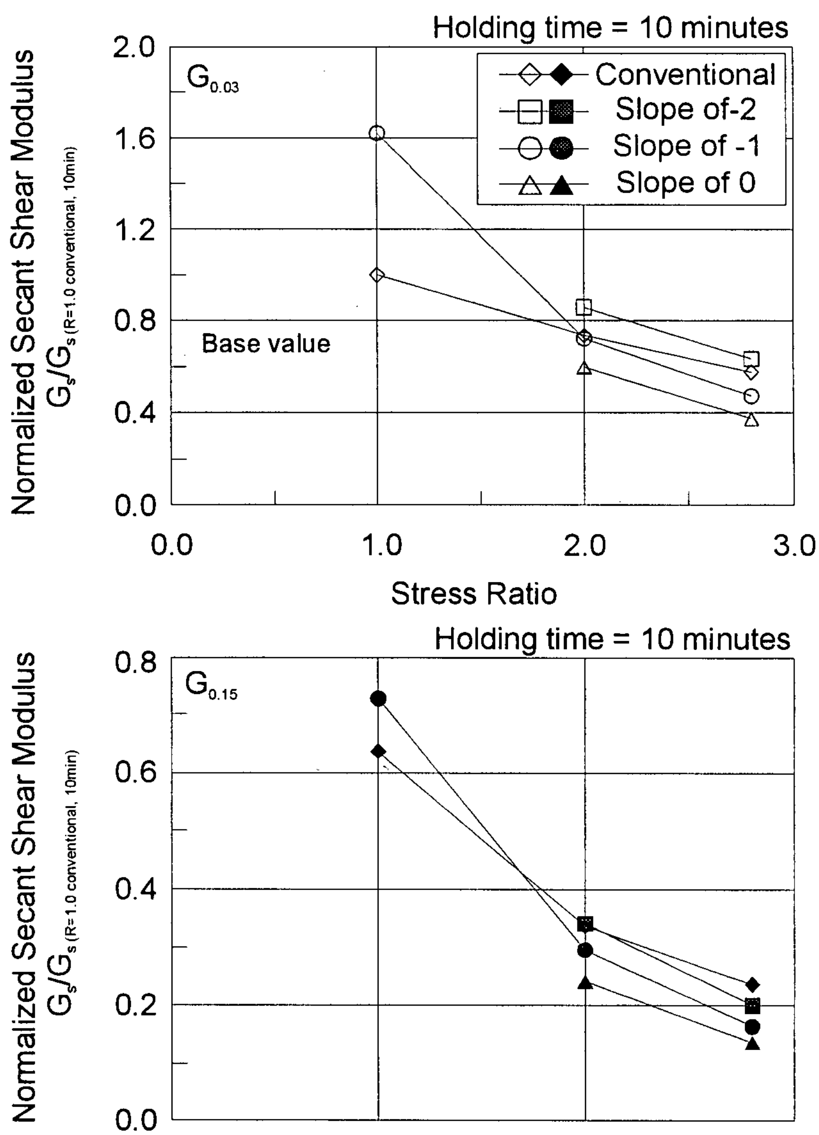

Figure 4.37 Effect of Applied Stress Paths

removed, the range at R=2.0 would be expected to become smaller. This range will be increased in the opposite direction at R=1.0. G_s for R=1.0 on a stress path with slope of -1 path has a higher value than the one on the conventional path. The effect of stress paths on $G_{0.03}$ has reversed by the time sample has reached R=2.0.

The stress path effect is still recognized in $G_{s0.15}$. However, the trend becomes less significant at the larger shear strain. At this point, only one stress path is attempted, thus it is impossible to present the effect of the stress path at R=1.0. But according to all trends based on other stress ratios, this phenomenon is likely happening. Yu and Richart (1984) performed a similar type of test on samples with the same ageing duration, and concluded that the effect of stress path is unimportant. At the same time, they confirmed the important of stress ratio (Yu and Richart, 1984). This contradict the results of these series of test, especially for the shear modulus at R=1.0 and requires further study

4.6.3 Confining stress difference

Figure 4.38 shows how the ageing effect on modulus changes as confining stress increases. The values have been normalized to the value at 10 minutes at 100kPa. As expected, the stiffness increases as confining stress increases. The rate of increase reduces as confining stress increases, i.e. the increase is non-linear. It is conventional to represent the increase as a power of the confining stress, eq $f(\sigma_3)^n$. This is equivalent to a linear increase with the log of confining stress. This was confirmed by Porovic and Jardine (1994) who showed that the power "n" was dependent only on shear strain γ. Jovicic and Coop (1997) also presented test results for the effect of confining stress. Change in G_{max} under the bender

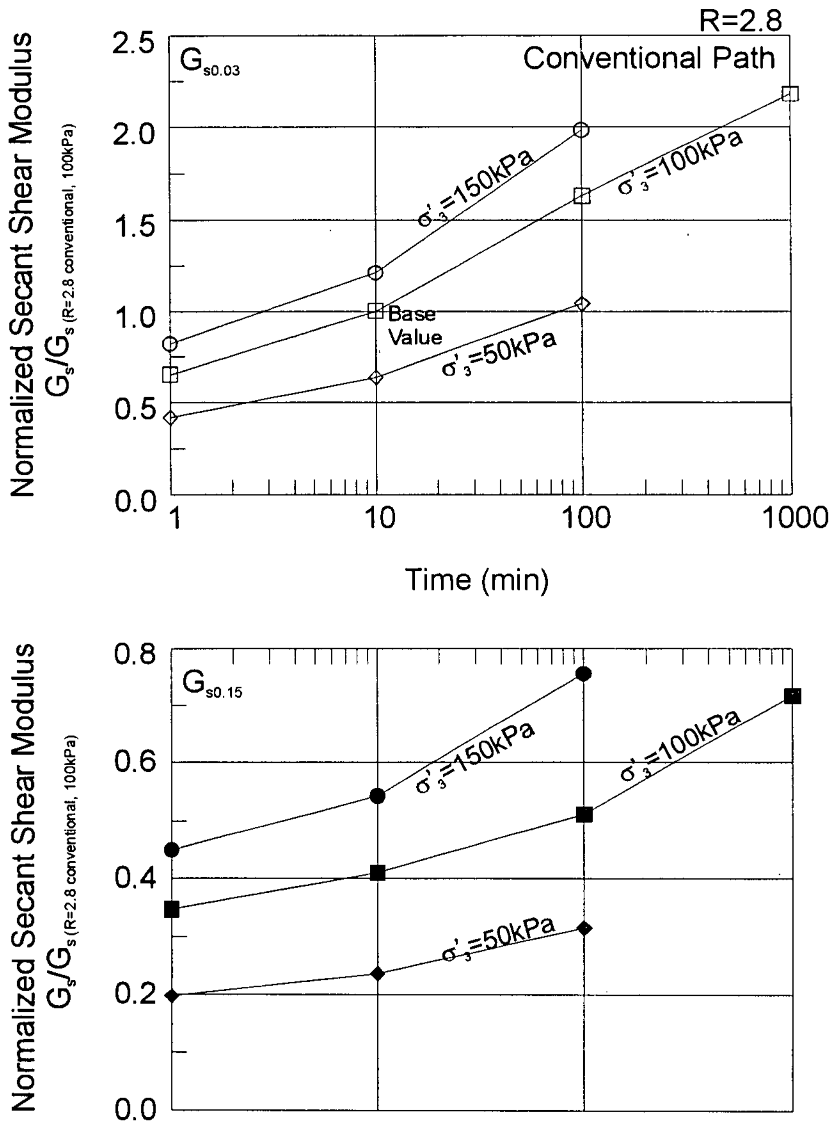

Figure 4.38 Secant Shear Modulus for Various Confining Stresses

element test were measured for different values of p' for different strain levels. All samples were consolidated isotropically. Regardless of the strain level, G_{max} increased as the magnitude of p' was increased. Also, the rate of logarithm G_{max} increment was constant against the logarithm of magnitude p' in all strain level. The larger confining stress seems to give higher magnitude in shear modulus regardless of a strain level or a stress ratio.

4.6.4 Effect of Stress Ratio on Shear Modulus

For continuous loading from an isotropic consolidation state along the conventional triaxial path, the shear modulus would be expected to reduce with shear strain as the stress ratio increased. As was shown earlier, if shearing is paused and the sample is held at a constant stress ratio, creep occurs. When loading is restarted, the sample is initially stiff but the stress-strain curve gradually rejoins the original stress-strain curve. In the tests reported here, the consolidation was carried out at constant stress ratios (proportional loading). Figure 4.39 shows the attenuation curves for each stress ratio on the conventional path. G_s is normalized by the mean normal stress σ'_m at the initial stress ratio prior to application of shear stress. The mean normal stresses are 100, 133 and 160kPa for R=1.0, 2.0 and 2.8 respectively. This value was chosen to focus on only the effect of stress ratios. When the holding duration is 1 minute, the attenuation curves for each stress ratio are very similar in shape but with a difference in magnitude. Stiffness reduces with increased stress ratios.

When the holding duration becomes 10 minutes, the response at R=2.8 shows an increase in G_s in the small shear strain range compared with other curves. Figure 4.40 shows the effect of ageing for 100 and 1,000minutes. The stiffer response on the curve for R=2.8 in

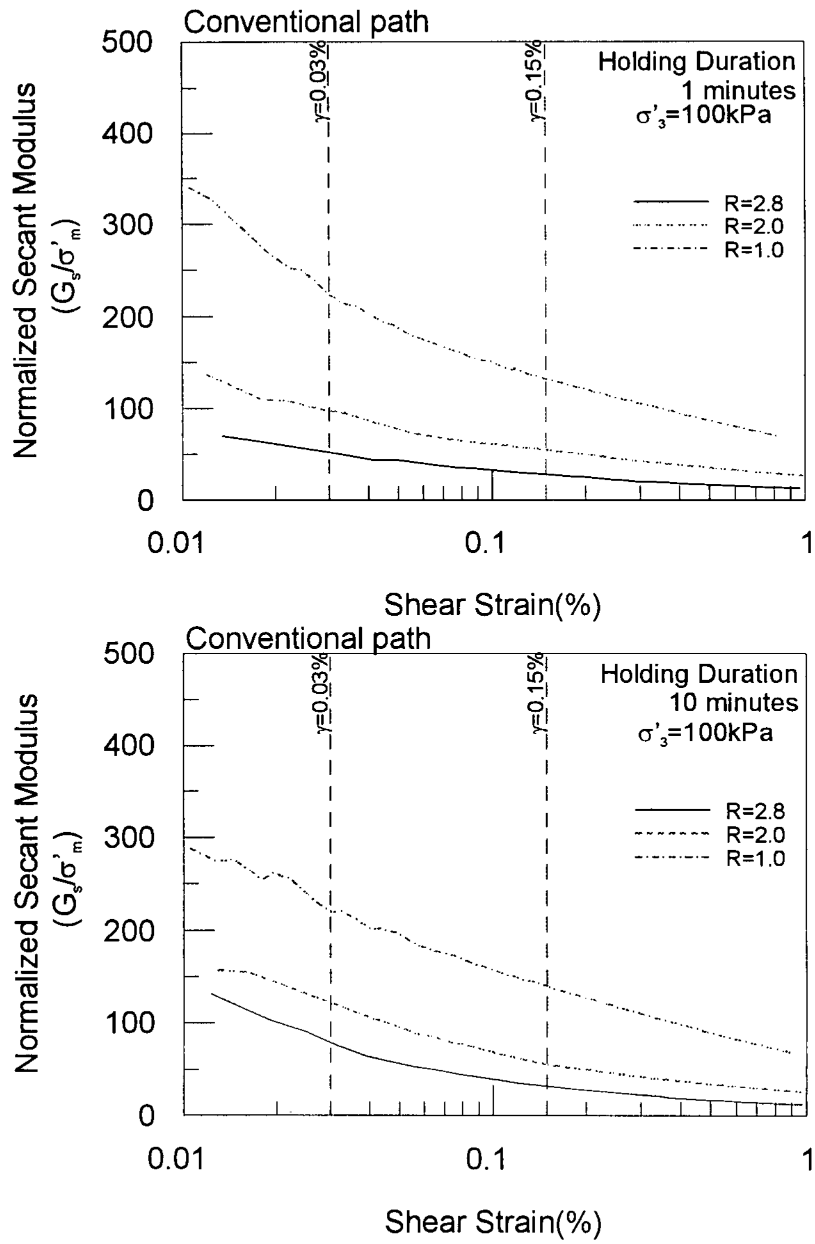

Figure 4.39 Attenuation Curves for Various Stress Ratios for different holding duration (1, 10 mins.)

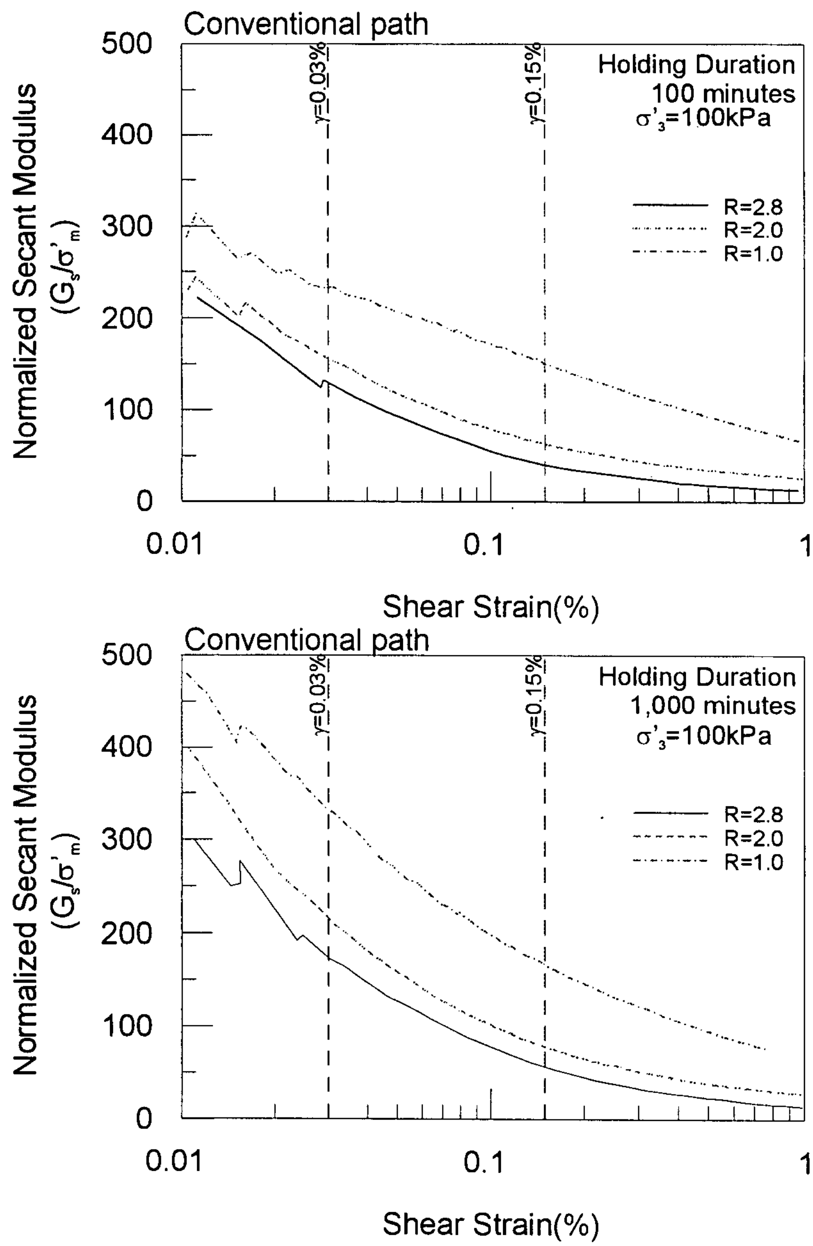

Figure 4.40 Attenuation Curves for Various Stress Ratios for different holding duration (100, 1,000 mins)

the previous figure is now observed on the curve for R=2.0 and especially the curve for R=2.8 is close to the one for R=2.0 in the range of smaller strain. However, the curve for R=1.0 still retains the identical shape as for 10 minutes duration and not much increase in shear modulus is observed. Once the holding duration reaches 1,000 minutes, the curve for R=1.0 also has a significant increase in shear modulus, and its shape becomes similar to other two curves. This effect can be seen clearly on Figure 4.41 and 4.42 in which G has been normalized with the mean normal stress. This shows that the sample becomes stiffer and more brittle for the shorter ageing, if the sample is aged at the higher stress ratios. This may be explained for the fact that the ageing deformation is larger at the higher stress ratios. When the sample is at rest under constant stress ratio, the magnitude of both axial and volumetric creep strains are higher for higher stress ratios. As seen in Figure 4.17, this deformation results in the accumulated strain level at the first application of shear stress being large. When the shear stress is applied, the stress-strain curve is stiff until it rejoins the original line. Until the stress-strain curve reaches the original line, the expected strain development will be very small. This causes an increase in small strain modulus. Ultimately, the attenuation curve for each stress ratio becomes a similar shape when the sample is aged longer.

Figure 4.41 shows the effect of ageing time and stress ratio for the conventional triaxial test.The data have been normalized by mean normal stress according to each stress level. It clearly shows that the magnitude of the shear modulus increases as the ageing period is longer, regardless of the stress ratios. However, the increase rate between R=2.0 and 2.8 seem to be identical whereas the increase in R=1.0 is different in comparison to the others.

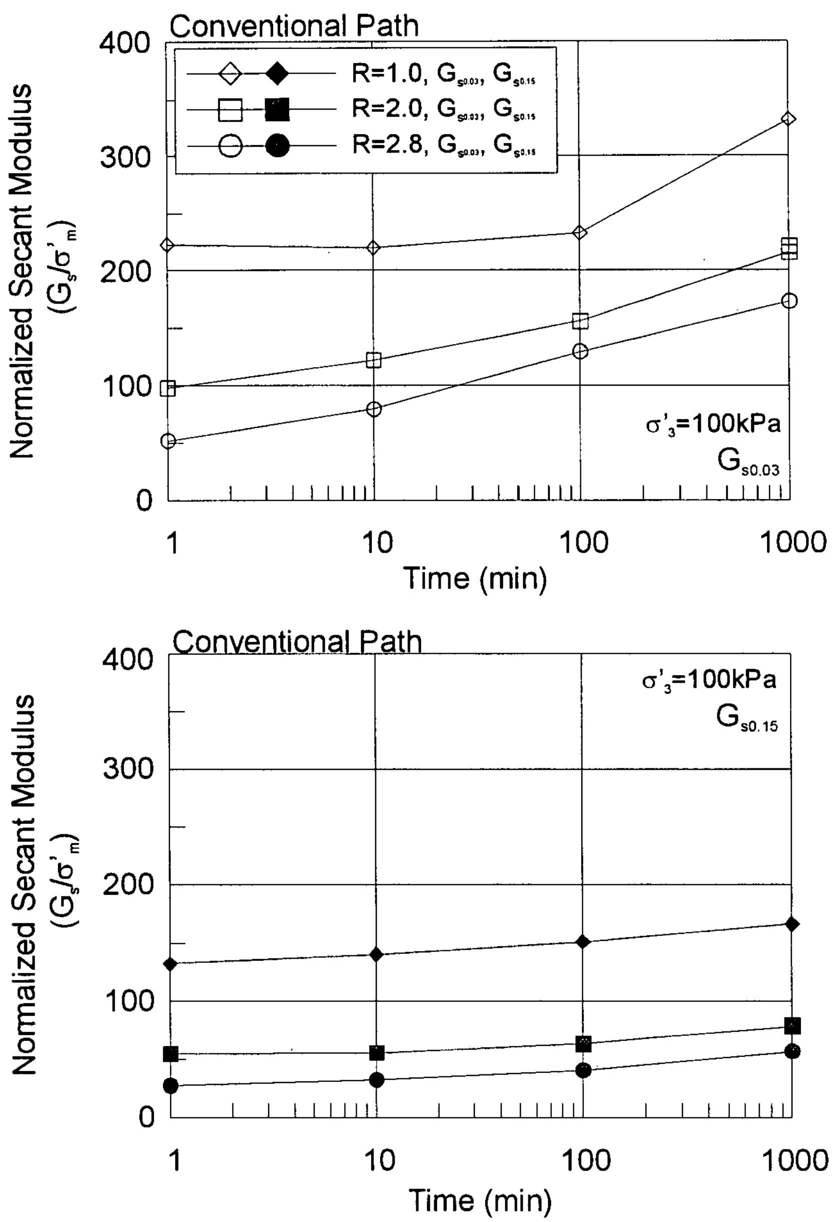

Figure 4.41 Effect of Stress Ratio for Different holding durations

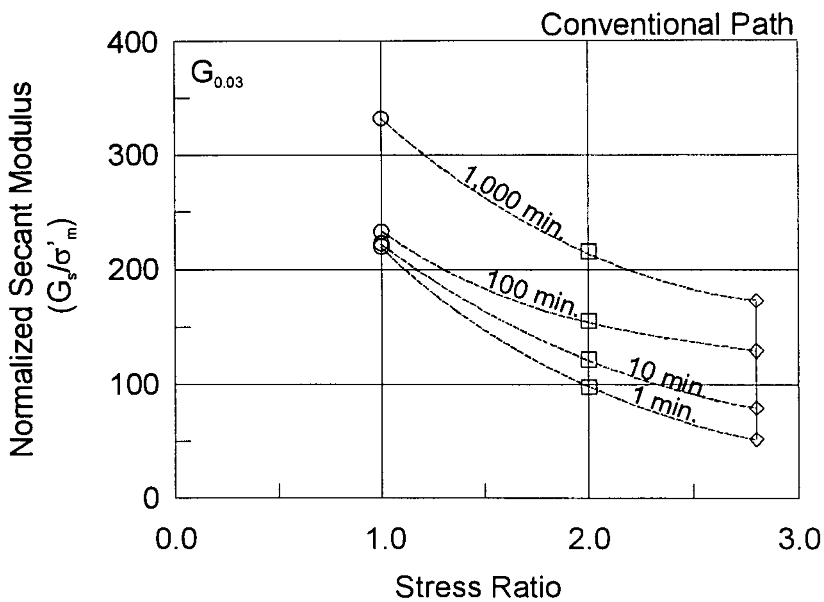

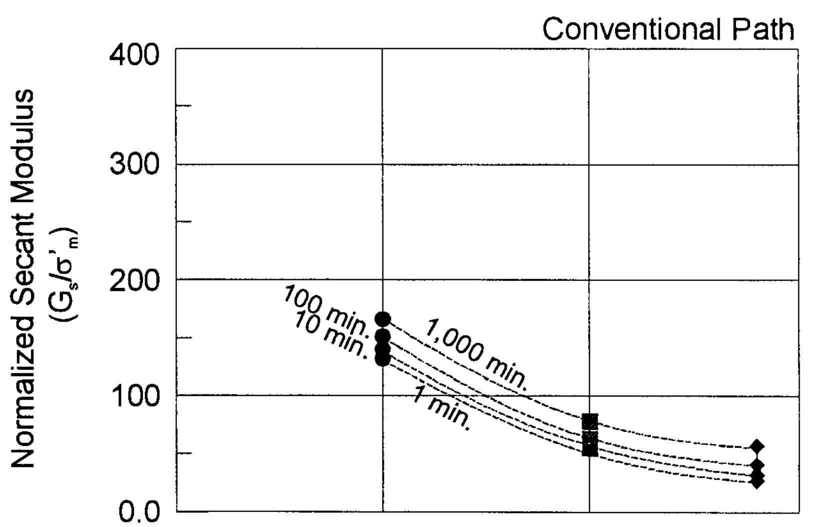

Figure 4.42 Effect of Stress Ratio for Different holding durations

Since there is only one data set presented here for R=1.0, it is hard to define the cause of this phenomenon. The only possible explanation with this test result is the amount of strain generated in the ageing period prior to shear tests. As stated in previous section, the amount of axial strain is very small at R=1.0. Once the ageing period reaches 1,000 minutes, the axial strain is about 0.03% which is the amount generated in 1 minute and 10 minutes at R=2.8 and 2.0 respectively. Regarding the value of 0.03%, further study is required to define this matter, i.e. setting a lateral stress higher than 100kPa and letting axial strain develop more within shorter ageing period. This phenomenon seems to disappear by the time strain reaches to 0.15% shear strain. The increase in $G_{s0.15}$ with time is much less dependent on the logarithm of holding duration.

Figure 4.42 shows the effect of ageing for each stress ratio more clearly. All values are normalized with mean normal stress at each stress level. As previously stated, the short duration make $G_{s0.03}$ increases significantly if the stress ratio is higher. Initial stiffness is smaller at higher stress ratio for no ageing. With ageing, initial stiffness increases by 300% at R=2.8. Only a small time effect is observed on $G_{s0.03}$ under the hydrostatic condition if the holding duration is less than 100 minutes. The modulus increase is not significant until the holding duration reaches 1,000 minutes (ref. Figure 4.35) and it is about 50% increase.

Yu and Richart (1984) conducted a series of tests in order to evaluate the influence of stress ratio on the shear modulus. The shear modulus was measured in the resonant column test and triaxial test. Before each test, a sample was left for 30 minutes at the constant stress state, which they suggested was enough time for sand to reach stable values of dynamic modulus. They observed that as the shearing stress or stress ratio increased, the shear modulus decreased. They noted, however, if the stress ratio is smaller than 2.5-3.0, the effect of shearing stress on shear modulus is less than 10%, and this is considered within the experimental error in evaluating shear modulus. According to Yu and Richart (1984), most previous researchers performed their tests within this range of stress ratios and that is probably why they concluded there was no effect of stress ratio.

From the results presented here, the effect of the stress ratio does exist in the strain range presented here. Shear modulus will decrease as stress ratio gets higher. It is the relationship of the applied stress ratio to the maximum value of stress ratio that governs the

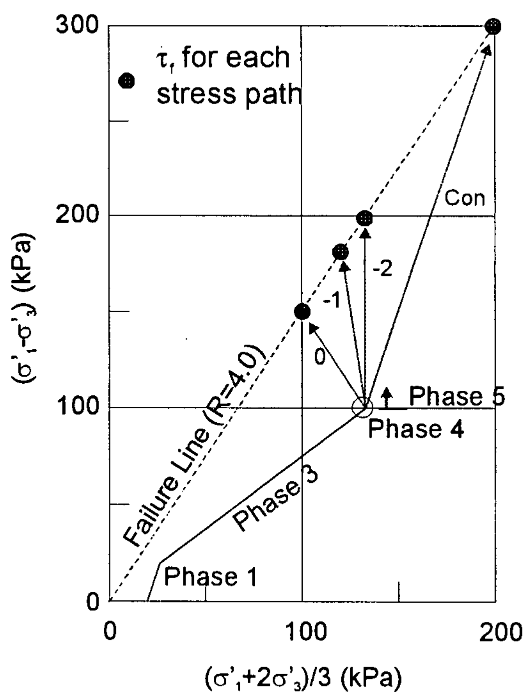

Figure 4.43 Diagram for τ_f estimate

modulus reduction. Increasing the stress ratio decreased the shear modulus, up to a maximum of 20%-30% (Yu and Richart, 1984).

From this series of tests, results for each condition are plotted in the same figure in Figure 4.44. The x-axis is τ normalized by τ_f, which is calculated from the stress state at

R=4.0 which is estimated to be the failure point for the samples as seen in Figure 4.43. The y-axis is the shear moduli normalized by effective mean normal stress with atomospheric pressure, i.e. $(\sigma'_m/Pa)^n$. These attempts are to eliminate the effect of confining stress, stress ratio and applied stress paths. The value "n" is chosen from the test results for three different confining stresses at R=2.8 on the triaxial conventional test (ref. Appendix A26). Shear modulus is higher at lower stress ratios but the effect of the holding duration is more significant at higher stress ratios. The denser sample indicates simply a stiffer response. However, the significant effect of ageing is observed regardless of relative density.

Regarding the effect of confining stresses, as seen in Figure 4.45, higher confining stresses make the relative density of samples denser until reaching the desired stress state, thus samples under lower confining stress have a slightly smaller relative density. These few percentage changes in the relative density may change the magnitude of shear modulus slightly.

In the range of a very small strain (0.01% or less), it is difficult to define the effect on shear modulus of all the different factors such as ageing, magnitude of stress ratios and the direction of applied stress paths. As behaviour, very small strain range is defined to be the range which has approximately linear and the shear modulus, G'_0, is constant (Atkinson and Sallfors, 1991). Within this range, for all practical purposes, the soil exhibits a linear elastic stress-strain response and the Young's modulus, E_0, and shear modulus, G_0, can be regarded as the initial stiffness of the relevant stress-strain curves of a given soil. Both moduli, if properly normalized with respect to the void ratio and effective stresses, result to be equal or similar in magnitude regardless of the type of loading (monotonic or cyclic). (Jamiolkowski,

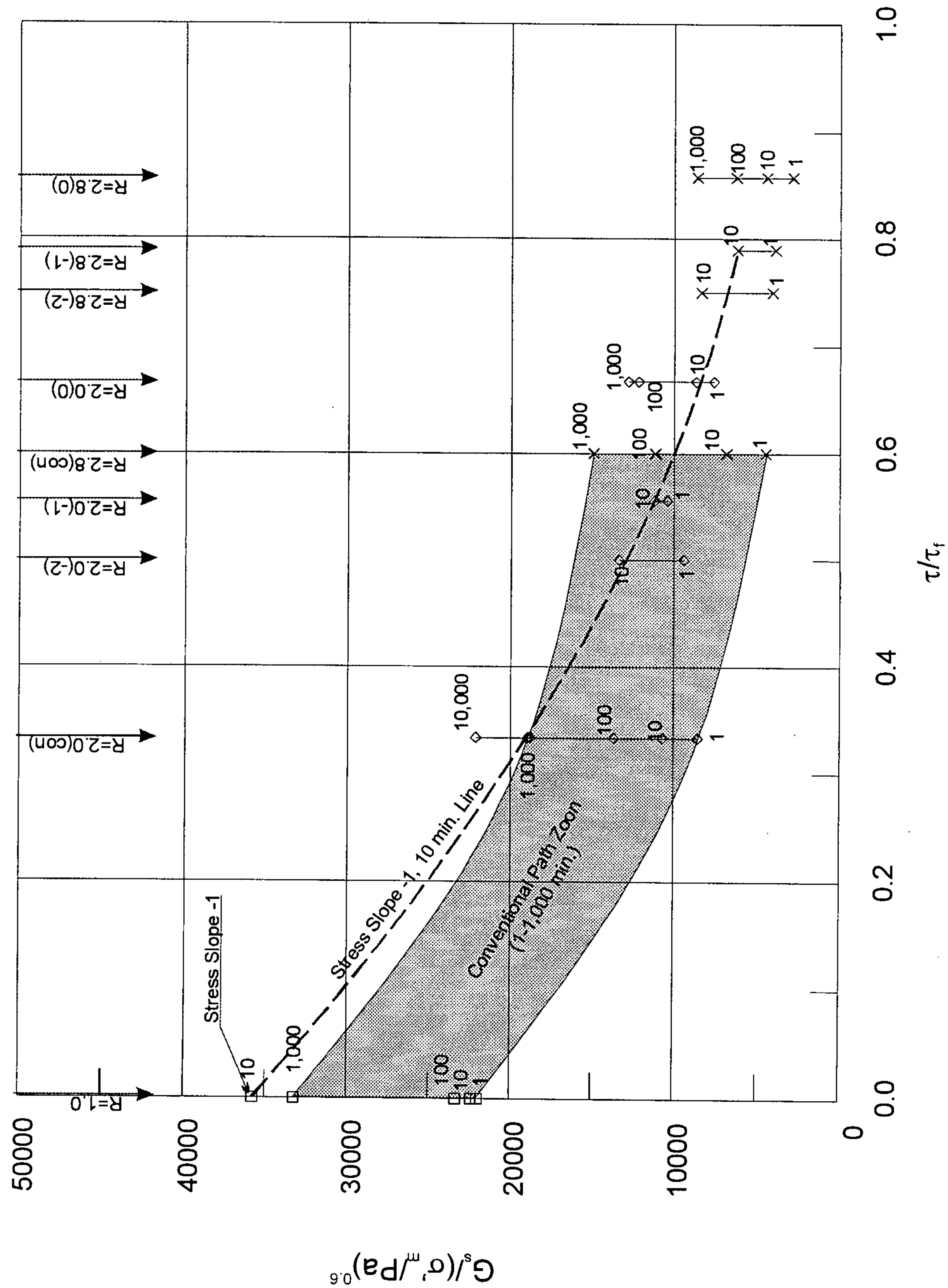

Figure 4.44 Normalized Shear modulus for loose samples

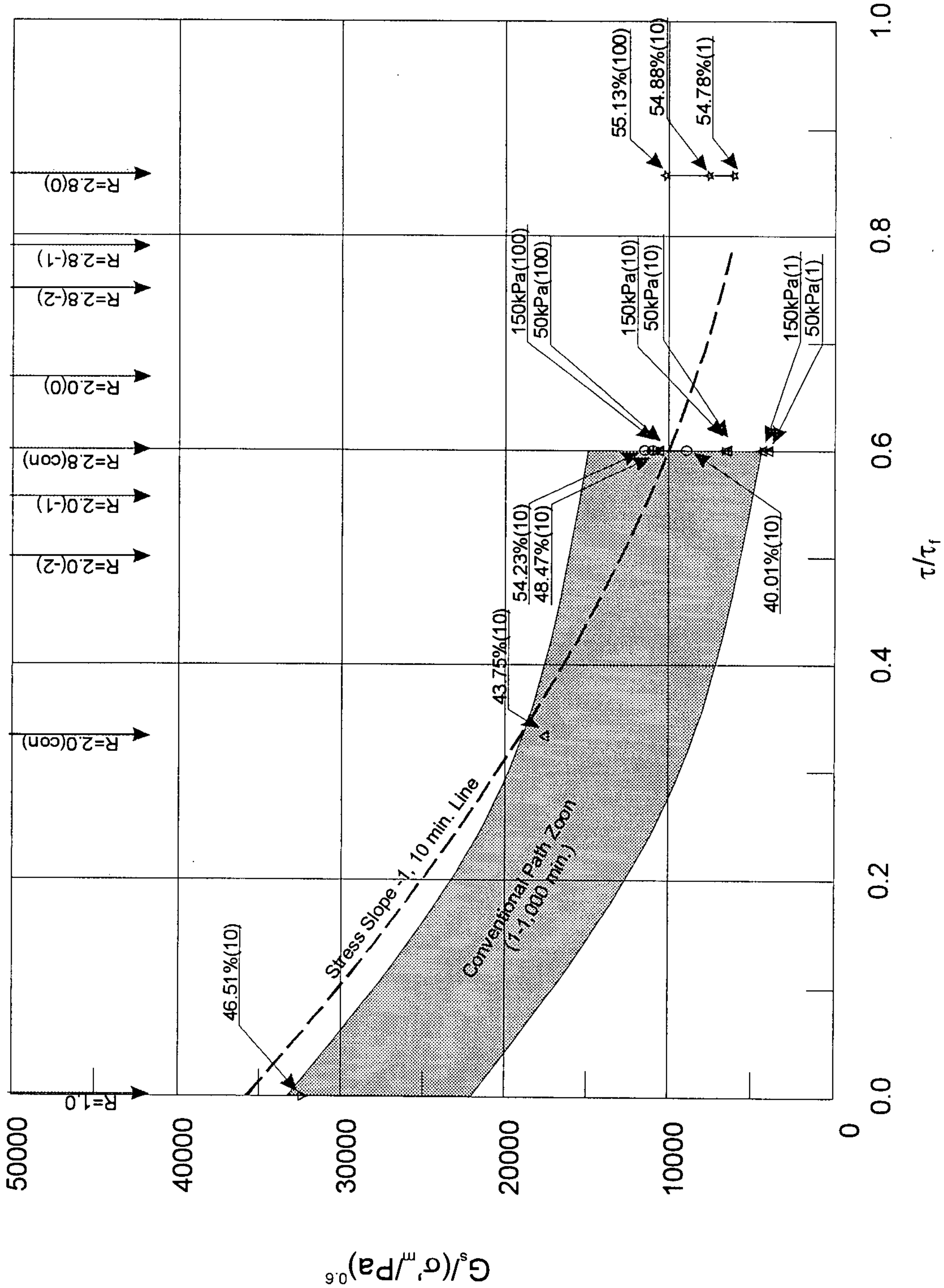

Figure 4.45 Normalized Shear Modulus with various conditions

LoPresti and Froio, 1998). In the same paper, Jamiolkowskie et al (1998) mentioned that both G_0 and E_0 increase with ageing time under constant stresses when subject to drained creep. Jovicic and Coop (1997) found out that a long period of rest before the bender element test to measure small strain stiffness caused the stiffness to increase by up to15% over a period of three days. This increase becomes insignificant as the isotropic confining stress level increase. Anderson and Stokoe (1978) presented the results of bender element tests under isotropic conditions showing a linear increase in shear modulus with logarithm of ageing time after consolidation. It is widely recognized that shear modulus in the very small strain range seems to increase depending on the length of ageing.

As stated before, at the very small strain range, it is widely accepted that higher mean normal stresses result in larger magnitude in shear modulus. Porovic and Jardine (1994) showed that, for isotropic and K_0 consolidated sand specimens, small strain shear modulus G_0 depends on the mean effective consolidation stress. However, Lo Presti (1995) showed that the magnitude of small Young's modulus is controlled only by the magnitude of axial stress. Regardless of which finding is applied, it should be expected that consolidation for constant σ'_3 at higher stress ratios will result in higher magnitude of small strain shear modulus considering the condition we applied in this research. However, the results in this research at a small strain level of γ=0.03% indicates the opposite tendency. For a given ageing period, stiffness is observed to decrease as stress ratios increase. Lo Presti (1995) presented the result of five triaxial tests in the study of the effect of stress ratio on Young's Modulus. All samples had the identical relative density (=55%) and effective vertical stress (=100kaPa) but with different values of the stress ratio, which was K_0 to K=2 (R=2.0 to 0.5). He concluded that Young's Modulus was only affected by the axial stress and was independent of stress ratios. Young's Modulus was determined at the axial strain of 0.005% or less. Beyond this strain range, the large reduction in attenuation curve was observed as the value of K is lower, i.e. higher in R. This may indicate that stiffness of the samples is highly dependent on the position of current stress state relative to failure. Samples reach an unstable state quickly if the current stress ratio during ageing is higher, which results in quick reduction in Young's Modulus.

From the finding in this thesis, only possible explanation for the reverse tendency is made by the reduction rate of shear modulus with strain level. The range focused on this research is small strain range unlike the range focused by other researchers, i.e. a very small strain range (0.01% or less) and it need to be taken into account. Further research is required to clarify this particular issue.

4.6.5 Time Effect for Different Relative Density

A number of tests with different relative densities were performed for the case of 10 minutes holding duration. The influence of void ratio is very strong in the case of reconstituted uniform quartz sand specimens, whilst it is less important for other kind of soils (Lo Presti, 1995). Figure 4.46 shows the magnitude of G_s for samples with different relative densities. The applied stress path is the conventional path with 10minutes holding duration. One denser sample for R=2.0 and 1.0 was tested and these data are plotted in the same figure. It seems that the development in G_s may have a linear relationship against the relative density in the range used in this research at R=2.8 for 10 minutes holding duration. In addition, the effect of the relative density on the shear moduli seems to remain at higher strain. Figure 4.47 shows the attenuation curves for samples with different relative densities. All lines are almost parallel with stiffness increasing with relative density at all strain levels. In the range between shear strain 0.03 and 0.15%, the effect of relative density difference is consistent for a given holding time for all strain levels. Under close observation, the reduction

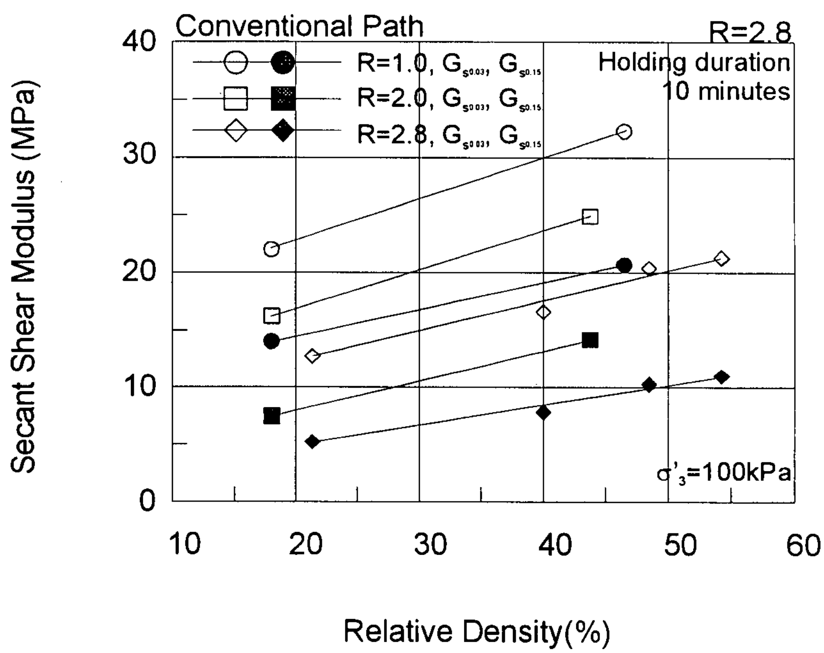

Figure 4.46 Effect of Relative Density on Secant Shear Modulus

seems to be slightly larger in percentage of each $G_{s0.03}$ for looser samples. The effect was observed for all three stress ratios investigated in this study. Similar tests were performed on Ham River Sand sample (Porovic and Jardine, 1994). All samples were prepared by the water pluviation technique. The relative density ranged from 18% to 70%. Changing the void ratio has a significant effect at very small strains (the densest sample showing a 30% higher G_{max} than the loosest) and the effects of density diminished as shear strain increases. The effect of

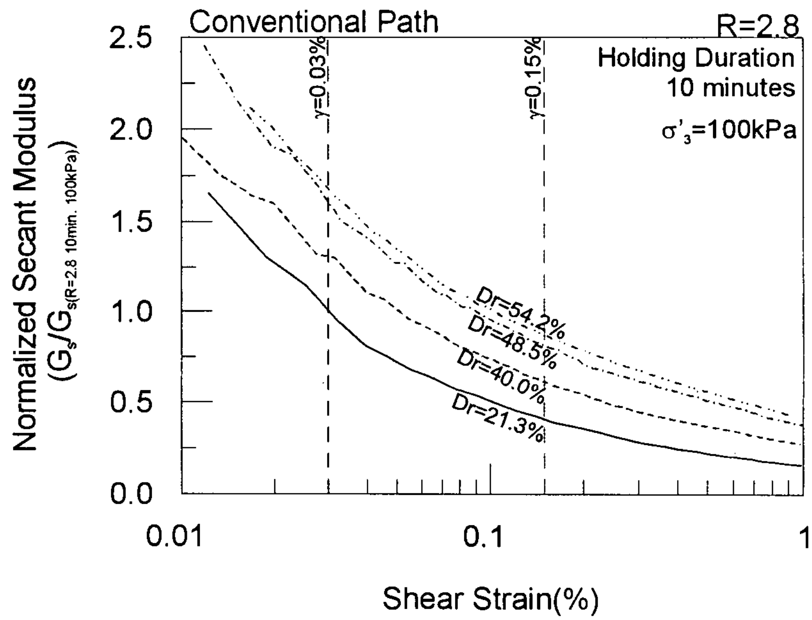

Figure 4.47 Attenuation Curves for Various Relative Densities

density appears more in this study and it still remains in the entire strain range unlike the study for Ham River Sand.

Figure 4.48 shows the variation in shear modulus with time for two different D_r(%) for loading along a stress path with slope of 0. Regardless of the magnitude of relative density, the time effect is still observed. The denser sample has a relative density of about 55%. Both lines are almost parallel. The increase in $G_{s0.03}$ per each logarithm cycle of time is 3.6to 4.0MPa. The increment in $G_{s0.15}$ for each logarithm cycle reduced down to 1.0 to 1.6MPa. From this result, the increase of shear modulus for each logarithm cycle may not be a function of relative density but the base value is.

As previously stated, dilative volumetric deformation is observed on paths accompanied with reduction in the confining stress. This trend is also observed in denser samples.

Figure 4.49 shows a comparison of volumetric strain observed in tests on different

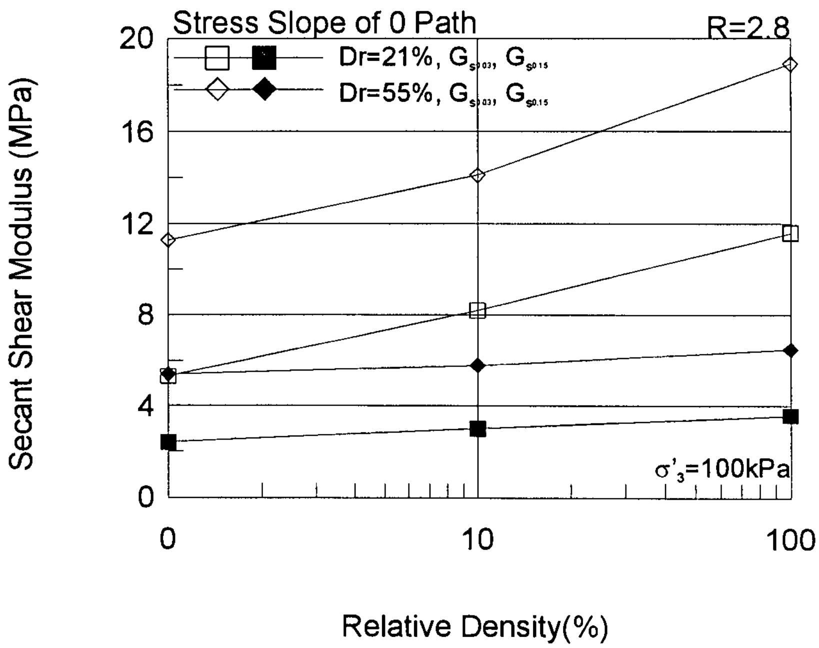

Figure 4.48 Secant Shear Modulus Development with Two Different Relative Densities

relative densities on a constant σ'_1 path at R=2.8. The relative densities for loose samples and medium dense samples were about 20 to 24% and about 54 to 55 %, respectively. In this series of tests, four stress paths were applied, i.e. the triaxial conventional, constant p', constant $1/2(\sigma'_1+\sigma'_3)$ and constant σ'_1 paths. In the case of a loose sample, the initial dilation was not recognized in the triaxial conventional path on any levels of stress ratios. The small dilation was observed in constant p' path (0.002%) and as the stress path was rotated further anti-clockwise, this phenomenon became significant as shown in the figure. In this figure, the medium dense sample starts dilating at the beginning of shear stress application, and the ageing does not seem to have a huge effect on the manner of volumetric response. However, a longer ageing period creates a significant difference in the manner of volumetric strain in loose samples. When the ageing is 10 minutes or less, the dilation is still small and samples start contraction in volume by ε_a=0.2%. For samples aged for 100 minutes or longer, dilation

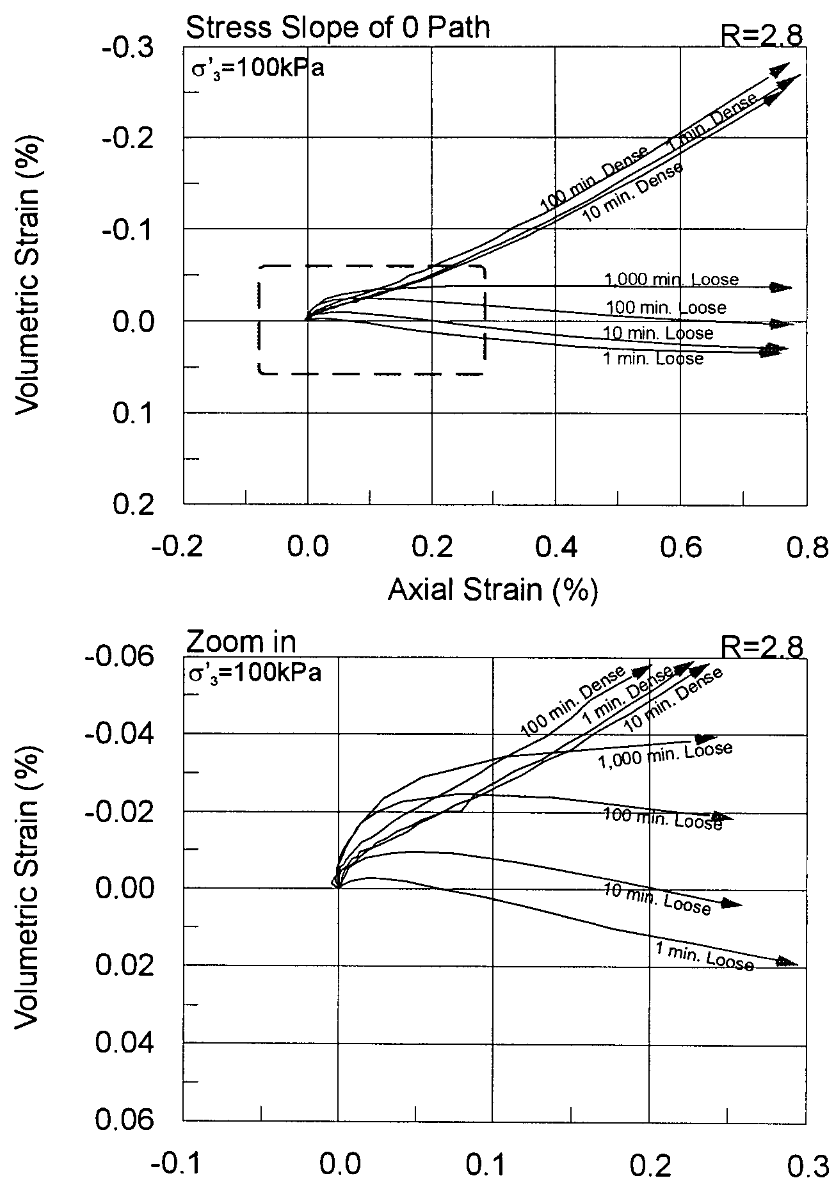

Figure 4.49 Initial Dilative Volumetric Strain for Stress-Slope of 0 path, R=2.8

in the small strain range actually develop more than one of denser samples and it does not contract, if at all, until large axial strain is generated, although it slows down at ε_a=0.1%. This dilation may be explained with the relationship between stress ratio and mean normal

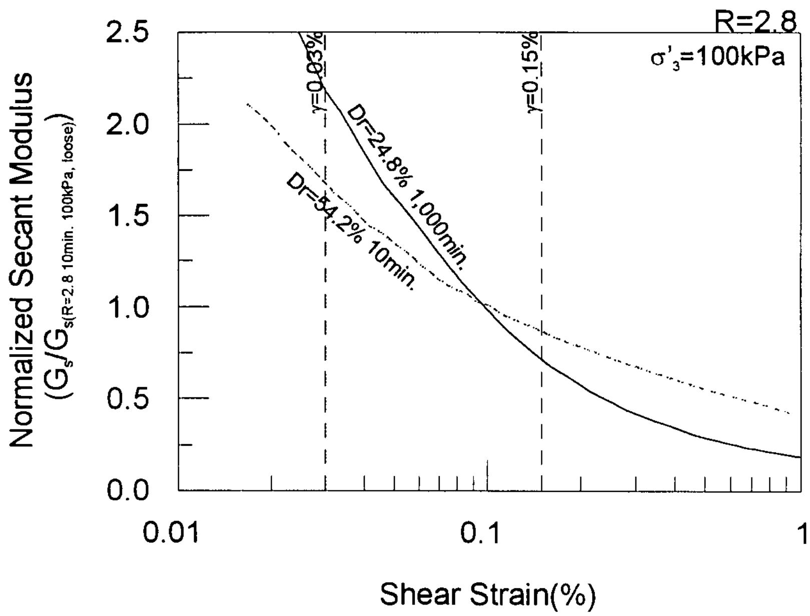

Figure 4.50 Comparison Between the Effect of Time and of the Relative Density (Triaxial Conventional Path)

stress. Both stress ratio and mean normal stress increases on the triaxial conventional path but not in other stress paths. Decreased mean normal stress may create the initial dilation in the small strain range, which dominates the volumetric strain behaviour. But an increased stress ratio quickly causes the contractive response. In addition, during ageing in Phase 4, the sand particles settle into more stable positions for longer durations. When viewed in q-p stress space, the zone of small strain deformation expands. Once the shearing phase is started, all stress paths, except constant or the conventional path, have reduction in mean normal stress which cause the rebound of particles structure. This may cause significant dilation in loose samples for longer duration. As for the time effect in denser samples, the samples are stiffer and the effect of ageing on the particle structure and G_0 is less, therefore less rebound occurs, and only small difference is observed between samples with different ageing duration.

Figure 4.50 shows attenuation curves for a denser sample with 10 minutes duration and a loose sample with 1,000 minutes duration. The relative density is one of the main factors influencing the magnitude of G_s. However, the loose sample with longer holding duration actually shows a stiffer response than one for a dense sample with shorter holding duration. From this figure, the holding duration has more effect on the magnitude of G_s than relative density in the small strain range. Beyond 0.1% strain, the denser sample is stiffer.

4.6.6 Shear Modulus for Geological Scale Ageing

Since the sample with 10,000minutes duration at R=2.0 has a technical difficulty with the apparatus used for this series of tests, it is still not defined whether Young's modulus and shear modulus keeps increasing with time. Figure 4.51 shows the calculated shear modulus against the logarithm of time exceeding 1,000minutes based on projecting the results at the same rate increase per logarithmic cycle. The increment of $G_{s0.03}$ is about 6MPa and for $G_{s0.15}$ is about 1.4MPa/log cycle

The resonant column tests performed by Anderson and Stokoe (1978) shows about 1% increase in shear modulus at 0.001% shear strain. This value is calculated relative to the shear modulus at 1,000minutes as a base value. All tests are performed after the hydrostatic consolidation. Figure 4.52 shows the result from their study. The shear modulus increases

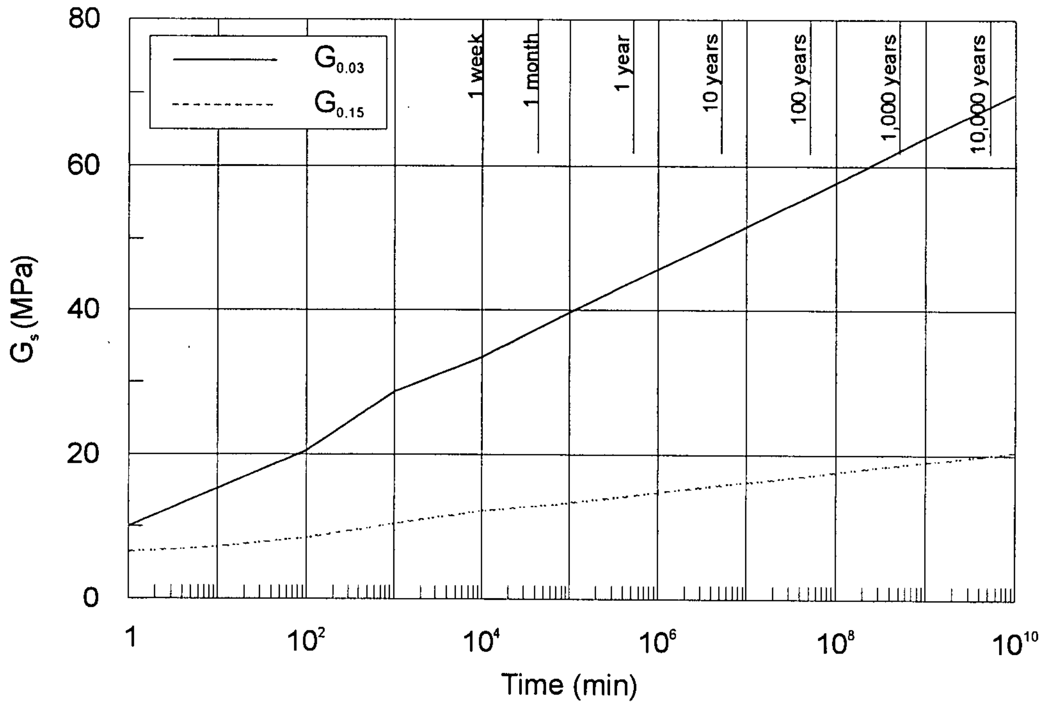

Figure 4.51 Secant Shear Modulus for Longer Duration, R=2.8

linearly against the logarithm of time. From Figure 4.51, the increment in shear modulus for each logarithmic cycle of time is about 6MPa. If shear modulus at 1,000minutes is taken as a base value, which is about 28MPa, the increment is about 20% (ref. Figure 4.29). Regarding

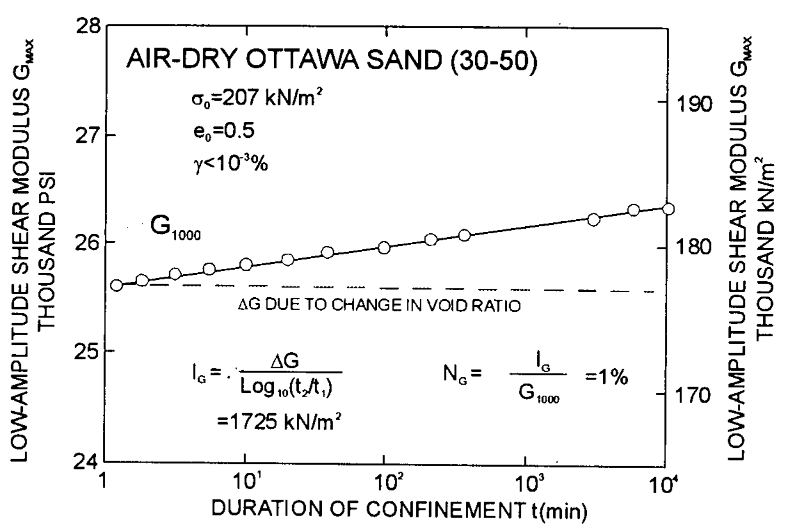

Figure 4.52 Effect of Time from Resonant Column Test (Anderson and Stokoe, 1978)

the stress ratio difference at 1,000minutes duration, Figure 4.41 shows that the shear modulus for every stress ratio has similar values and it may increase similarly after 1,000minutes. As stated before, the tests with 10,000minutes have not succeeded yet with the apparatus in use for these tests. From the results of other researchers, it is possible to assume that it will increase continuously as time increases.

4.7 Total strain for Creep and Shear Phase

4.7.1 Axial and Volumetric strain behaviour

In previous sections, the strain that would have resulted from creep deformation is removed from the stress-strain curve during shear. However, it may give better insight if creep deformation and stress-strain response are presented together. In this section, the strain used is a value before correction is applied to see the overall relation between creep deformation and stress-strain response.

Figure 4.53 shows the stress-strain curves for R=1.0, 2.0 and 2.8. In this time, both stress and strains are plotted using total values. All samples in this figure have 10 minutes holding duration in the conventional path. Stress-strain curves seem to merge into one common line as further load applications take place. The initial condition for each sample is identical after the B value was measured. Regarding the volumetric strain, since the time required to reach a desired stress ratio is different depending on the stress path, volumetric strain develops at a different rate depending on each stress ratio. For example, it takes about 33 minutes for the sample consolidated isotropically to reach R=2.0. On the contrary, it takes

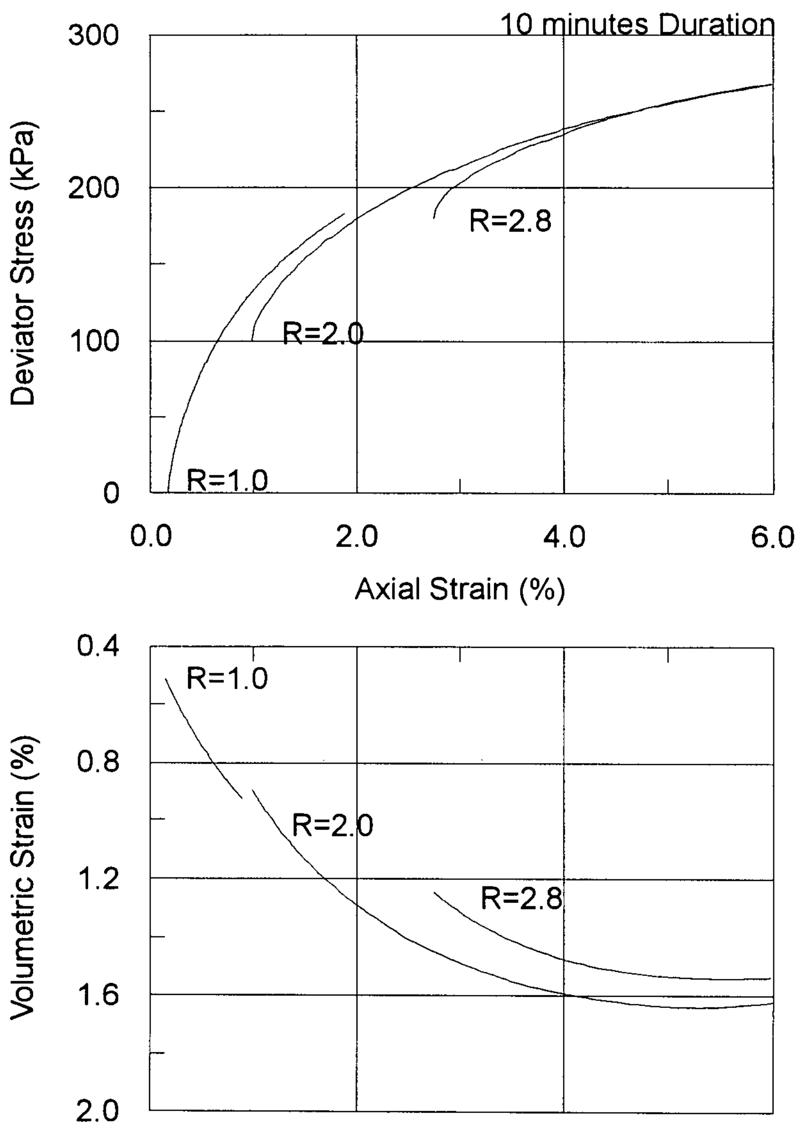

Figure 4.53 Strain Development at Each Stress Ratio.

only 11 minutes to reach R=2.0 following the R=2.0 path. This time difference between both paths will generate a difference in volume changes. Also, this volume change may be created by the stress history differences. At this point, it is impossible to separate both factors based on these results.

Figure 4.54 show the results for R=2.0 on the conventional path with various holding durations. This figure is plotted from the beginning of Phase 4 setting strain to zero at the beginning. For the longer duration ageing, the initial response during shear is stiffer. Depending on the amount of creep deformation, the starting position of the stress-strain curve is shifted to the right in the figure. Because of the tendency to go back to the original

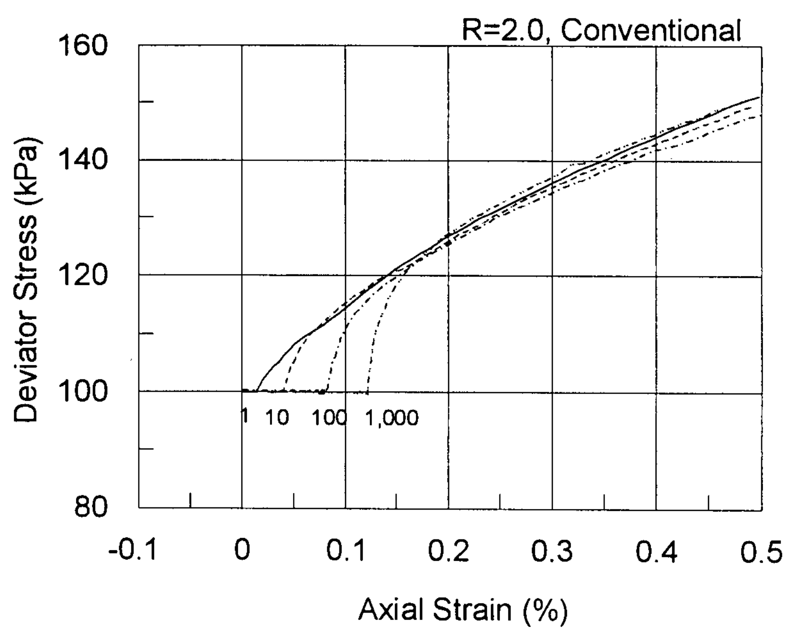

Figure 4.54 Strain Development for Phase 4 and 5 with Various Durations

line, the stress-strain curve climbs up faster which results in a stiffer response in the small strain range. The additional deviator stress required for a stress-strain curve to reach the original line is about 20kPa in the case of the conventional path. The value is also about

20kPa to go back to the original line on the conventional path in other stress ratios. If the stress path, however, is not the conventional path, this value seems to change depending on its stress ratio and relative density. For example, it only took 10kPa to reach the original line for the samples with the stress-slope of 0 at R=2.8. It may be possible to say that the required additional loading in order to eliminate the time effect is about 20kPa for the conventional path under the confining stress of 100kPa regardless of the magnitude of stress ratios. This indicates that the stiffness increased by time effect only exists when the additional loading is less then a certain threshold value.

Since this series of tests was performed under stress control, the relationship between the volume change and the deviator stress are plotted. Figures 4.55 and 4.56 show the relationship between the deviator stress increase, which is constant, and volumetric strain which is a result of load application. Figure 4.55 shows the volumetric strain on the

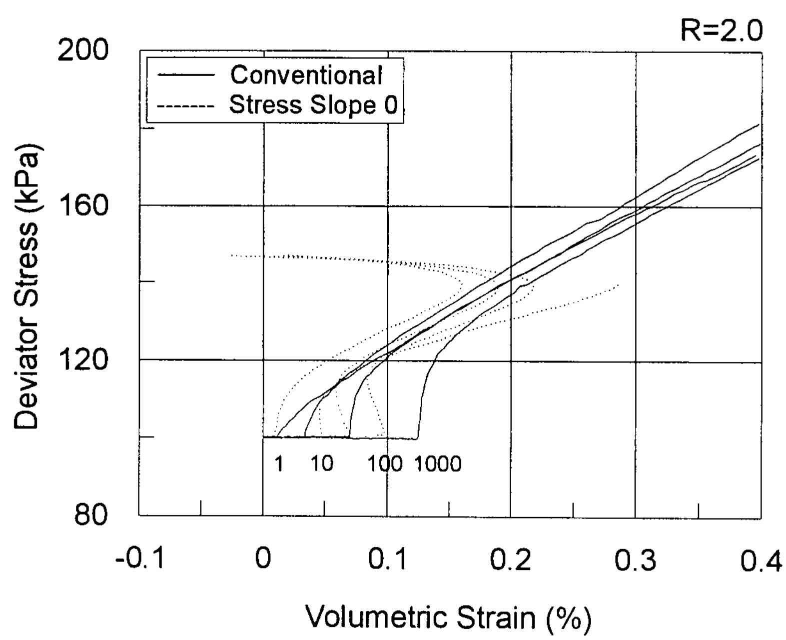

Figure 4.55 Volumetric Strain against Deviator Stress on Two different Stress Paths for Phase 4 and 5

conventional and stress-slope of 0 path for R=2.0. Since there is a difference in the relative density for each sample, it is not quite following the one clear line. However, the trend is recognizable. When the holding duration is more than 10 minutes, the volumetric strain

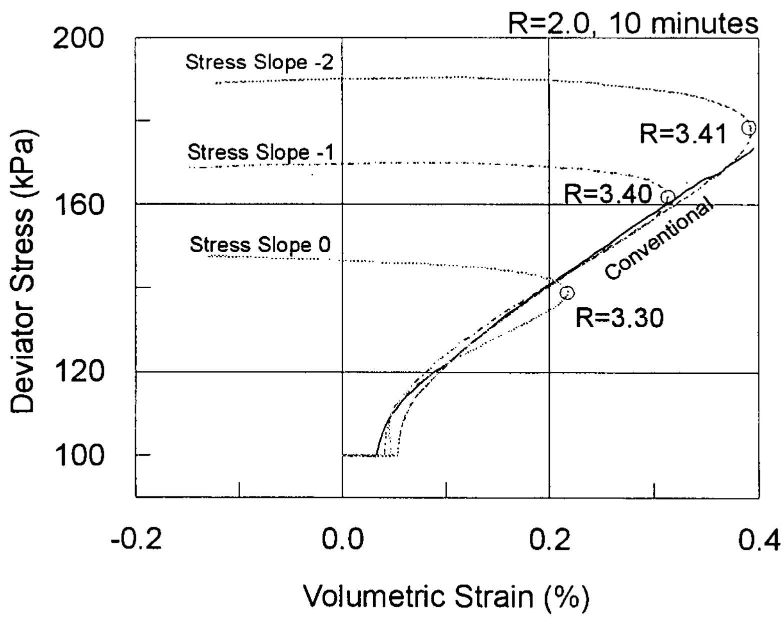

Figure 4.56 Volumetric Strain against Deviator Stress on Various Stress Paths for Phase 4 and 5

development become dilative initially. But this dilation seems to cease when the volumetric strain reaches to the line of the conventional path. After reaching the strain path for the sample on the conventional path, contraction begins and the volumetric strain develops with following the same path until the stress ratio reaches to certain value for dilation. This tendency becomes more obvious when the stress ratio is a higher value. Figure 4.56 shows also the volumetric strain for various applied stress paths with 10 minutes holding duration. Regardless of the applied stress path, the volumetric strain develops on the unique path. Since these figures are plotted in terms of σ_d, the dilation point for each sample seems to be different. However, all dilation happens around R=3.3 to 3.4 regardless of the relative density. In the case of R=2.0 and 2.8, once the additional stress is applied, the volumetric strain seems to go back to a unique line if samples have the same relative density. Once it reaches to the original line, regardless of the applied stress path, volumetric strain follows the original line until it reaches to the dilation point. This may indicate that the development of volumetric strain up to phase transformation point is dominated only by applied deviator stress.

However, volumetric strain has different behavior at R=1.0. There is no indication of coming back to the original line. This phenomenon is also observed in the sample for R=2.0 with 1 minute holding duration. The volumetric strain develops beyond that for the conventional path, which is the same in the sample for 10minutes duration at R=1.0. The difference in the relative density may be reason, since the volumetric strain is very sensitive to the relative density. There is about 3 to 4% difference in these particular samples for two different applied stress paths. This phenomenon becomes more obvious for the lower stress ratio. At this point, this is inconclusive since there is only one sample tested on the different applied stress path at R=1.0.

After about 20kPa of additional stress, the time effect seems to be disappearing. The axial strain development at σ_d of 20kPa is about less than 0.2% which indicates the improvement in response by the time effect is only recognized in the small strain range.

Summary

The major findings of the laboratory testing program may be summarized as follows:

- Stiffness increases with time under ageing at constant stress conditions regardless of the magnitude of the stress ratio, applied stress paths and the relative density of sample.
- The rate of increase in stiffness with time is greater at higher stress ratios.
- Stiffness increase with time is a greater percentage of the initial value in looser samples, but the rate of increase is constant regardless of the magnitude of the relative density.
- Ageing reduces the amount of volumetric contraction occurring during the initial stages of shearing along stress paths in which stress ratio increases.
- Initial expansion occurs when shearing occurs along stress paths with σ'_3 reduction, and the amount of expansion is greater with longer ageing.
- The magnitude of stiffness increase with time is greater on the conventional path and it becomes decrease as stress path rotates in the anti-clockwise direction at R=2.0 and 2.8.
- The time effect on stiffness is only apparent in the early stages of shearing. It disappears after a small increments in shear stress (about 20kPa) or strain (about 0.05%).

CHAPTER 5

Conclusion

The effect of ageing on the stress-strain behaviour of Fraser River Sand was studied under triaxial conditions. Reconstituted specimens were tested under three different consolidation stress ratios. Shear tests were performed along four different stress paths to study the effect of stress path on the stress-strain response and primarily stiffness of the aged samples. Most samples were prepared in a loose state but some medium dense samples were tested. The effects of confining stress were also studied. The purpose of the study was to separate the effect of time from other effects.

Samples were consolidated along paths of constant stress ratio to the desired stress state, and were allowed to age at constant stress ratio. Samples continued to creep at a constant ratio of $\varepsilon_v/\varepsilon_a$ independent of relative density, confining stress and time. The ratio $\varepsilon_v/\varepsilon_a$ depends on stress ratio alone and decreased as stress ratio increased.

After the shear stress is applied, the creep deformation most likely continues to take place, which will create additional strain development in both axial and volumetric strain. When samples were not aged long enough, this continuous creep deformation will be significant during the shear test. From this test, the major additional strain is recognized in samples with the holding duration of 10 minutes or less. If samples are not aged long enough, the stress-strain response may become softer because of the continuous creep deformation.

The study concentrated on secant shear modulus at two levels of shear strain, 0.03% and 0.15%, i.e. $G_{s0.03}$, $G_{s0.15}$. For the loose sand, the shear stiffness increases at a constant stress ratio for ageing time up to 1,000 minutes. The increase in stiffness is greater for $G_{s0.03}$ than for $G_{s0.15}$, i.e. ageing effects appear to be greater at smaller strain. The percentage increase in secant modulus dur to ageing becomes much greater as the consolidation stress ratio increases. The increase is approximately linear against the logarithm of time. The absolute value of the increase per log cycle appears to be relatively constant regardless of relative density but, as the base value of G increases with D_r, the percentage increase is less at higher D_r.

At a given stress ratio, the stiffness is related to the current stress state relative to the failure state. When G_s is normalized to remove the effect of increased mean normal stress, G_s reduces with increasing stress ratio independent of ageing time.

Poisson's Ratio depends on the magnitude of stress ratio. There is a general idea that Poisson's Ratio is assumed to be 0.1 to 0.2. From the result presented here, this may be only applicable at isotropically consolidated (R=1.0) samples. If the stress ratio is higher, Poisson's Ratio is expected be higher.

Increasing ageing time resulted in the sample become more dilative during the initial stages of shearing. This dilative phenomenon will become obvious as the applied stress path becomes closer to horizontal to the direction with σ'_3 decrease.

In addition, it was shown that the substantially increased stiffness was only effective for small increments of shear stress. For the conventional path, the stiffness effect disappeared after a shear stress increase of only about 20kPa for consolidation stress ratio of 2.0 and 2.8.

The above findings suggest that it is extremely important to control the ageing time of reconstituted samples used in studies of small strain behaviours of sands. In addition, great care is required when relating properties measured in the laboratory or in reconstituted chamber specimens to field condition.

Suggestion for further research

The effect of ageing time for Fraser River Sand was studied in this thesis. In future research, it is recommended that the following factors should be considered to clarify the changes in stress-strain response caused by ageing.

- Behaviour in the very small strain range (<0.01%) needs study. The transducers used in this research could not reliably measure smaller axial and volumetric strain due to their resolutions. Use of transducers with higher resolution may be appropriate.
- The use of Bender elements is one option to measure very small strain behaviour and it may give interesting insight into the relationship between shear modulus and time effect.
- Tests should be run with ageing under additional values of applied stress ratio.

This will clarify the effect of stress ratio during ageing on stiffness, which seems to be reversed *(what do you mean "reversed"?)* around the K_0 condition.

- The longer duration for stress slope of -2 and -1 should be completed for further understanding the effect of stress path. In addition, samples should be aged for longer durations, such as 10,000 minutes or longer, under each condition, to investigate whether the observed rate of increase continues. This will require stringent control of test conditions.
- Tests under other stress paths, such as directions with the stress ratio decrease and confining stress increase, will help to understand how the ageing effect expands the envelope of elevated stiffness in stress-space.
- Deformation at the ageing period under the different lateral pressure could give the further understanding relationship between ageing deformation and ageing effect on stiffness. This attempt also gives how long the ageing effect last under higher lateral pressures.
- Between the stress applications under the shear test, additional records are useful during 15 seconds waiting. This may show the behaviour of sand between the stress applications in detail.
- Tests in this thesis were carried out with constant lateral stress and variable stress ratio. Shear tests under the constant vertical stress at the different stress ratios may provide further insight into the effect of stress ratios.

Reference

1. Anderson, D. G. and Stokoe, K. H, (1978), "Shear Modulus: A Time-Dependent Soil Property", Dynamic Geotechinal Testing, ASTM STP654, American Society for Testing and Materials, pp.66-90.

2. Atkinson, J. H. and Sallfors, G., (1991), "Experimental determination of stress-strain-time characteristics in laboratory and in situ tests", Proc. 10th European Conf. On SMFE, Florence, Italy, Vol.3, pp.915-956, Balkema, Rotterdam

3. Atkinson, J. H., Richardson, D. and Stallebrass, S. E., (1990), "Effect of recent stress history on the stiffness of overconsolidated soil", Geotechnique, 40, No.4, pp.531-540

4. Berardi, R., Jamiolkowski, M. and Lancellotta, R.., (1991), "Settlement of shallow foundations in sands: selection of stiffness on the basis of penetration resistance", Proc. ASCE Geotech. Engng Congress, Geotechnical Special Pub. No.27, Vol.1, pp.185-200, Boulder, Colorado

5. Bishop, A. W. and Henkel, D. J., (1957), "The measurement of soil properties in the triaxial test", EDWARD ARNOLD LTD., London

6. Burland, J. B., (1989), "Ninth Laurits Bjerrum Memorial Lecture: "Small is Beatiful" - the stiffness of soils at small strains", Canadian Geotechnical Journal. 26, pp.499-516.

7. Charlie, W. A, (1992), "Time-Dependent Cone Penetration Resistance due to Blasting", Journal of Geotechical Engineering, Vol.118, No.8, pp.1200-1215

8. Daramola, O., (1980), "Effect of consolidation age on stiffness of sand,", Geotechnique, 30(2), pp.213-216

9. Fahey, M., (1998), "Deformation and in situ stress measurement", Geotechnical Site Characterization, Robertson & Mayne (eds), pp.49-68

10. Garrison, R. E., Luternauer, J. L. Grill, E. V., Macdonald, R. D. and Murray, J. W., (1969), "Early diagenetic Cementation of Recent Sands, Fraser River Delt, British Columbia", Sedimentology, Vol.12,, pp.27-46

11. Howie, J. A., (1990), "Factors Affecting The Analysis and Interpretation of Full-Displacement Pressuremeter Tests", Ph-D Thesis,"Dept of Civil Engineering, The University of British Columbia

12. Jamiolkowski, M., Lo Presti, D. C. F and Froio, F, (1998), "Design parameters of granular soils from in situ tests", Geotechnical Hazard, Maric, Lisac & Szavits-Nossan (eds), pp.65-94Balkema, Rotterdam

13. Jardine, R. J., (1992), "Some Observations of the Kinematic Nature of Soil Stiffness", SOILS AND FOUNDATION Vol.32 No.2, pp.111-124, Japan

14. Jovicic, V. and Coop, M. R., (1997), "Stiffness of coarse-grained soils at small strains", Geotechnique 47, No.3, pp.545-561

15. Kuerbis, R. H. and Vaid , Y. P., (1990), "Corrections for membrane strength in the triaxial test."Geotechnical Testing Journal, Vol.13, No.4, pp.361-369

16. Lade, P and C-T. Liu, (1998), "Experimental Study of drained creep behaviour of sand.", Journal of Geotechnical Engineering., ASCE 124(8), pp.912-920.

17. Lambe, T. W. and Whitman, R. V, (1968), Soil Mechanics, SI Version, John Wiley and Sons, Inc

18. Lo Presti, D. C. F., (1995), "General report: Measurement of shear deformation of geomaterials in the laboratory", Pre-failure Deformation of

Geomaterials, Shibuya, Mitachi & Miura (eds), pp.1067-1088, Balkema, Rotterdam

19. Mejia, C. A., Vaid, Y. P., and Negussey, D., "Time Dependent Behaviour of Sand"

20. Mesri, G. and Feng, T. W., (1990), "Postdensification penetration resistance of cleansands.", Journal of Geotechnical Engineering., ASCE 116(7), pp.1095-1115

21. Mesri, G. and Feng, T. W., (1990), "Postdensification penetration resistance of clean sands.", Journal of Geotechnical Engineering., ASCE 116(7), pp.1095-1115

22. Michell, J. K., (1976), Foundations of Soil Behavior, John Wiley and Sons, Inc, , New York, New York City

23. Michell, J. K. and Solymar, Z. V., (1984), "Time-dependent strength gain in freshly deposited or densified sand.", Journal of Geotechnical Engineering., ASCE 110(11), pp.1559-1576.

24. Murashev, A. K., (1997), "Effect of age-strengthening on initial stiffnesses

and settlements of soils", Theme Lecture, Proc. 14th Int. Conf. SMFE, Hamburg, Germany, Vol 1, pp.167-173.

25. Negussey, D., (1984), "An experimental study of the small strian response of sand., Ph-D Thesis", Dept of Civil Engineering, The University of British Columbia

26. Nutt, N. R. F. and Houlsby, G. T., (1995), "Time dependent behaviour of sand from pressuremeter tests", The Pressuremeter and its New Avenues, Ballivy (ed.), pp.95-100

27. Porovic,E and Jardine, R. J., (1994), "Some observations on the static and dynamic shear stiffness of Ham River sand", Pre-failure Deformation of Geomaterials, Shibuya, Mitachi & Miura (eds), pp.25-30, Balkema, Rotterdam

28. Schmertmann, J. H., (1991), "The mechanical aging of soils.", The Twenty-Fifth Karl Terzaghi Lecture", Journal of Geotechnical Engineering., 117(9), pp.1288-1330

29. Schmertmann.J.H, (1981), "General Time-Related Soil Friction Increase Phenomenon"ASTM STP 740, pp.456-484, Philadelphia, Pa

30. Tatsuoka,F., Santucci de Magistris,F., Hayano,K., Momoya,Y. and Koseki,J. (1998), "Some new aspects of time effects on the stress-strain behaviour of stiff geomaterials", Keynote Lecture, The Geotechnics of Hard Soils and Soft Rocks, Proc. of Second Int. Conf. on Hard Soils and Soft Rocks, Napoli (Evamgelista and Picarelli eds.), Balkema, Vol.2.

31. Vaid, Y. P. and Negussey, D., (1984), "A critical assessment of membrane penetration in the triaxial test.", Geotechnical Testing Journal, Vol.7, No.2, pp.70-76

32. Vaid, Y. P. and Sivathayalan, S, (1999), "Fundamental factors affecting liquifaction susceptility of sands", Physics and Mechanics of Soil Liquifaction, Lada & Yamamuro (eds)Balkema, Rotterdam

33. Whitman, R. V., Millar, E. T., and Moore, P. J., (1964), "Yielding and locking of confined sand."J. Soil Mech. And Found. Eng. Div., 90(4), pp.57-84

34. Yu, Peiji and Richart, F. E. Jr, (1984), "Stress Ratio Effects on Shear Modulus of Dry Sands"Journal of Geotechnical Engineering, Vol. 110 No.3, pp.331-345

Appendix

Loose Samples

σ'₃	Stress Ratio	Stress Slope	Holding Duraiton	Phase 1 e	Phase 1 Dr	Phase3 e	Phase3 Dr	Phase 4 e	Phase 4 Dr	Phase 5 e	Phase 5 Dr
100	2.8	Con	1	0.933	15.37%	0.929	16.56%	0.912	21.28%	0.912	21.35%
			10	0.936	14.66%	0.931	15.90%	0.913	21.05%	0.912	21.33%
			100	0.939	13.72%	0.935	15.03%	0.916	20.15%	0.914	20.73%
			1000	0.922	18.60%	0.918	19.72%	0.902	24.14%	0.899	24.80%
		-2	1	0.932	15.72%	0.928	16.81%	0.910	21.79%	0.910	21.87%
			10	0.919	19.42%	0.915	20.42%	0.899	24.84%	0.898	25.06%
		-1	1	0.935	15.03%	0.930	16.17%	0.913	20.97%	0.913	21.04%
			10	0.912	21.16%	0.909	22.11%	0.893	26.53%	0.892	26.85%
		0	1	0.921	18.76%	0.918	19.71%	0.902	23.98%	0.902	24.06%
			10	0.937	14.37%	0.933	15.59%	0.915	20.46%	0.914	20.73%
			100	0.938	13.96%	0.934	15.23%	0.915	20.38%	0.913	20.96%
			1000	0.926	17.27%	0.922	18.47%	0.905	23.21%	0.902	23.93%
	2	Con	1	0.933	15.53%	0.931	15.99%	0.918	19.73%	0.917	19.78%
			10	0.941	13.24%	0.939	13.76%	0.924	17.85%	0.924	18.04%
			100	0.940	13.56%	0.938	14.02%	0.924	17.88%	0.923	18.25%
			1000	0.940	13.52%	0.938	14.01%	0.924	17.99%	0.921	18.66%
		-2	1	0.947	11.53%	0.946	12.00%	0.931	16.06%	0.931	16.12%
			10	0.935	14.95%	0.933	15.38%	0.920	19.01%	0.919	19.23%
		-1	1	0.926	17.27%	0.925	17.58%	0.913	20.89%	0.913	20.95%
			10	0.942	12.91%	0.941	13.38%	0.927	17.23%	0.926	17.44%
		0	1	0.927	17.14%	0.926	17.53%	0.913	21.09%	0.912	21.13%
			10	0.932	15.73%	0.930	16.19%	0.916	20.08%	0.915	20.33%
			100	0.923	18.20%	0.922	18.58%	0.909	22.20%	0.907	22.57%
			1000	0.949	10.97%	0.947	11.55%	0.931	15.93%	0.929	16.47%
	1	Con	1	0.937	14.29%	0.937	14.29%	0.926	17.36%	0.926	17.42%
			10	0.934	15.28%	0.934	15.28%	0.924	17.88%	0.924	18.01%
			100	0.941	13.26%	0.941	13.27%	0.930	16.27%	0.929	16.53%
			1000	0.941	13.38%	0.941	13.39%	0.930	16.37%	0.928	16.85%
		-1	10	0.946	11.88%	0.946	11.88%	0.934	15.19%	0.933	15.36%
150	2.8	Con	1	0.933	15.47%	0.928	16.88%	0.901	24.44%	0.900	24.53%
			10	0.939	13.74%	0.935	14.88%	0.909	22.02%	0.908	22.39%
			100	0.943	12.83%	0.937	14.32%	0.909	22.03%	0.907	22.70%
		-2	10	0.940	13.44%	0.935	14.94%	0.911	21.64%	0.910	21.96%
50	2.8	Con	1	0.945	12.11%	0.941	13.37%	0.932	15.82%	0.931	15.89%
			10	0.936	14.77%	0.931	16.05%	0.923	18.33%	0.922	18.54%
			100	0.937	14.46%	0.932	15.77%	0.923	18.18%	0.922	18.56%

Midium Dense Samples

σ'₃	Stress Ratio	Stress Slope	Holding Duraiton	Phase 1 e	Phase 1 Dr	Phase3 e	Phase3 Dr	Phase 4 e	Phase 4 Dr	Phase 5 e	Phase 5 Dr
100	2.8	Con	10	0.854	37.27%	0.853	37.62%	0.845	39.87%	0.844	40.01%
			10	0.821	46.43%	0.820	46.75%	0.814	48.39%	0.814	48.47%
			10	0.800	52.09%	0.799	52.46%	0.793	54.15%	0.793	54.23%
		0	1	0.798	52.87%	0.797	53.14%	0.791	54.77%	0.791	54.78%
			10	0.798	52.88%	0.796	53.20%	0.791	54.82%	0.790	54.88%
			100	0.796	53.22%	0.795	53.47%	0.790	55.00%	0.789	55.13%
	2	Con	10	0.838	41.71%	0.837	41.91%	0.831	43.67%	0.831	43.75%
	1	Con	10	0.826	45.07%	0.826	45.07%	0.821	46.45%	0.821	46.51%

***All values are calculated at the beginning of each phase**

Table A1. Relative Density at the beginning of each phase

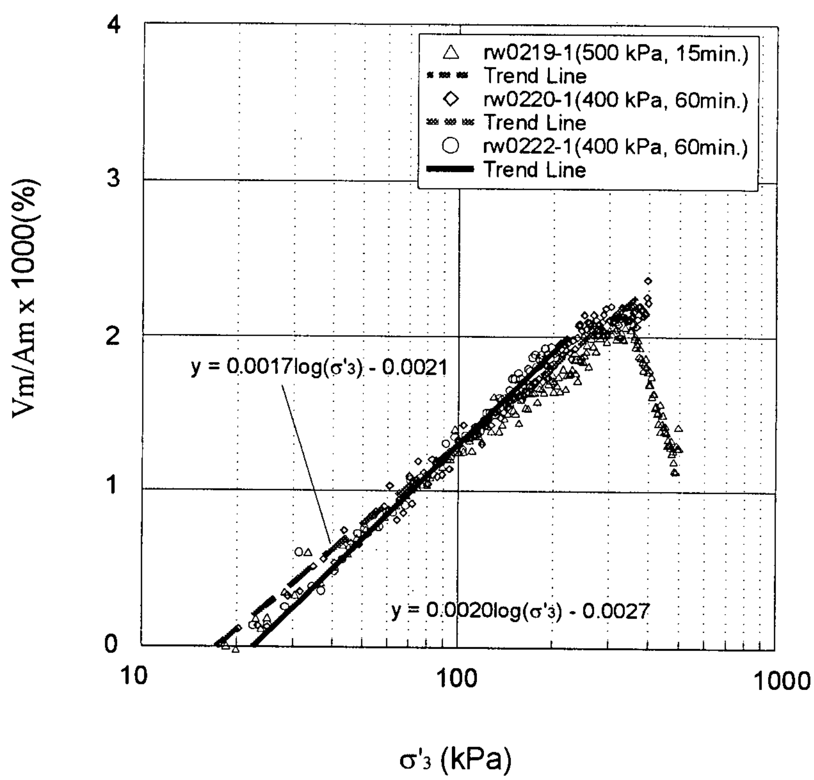

Figure A1. Membrane penetration for unit area of membrane with continuous reduction of stress.

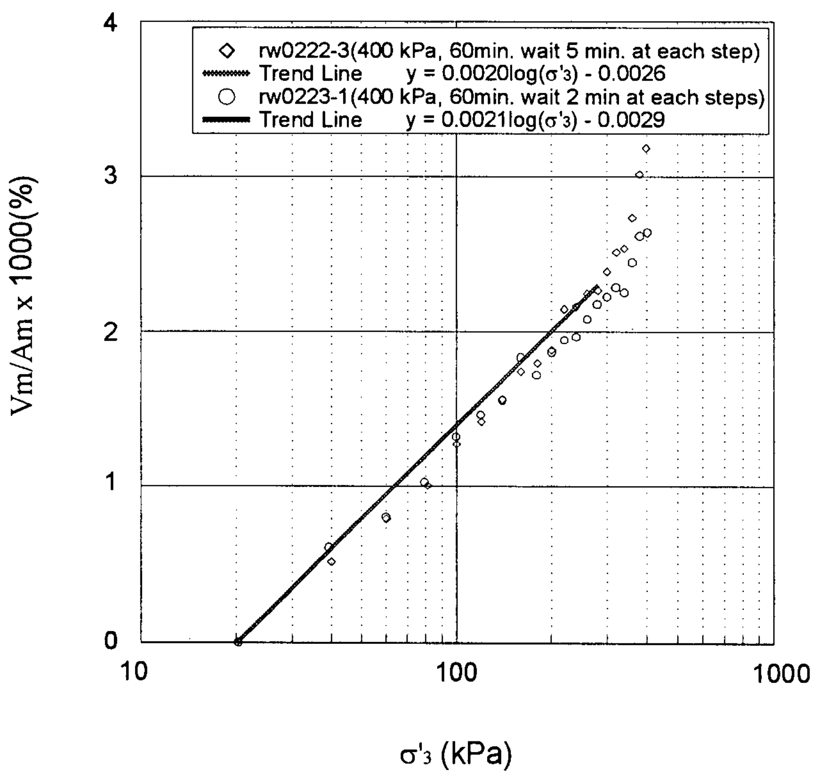

Figure A2. Membrane Penetration for a unit area of membrane with step reduction of stress.

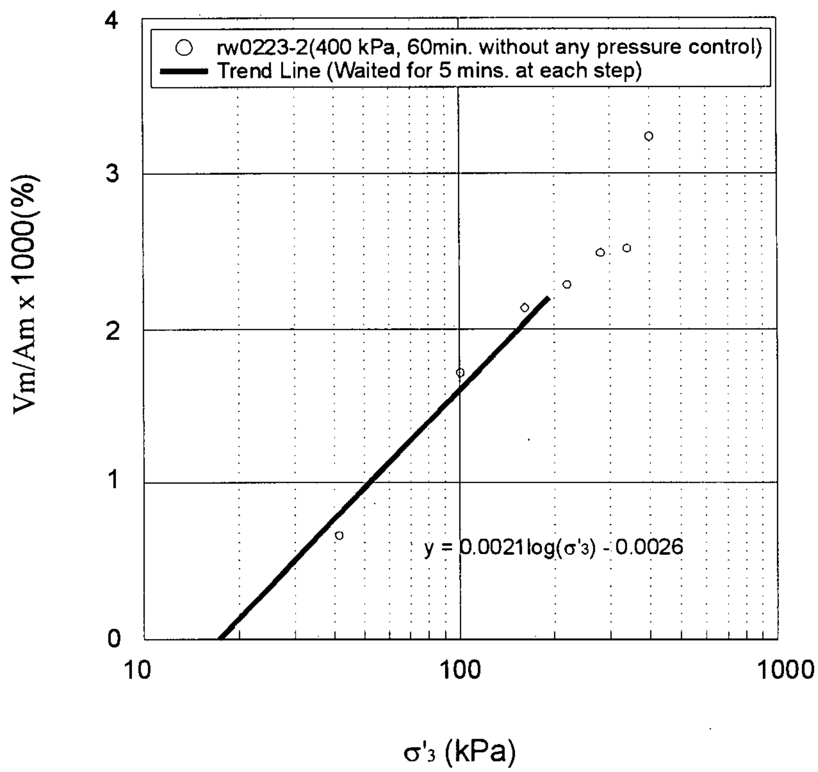

Figure A3. Membrane penetration for unit area of membrane with step reduction of stress without using stress control

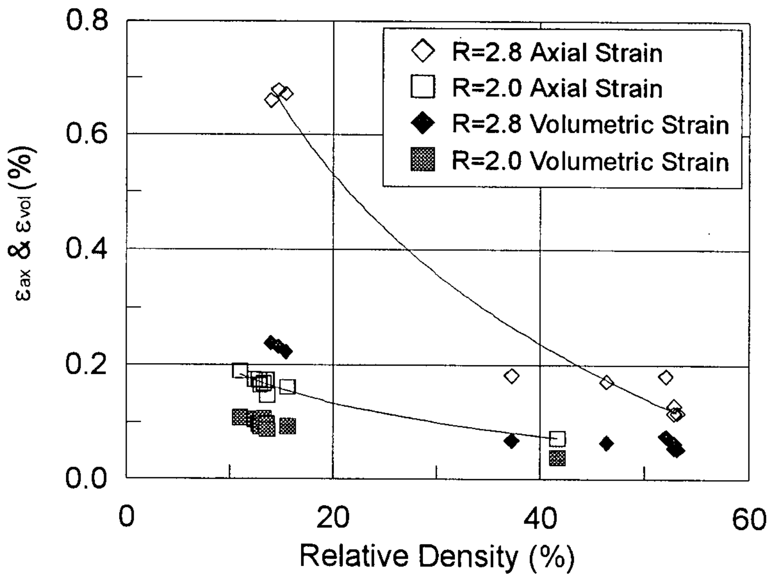

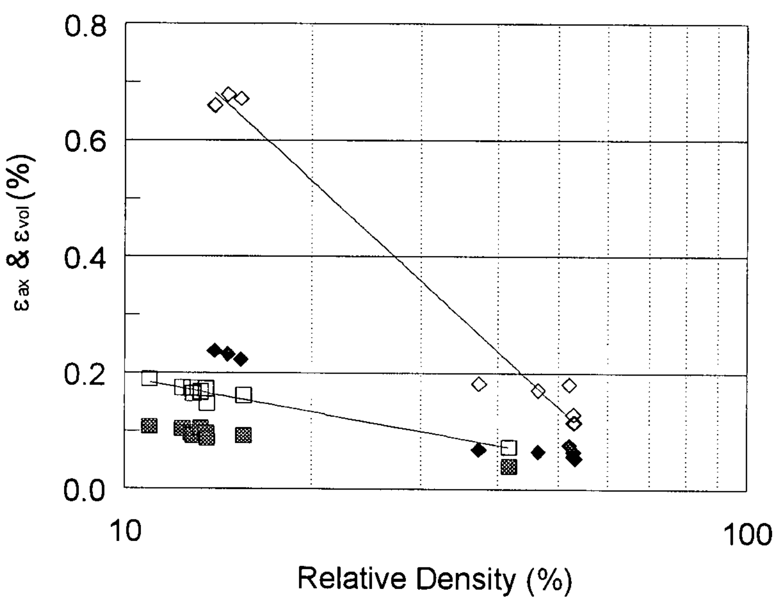

Figure A4. Strain development against Logarithm of the Relative Density in Phase 1

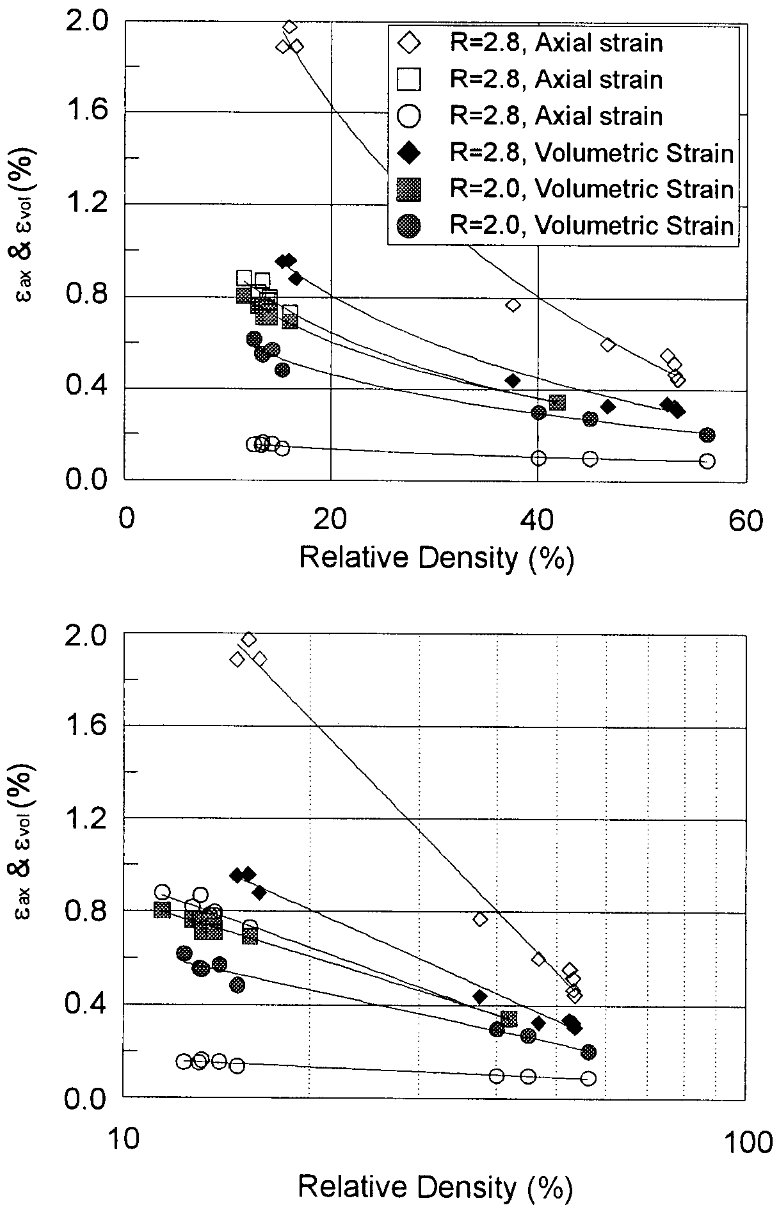

Figure A5. Strain development against Logarithm of Relative Density in Phase 3

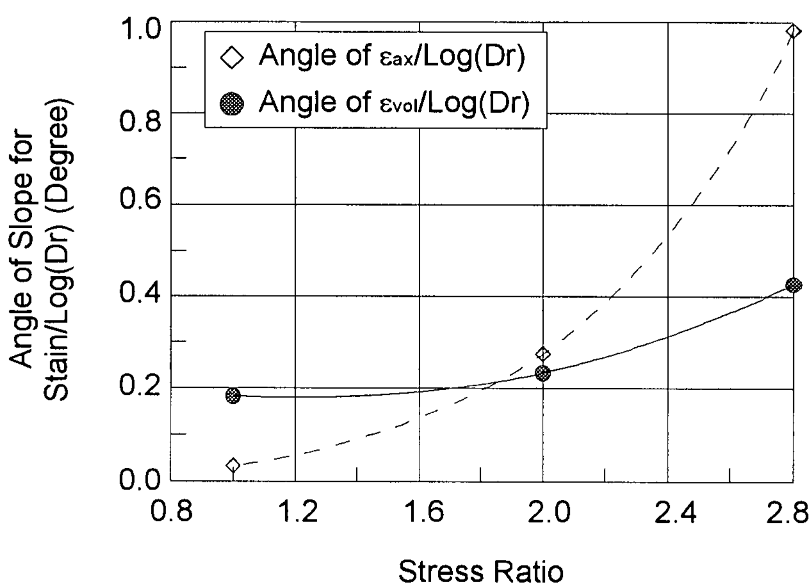

Figure A6. Angle of Strain/Log(Dr) for Stress Ratio

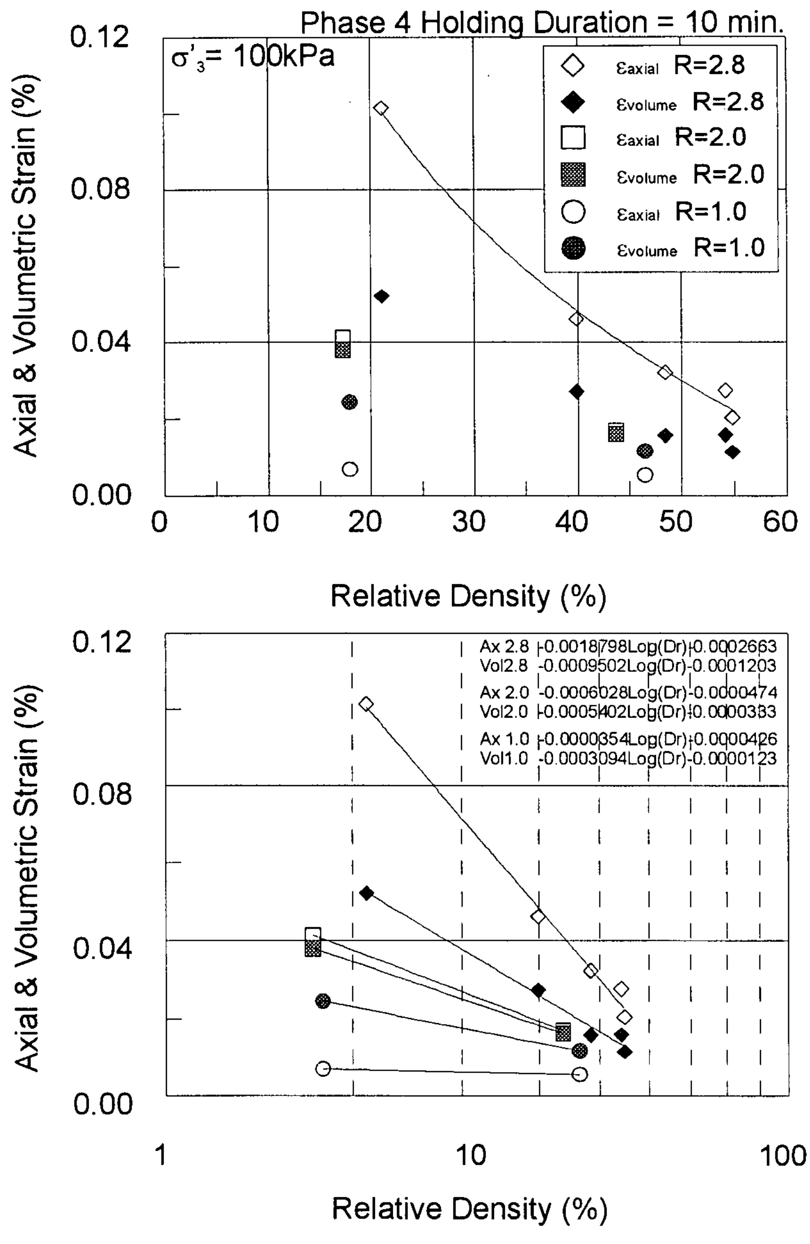

Figure A7. Relationship between strain and relative density for the stress ratio difference

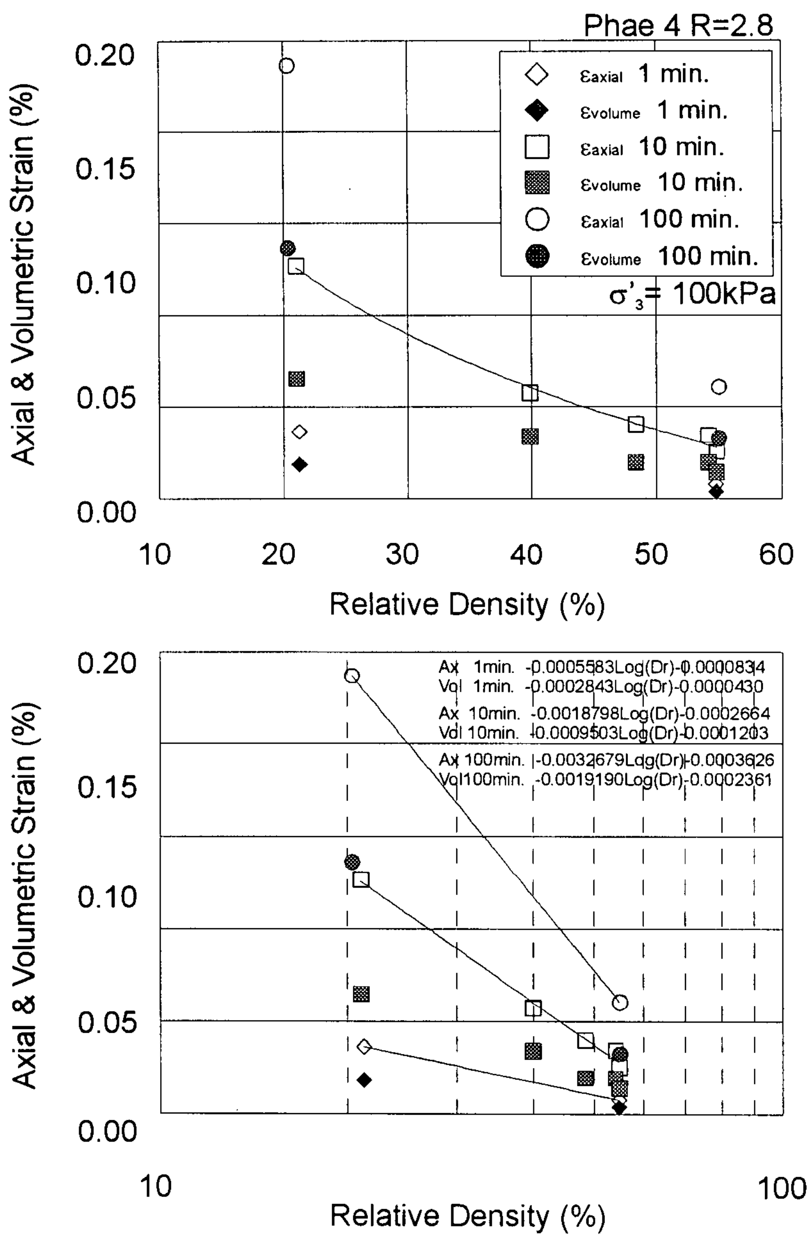

Figure A8. Relationship between strain and relative density for the holding duration differences

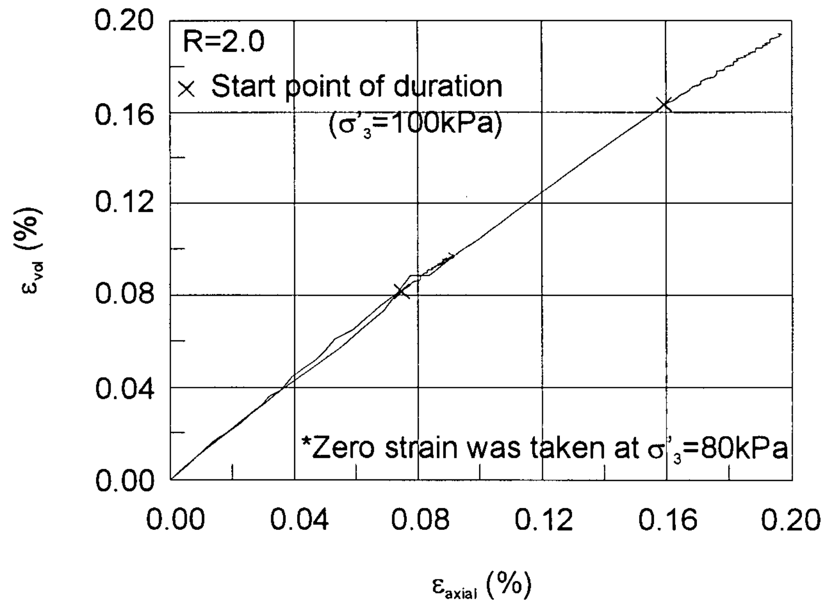

Figure A9. Stain Path Direction change through Phase 3 and Phase 4 at R=2.0

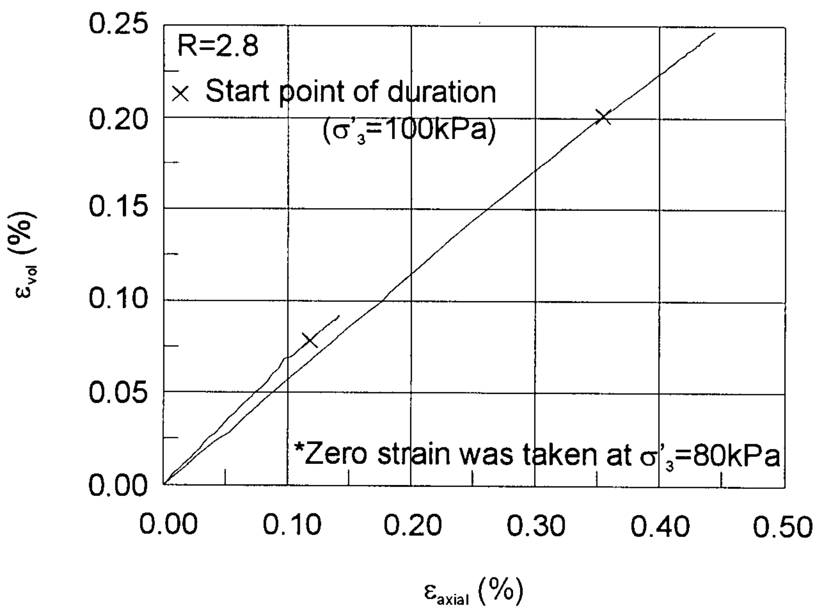

Figure A10. Strain Path Direction change through Phase 3 and Phase 4 at R=2.8

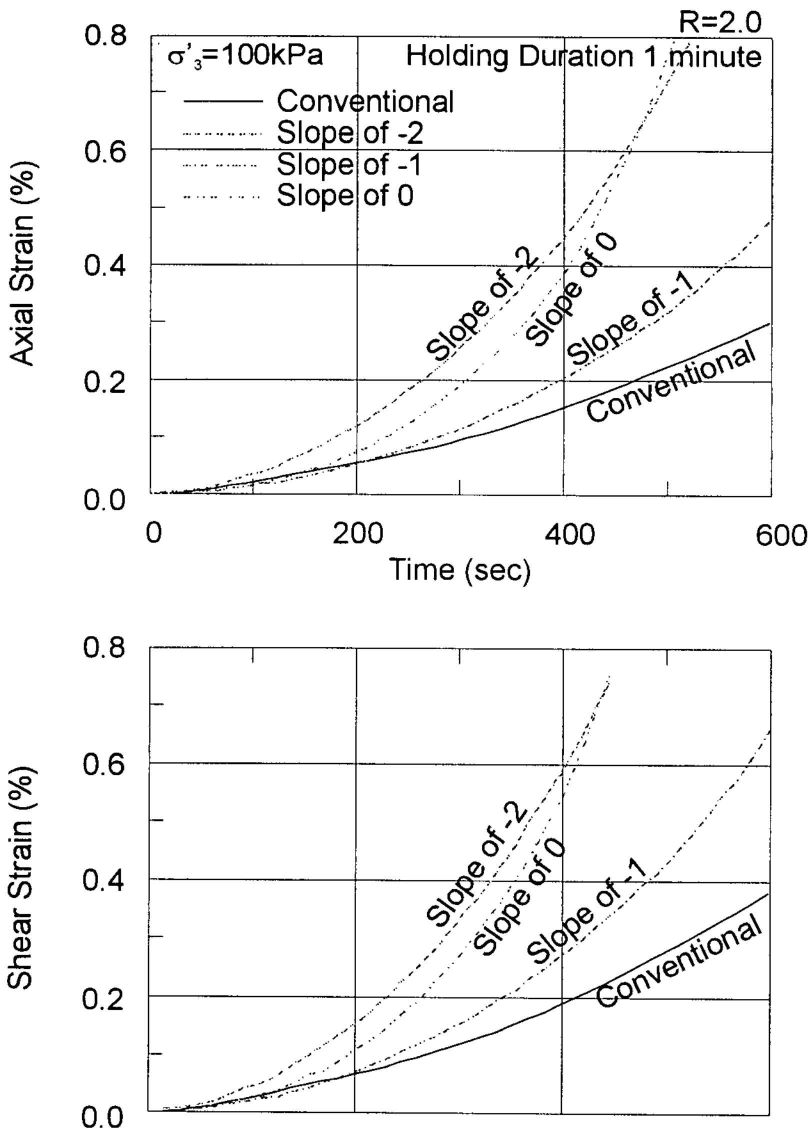

Figure A11. Axial and Shear Strain Rate on various applied stress paths for Phase 5 at R=2.0

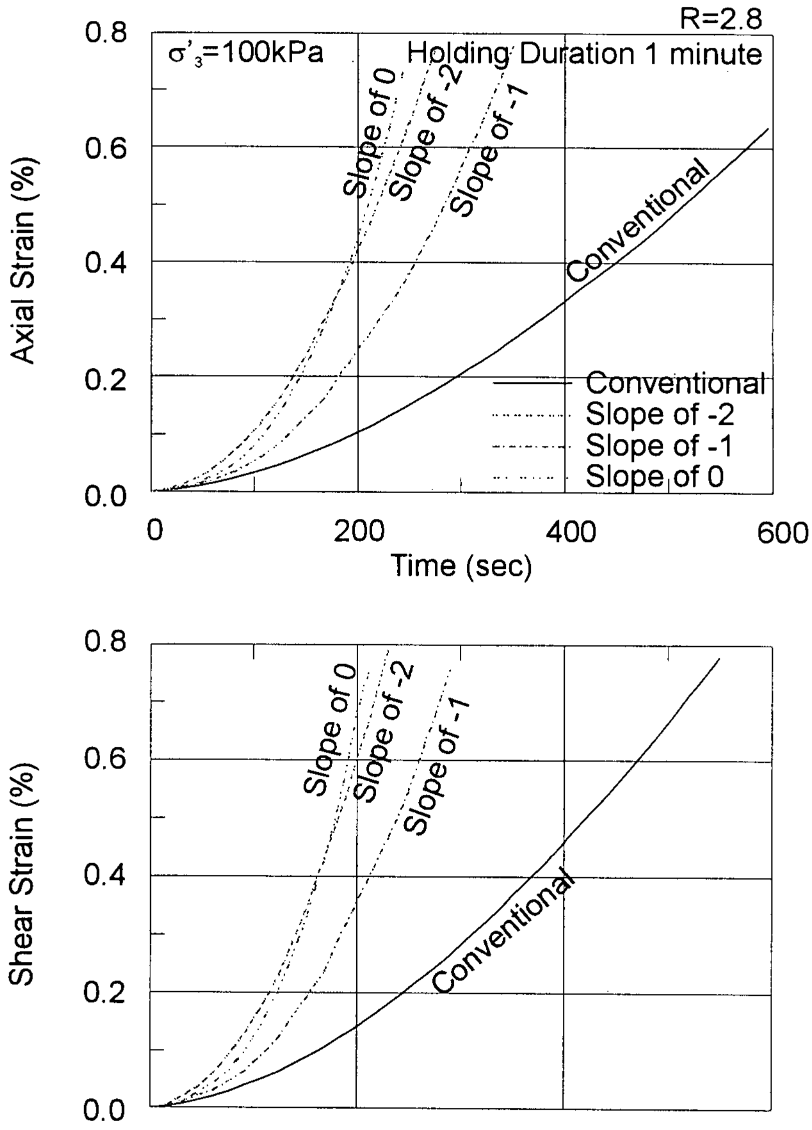

Figure A12. Axial and Shear Strain rate on various applied stress paths for Phase 5 at R=2.8

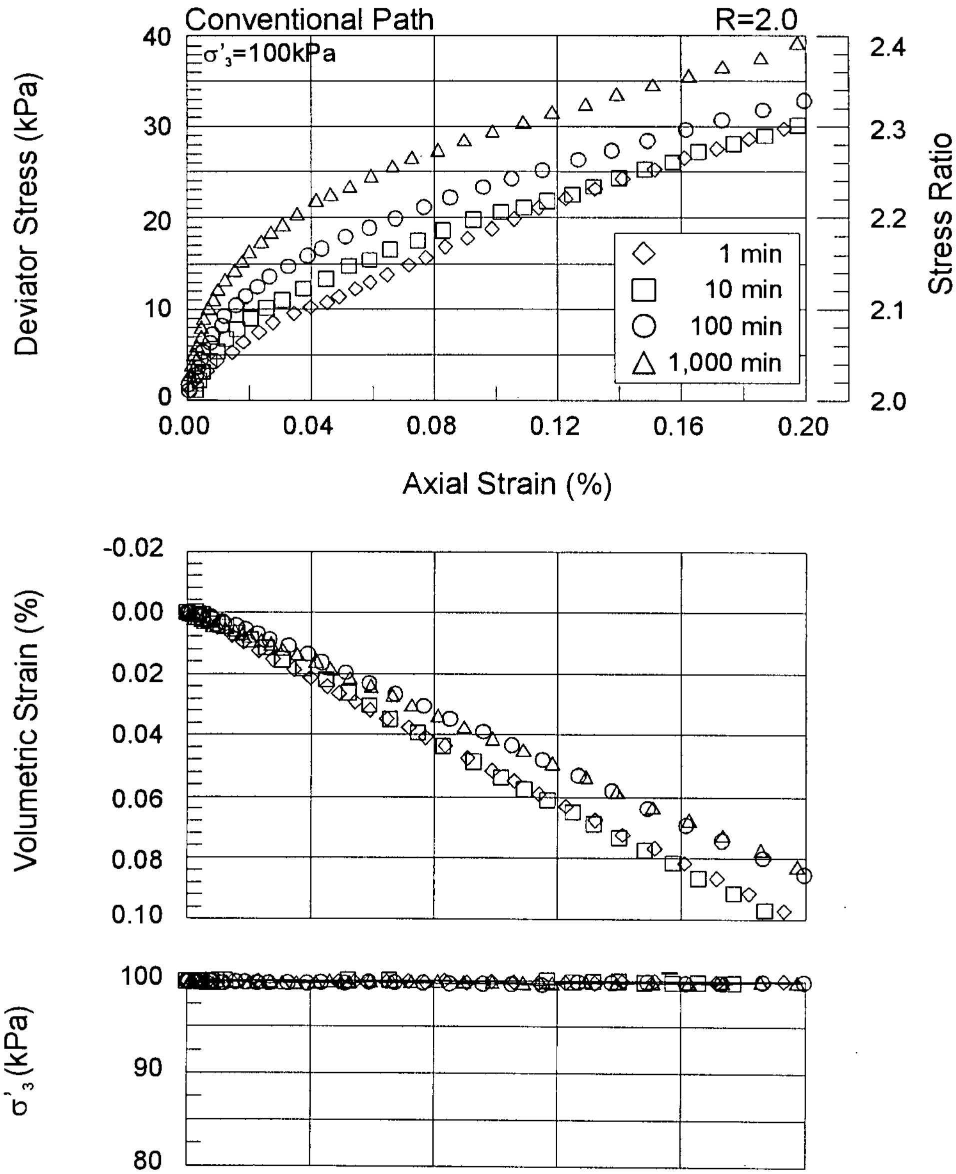

Figure A13. Stress-Strain curves with various holding time on conventional path at R=2.0

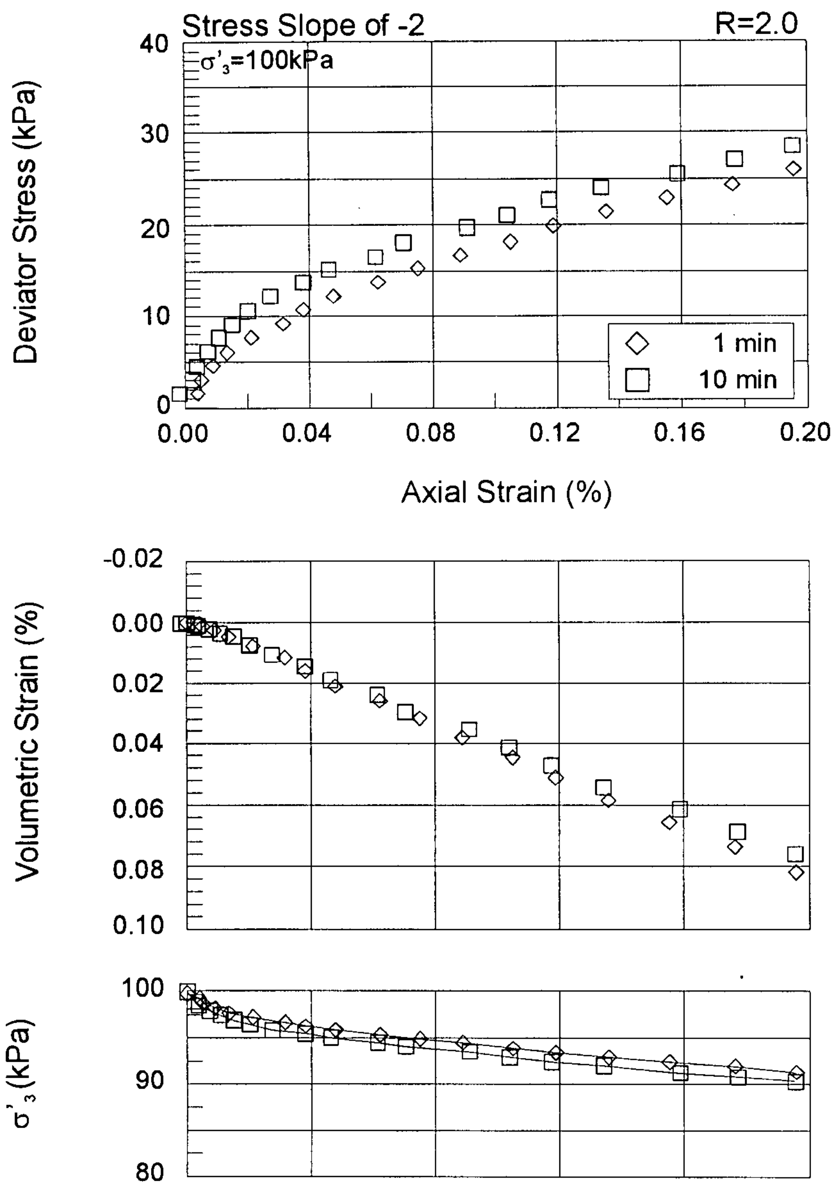

Figure A14. Stress-Strain curves with two holding time on Stress-Slope -2 Path at R=2.0

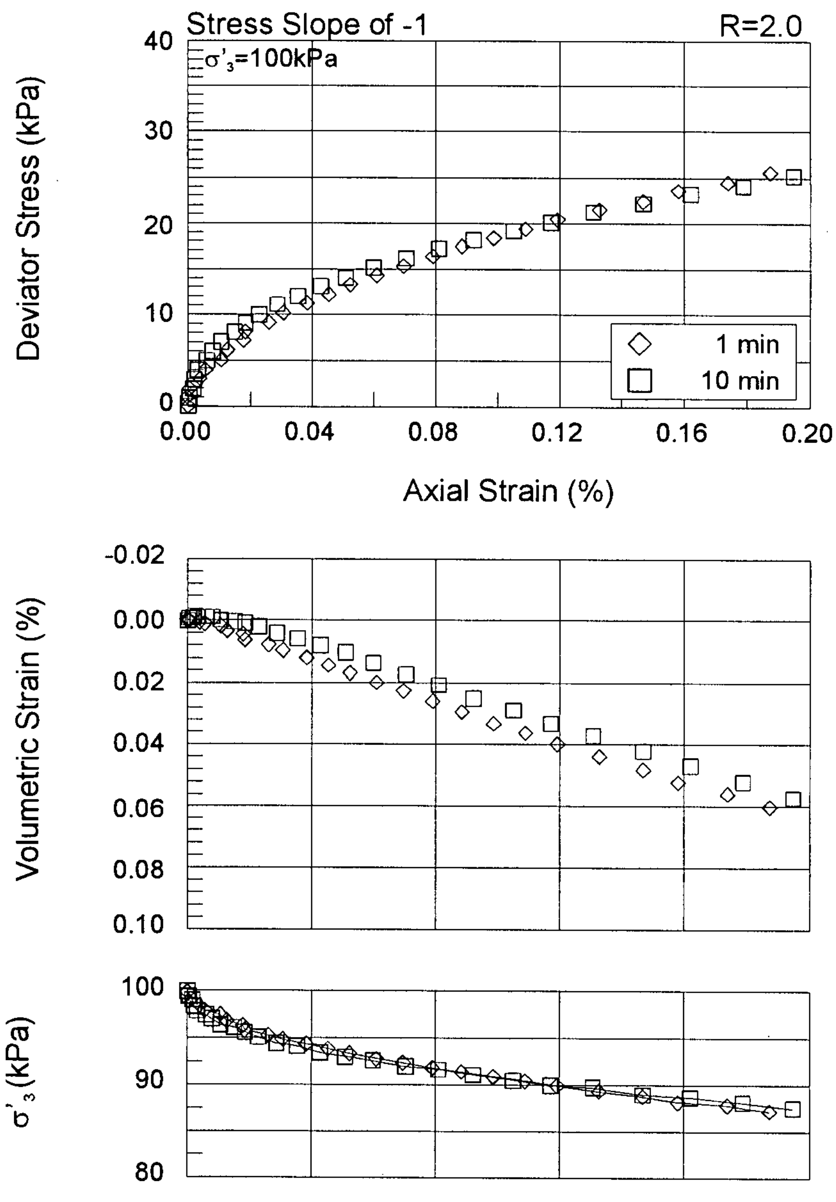

Figure A15. Stress-Strain curves with two holding time on Stress-Slope of -1 Path at R=2.0

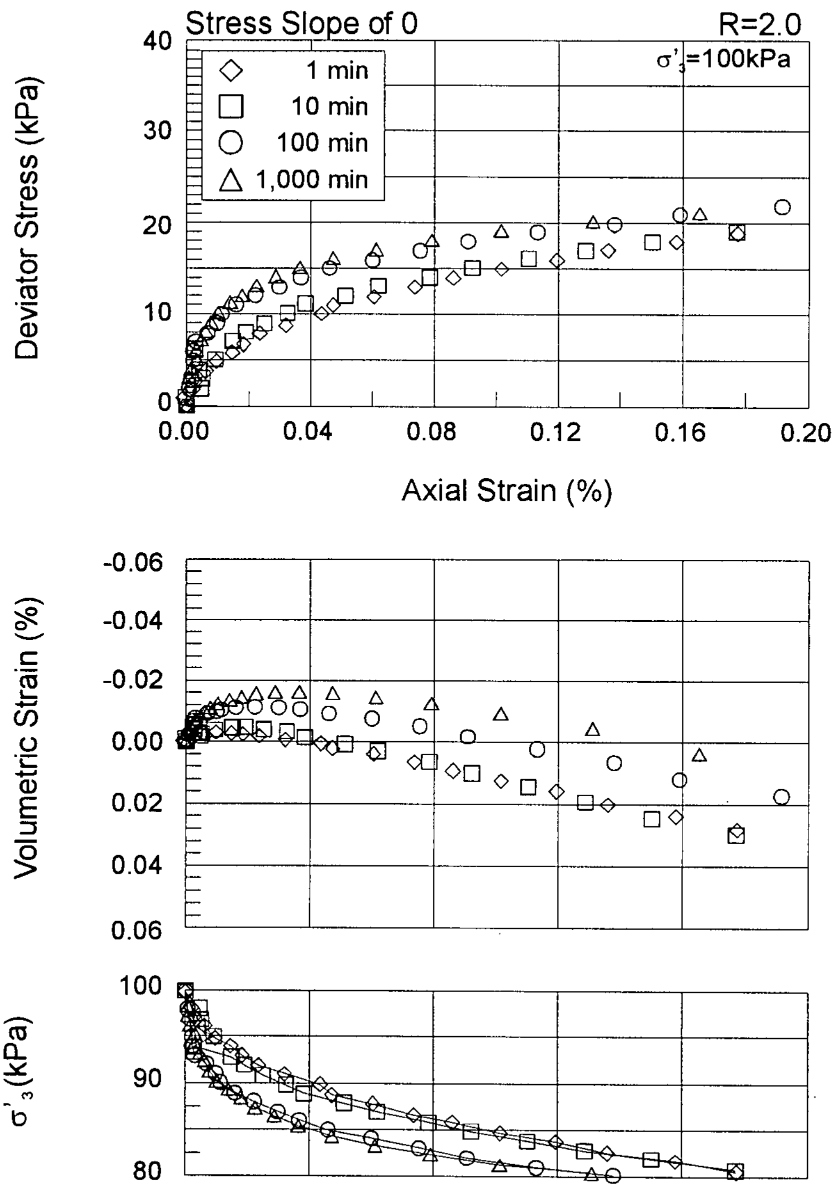

Figure A16. Stress-Strain curves with various holding time for Stress-Slope of 0 at R=2.0

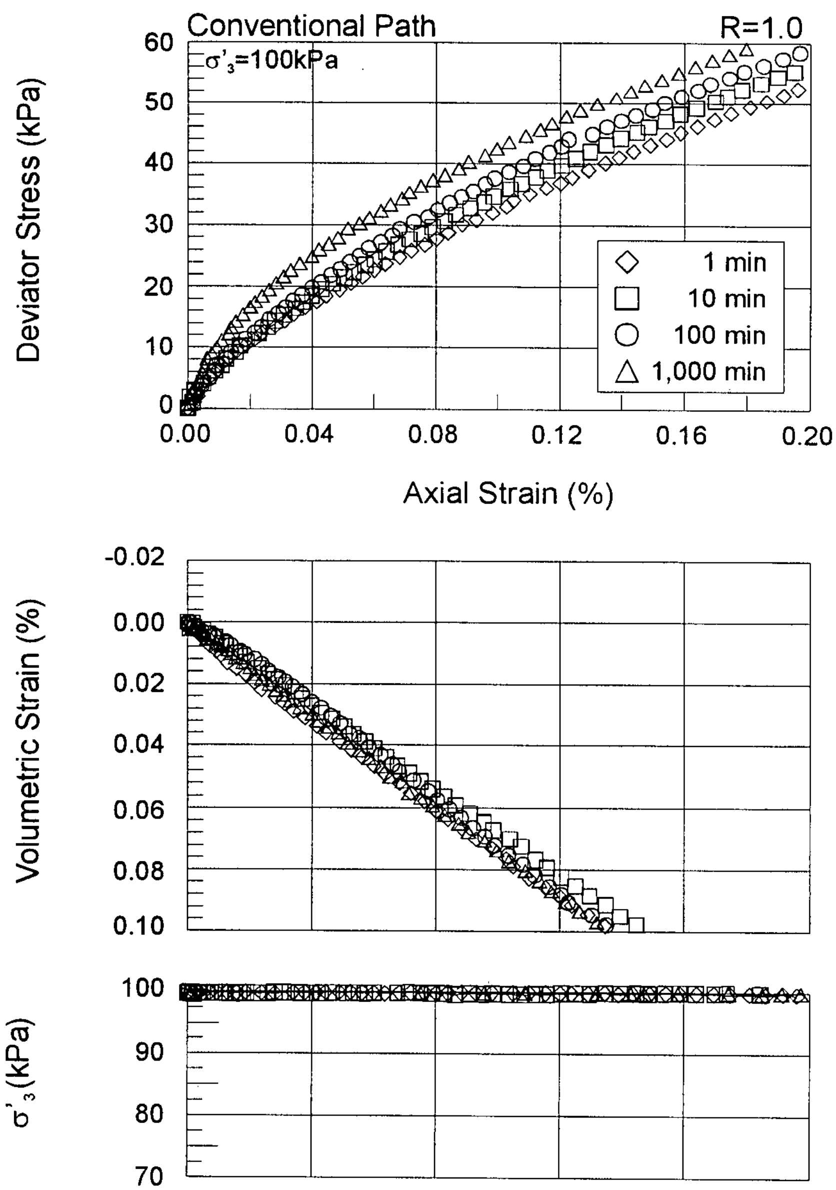

Figure A17. Stress-Strain curves with various holding time on Conventional Path for R=1.0

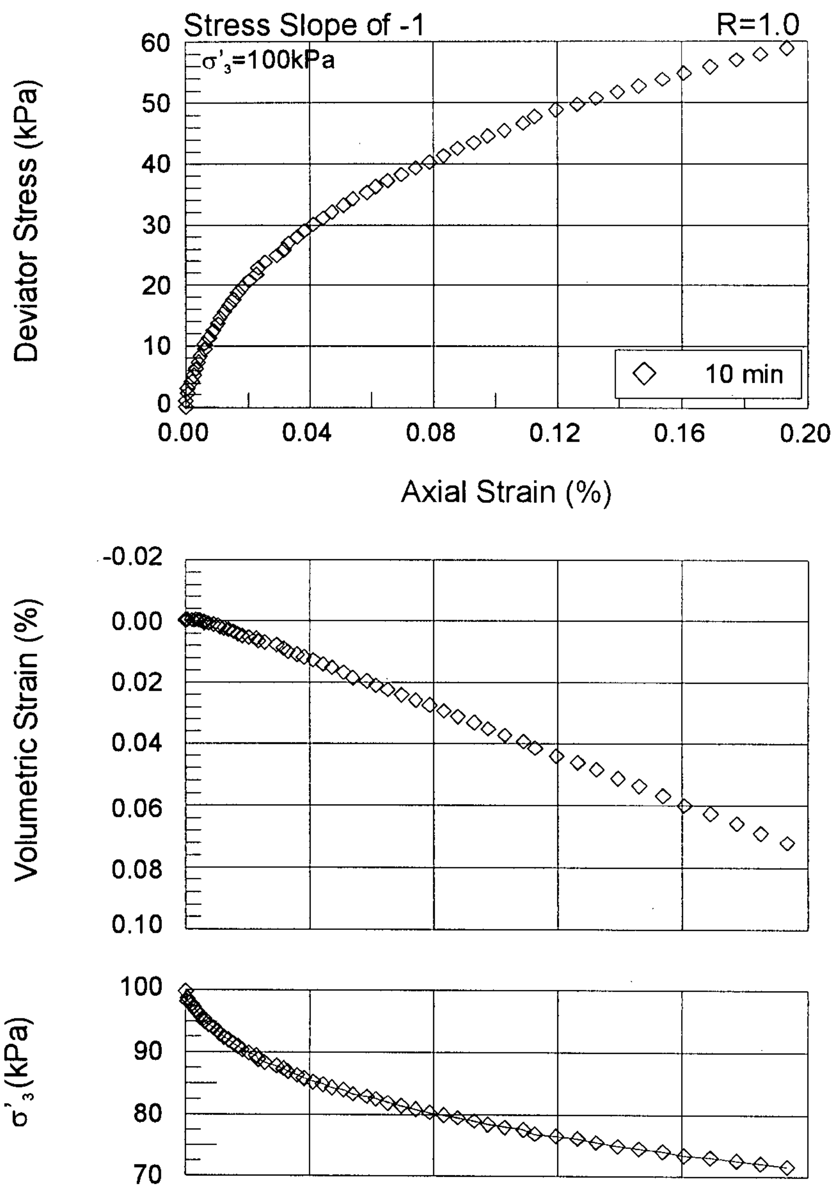

Figure A18. Stress-Strain curve with 10-min. holding time on Stress-Slope of -1 Path at R=1.0

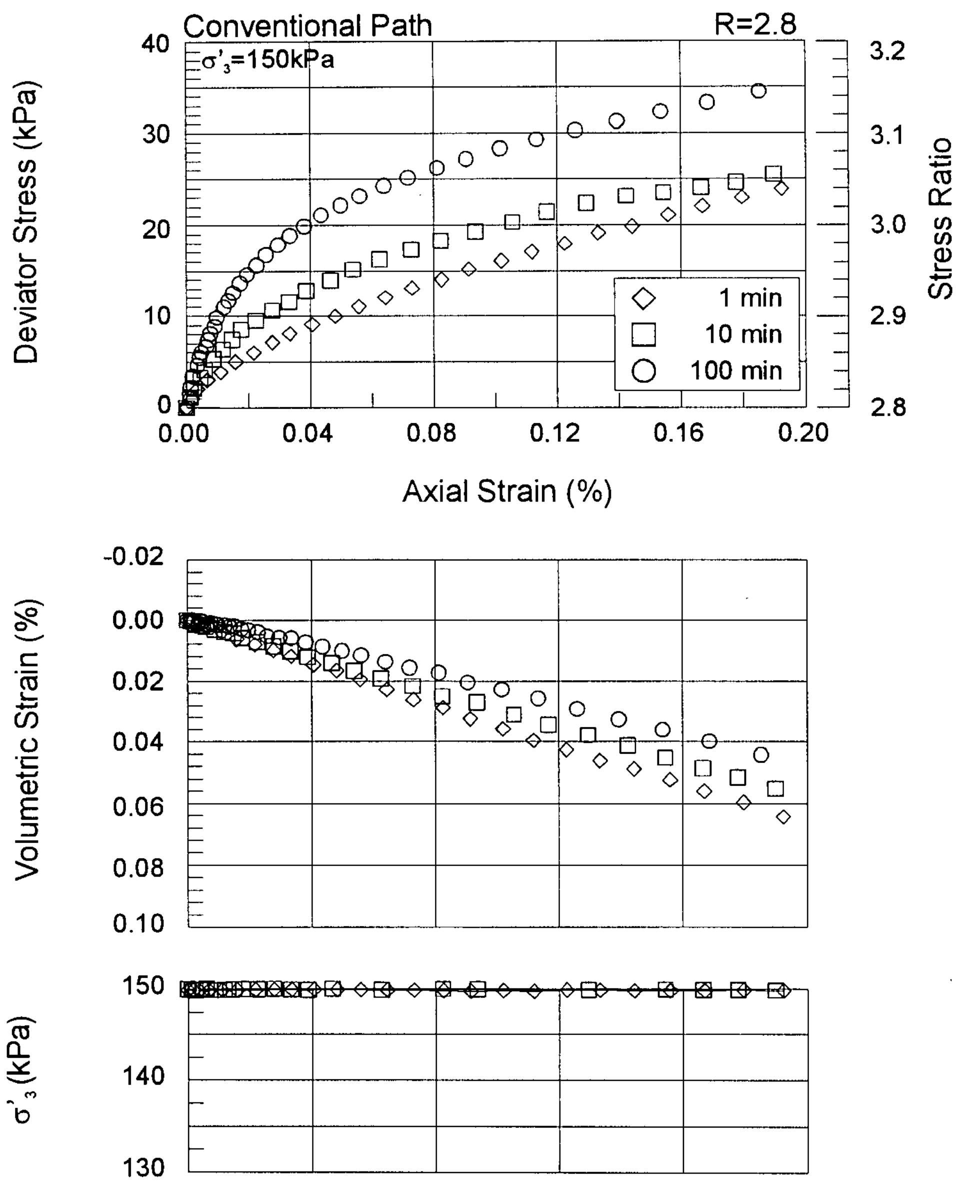

Figure A19. Stress-Strain curves with various holding time on Conventional Path at R=2.8 under 150kPa confining stress.

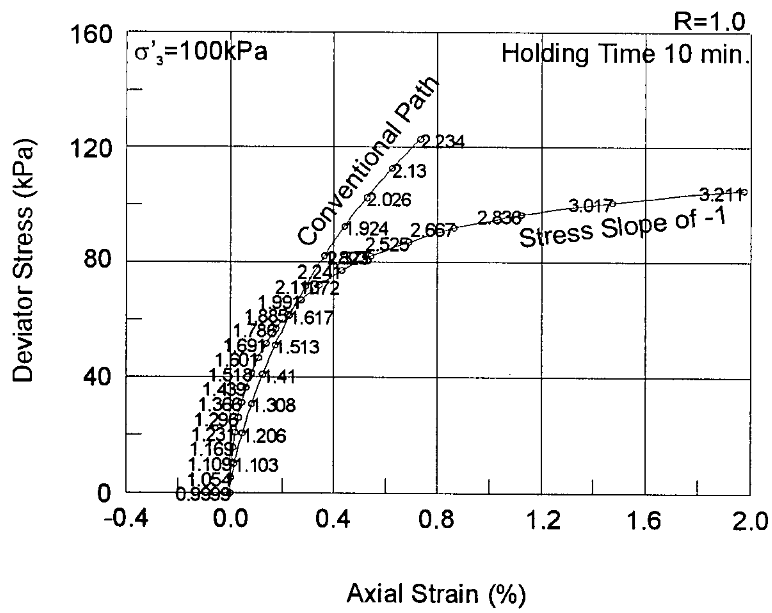

Figure A20. Two stress paths at R=1.0

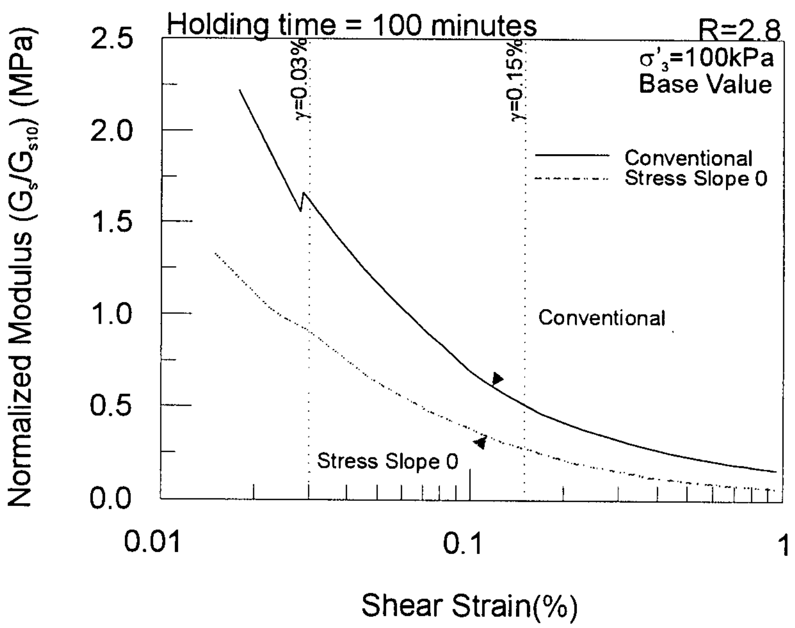

Figure A21. Attenuation Curves for Various Stress Paths with holding duration of 100 minutes at R=2.8

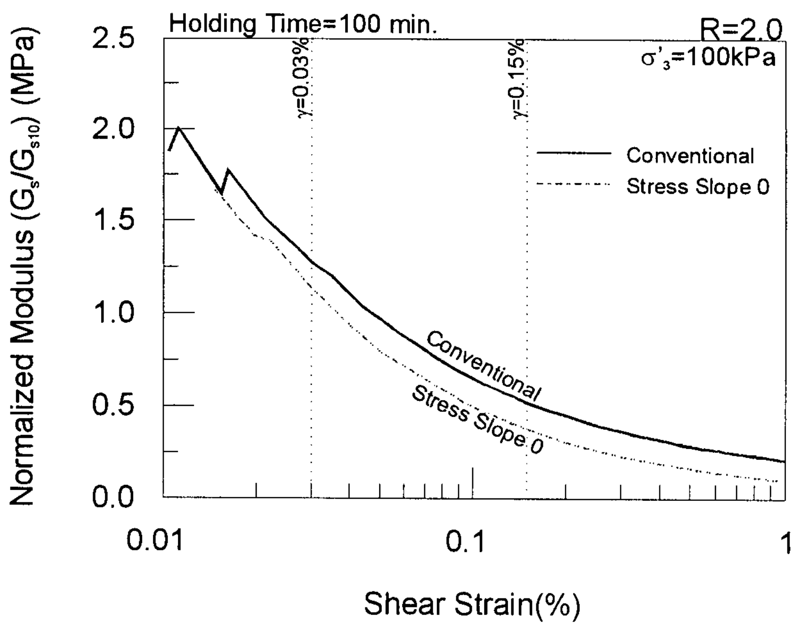

Figure A22. Attenuation Curves for Various Stress Paths with holding duration of 100 minutes at R=2.0

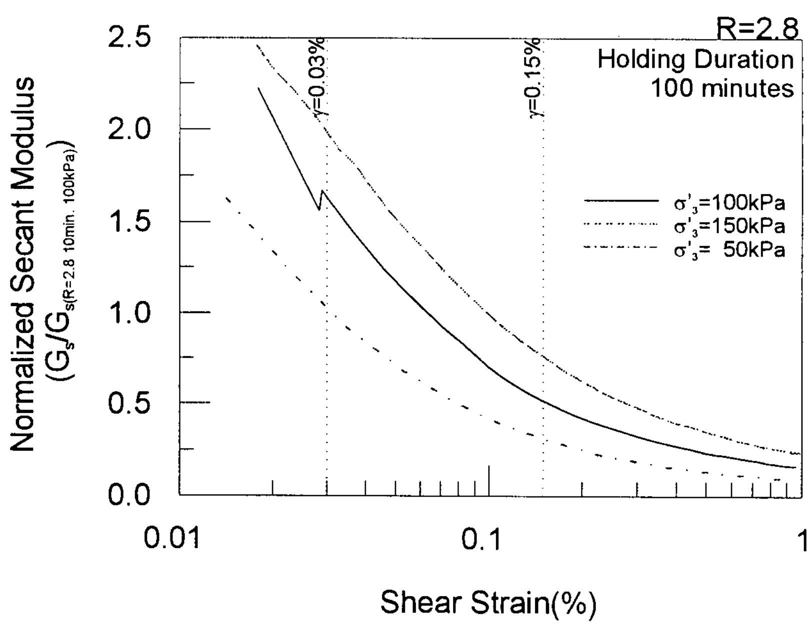

Figure A23. Attenuation curve for various confining stresses

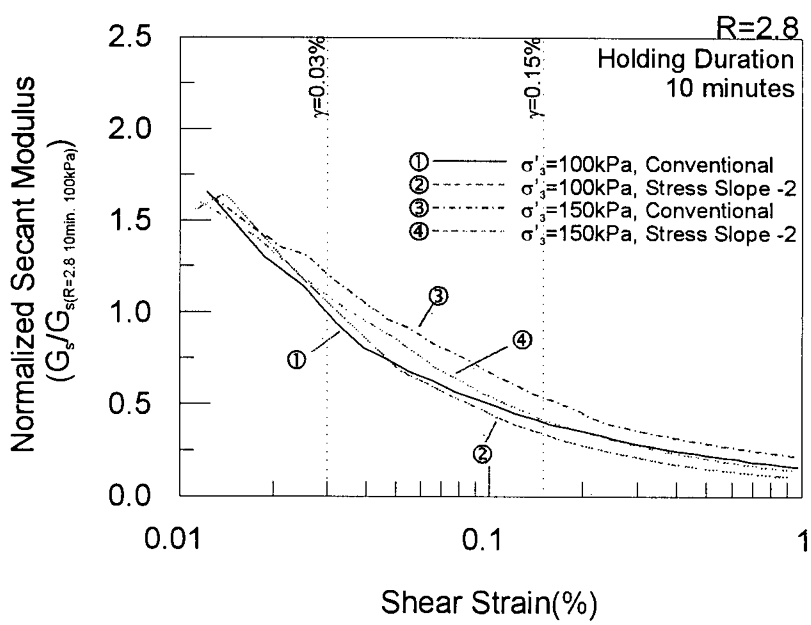

Figure A24. Effect of stress path for different confining stresses

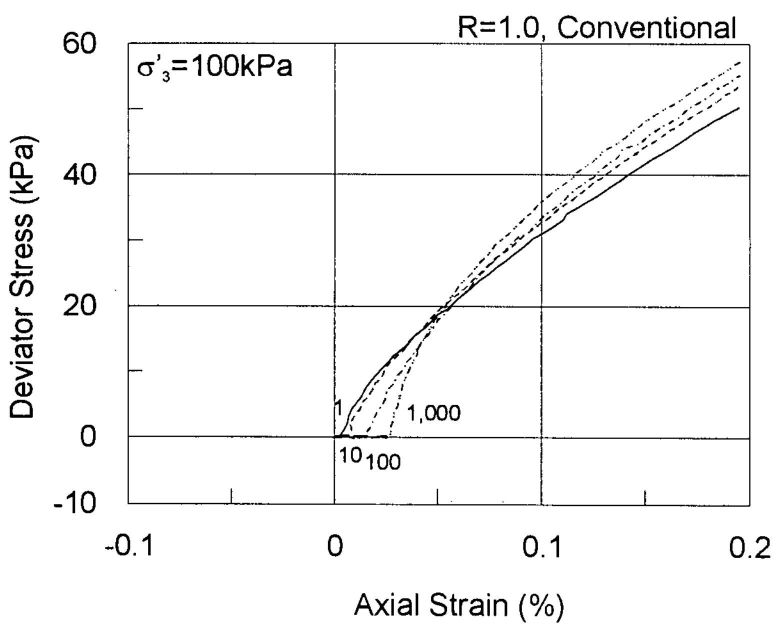

Figure A25. Axial strain development through Phase 4 and Phase 5 at R=1.0 on Conventional Path

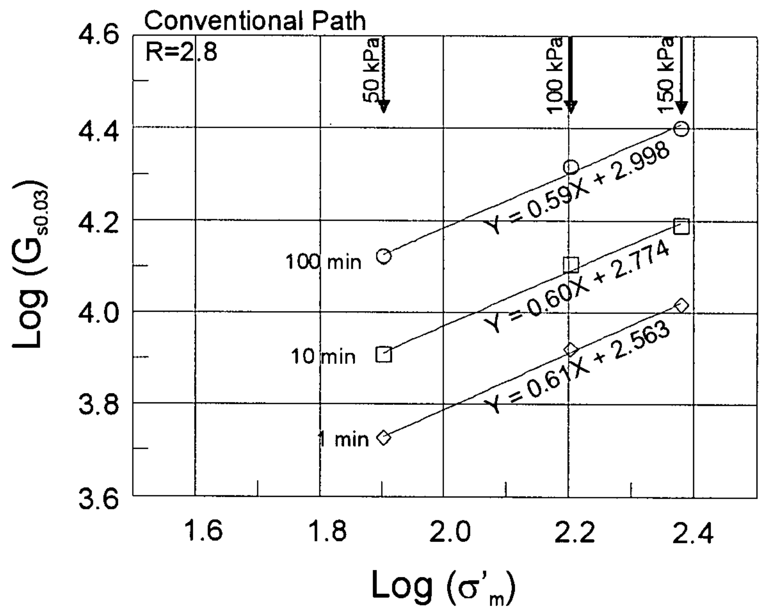

Figure A26. Relationship between Log($G_{0.03}$) and Log(σ'_m) for various holding time

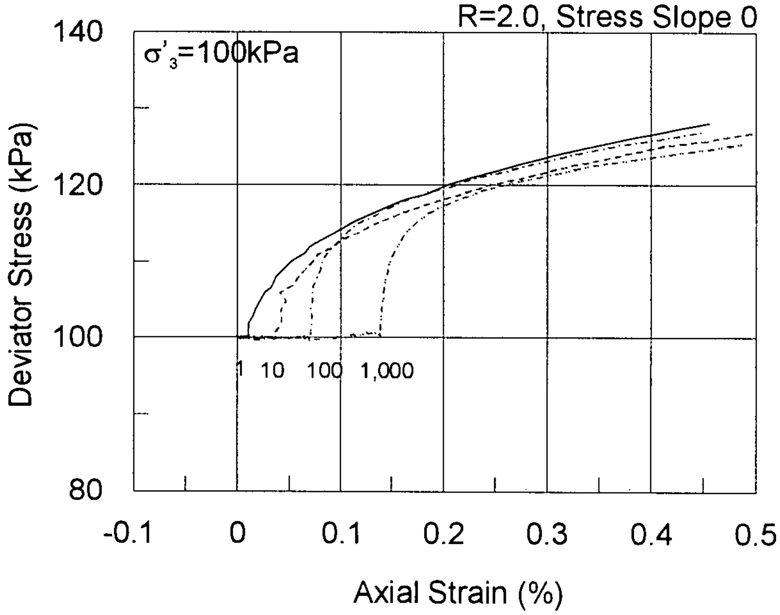

Figure A27. Axial strain development through Phase 4 and Phase 5 at R=2.0 on Stress-Slope of 0 Path

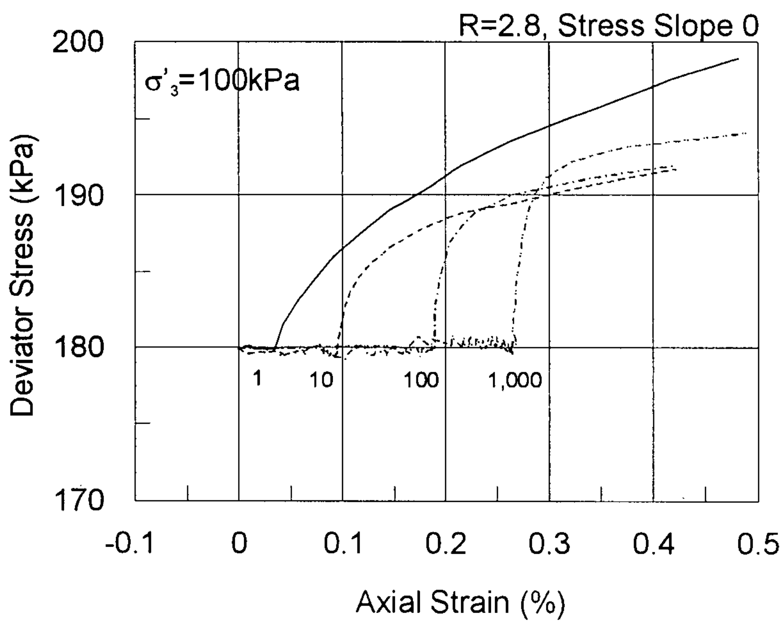

Figure A28. Axial strain development through Phase 4 and Phase 5 at R=2.8 on Stress-Slope of 0 Path

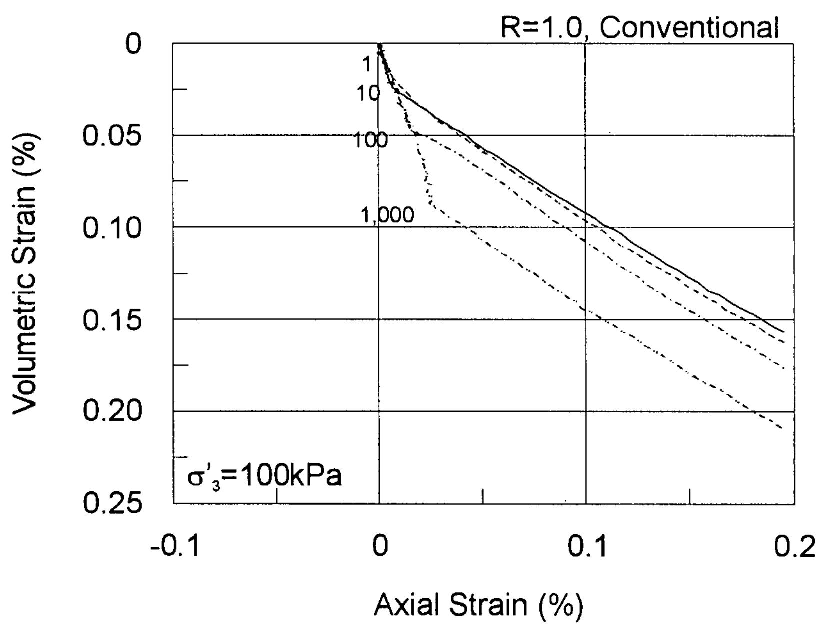

Figure A29. Axial and Volumetric strain development through Phase 4 and Phase 5 at R=1.0 on Conventional Path

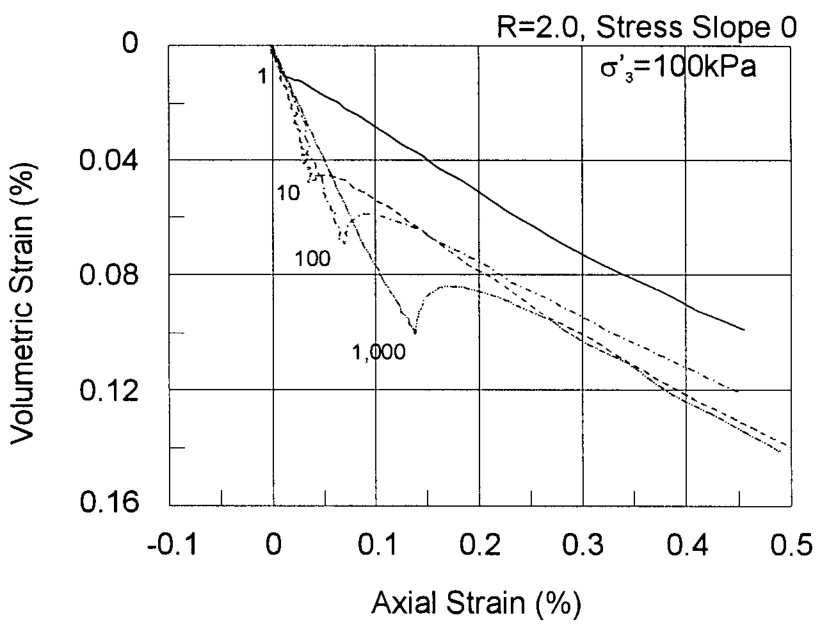

Figure A30. Axial and Volumetric strain development through Phase 4 and Phase 5 at R=2.0 on Stress-Slope of 0 Path

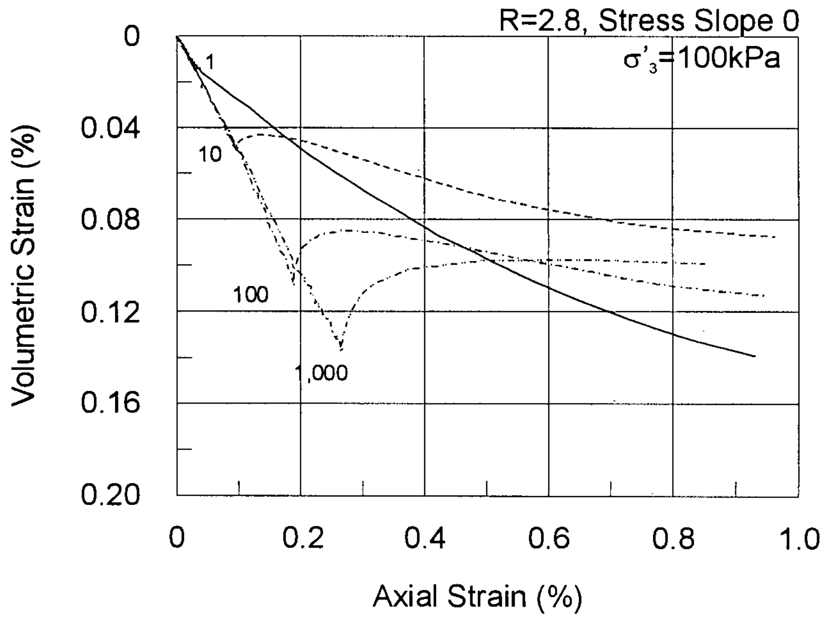

Figure A31. Axial and Volumetric strain development through Phase 4 and Phase 5 at R=2.8 on Stress-Slope of 0 Path

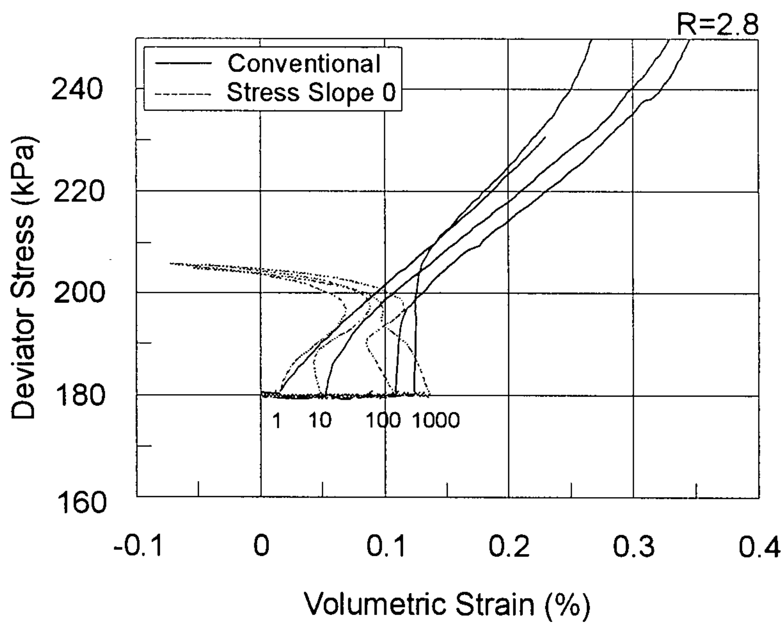

Figure A32. Volumetric strain development with various holding duration on Conventional and Stress-Slope of 0 Path at R=2.8

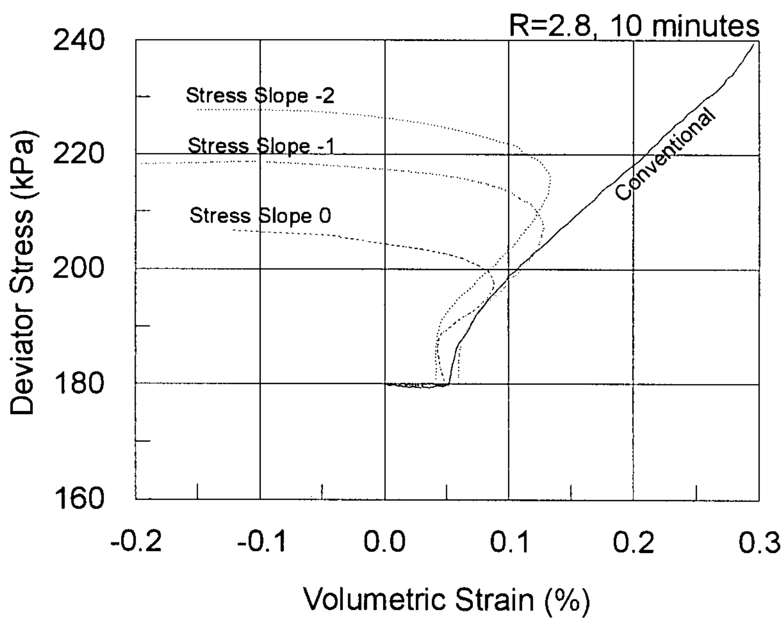

Figure A33. Volumetric strain development on various applied stress paths through Phase 4 and Phase 5 for 10-min. holding duration at R=2.8

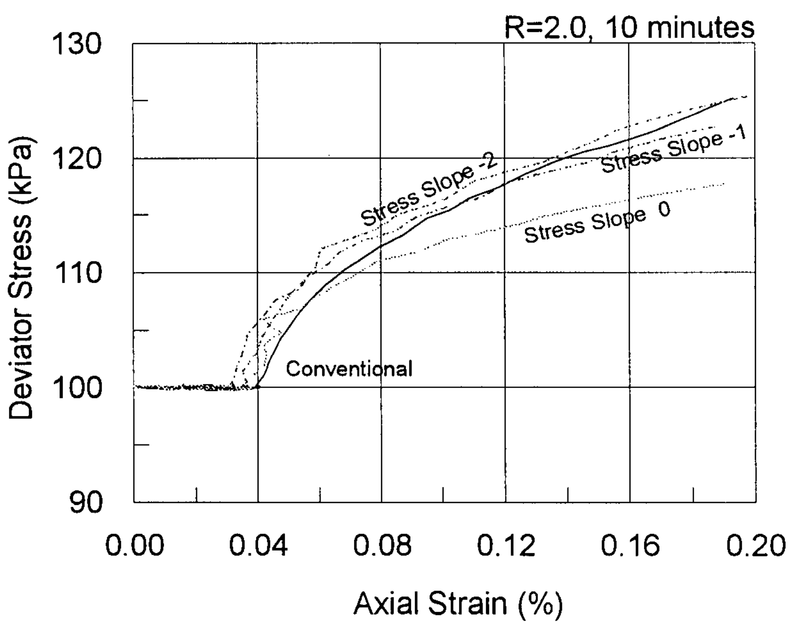

Figure A34. Axial Strain development on various applied stress paths through Phase 4 and Phase 5 for 10-min. holding duration at R=2.0

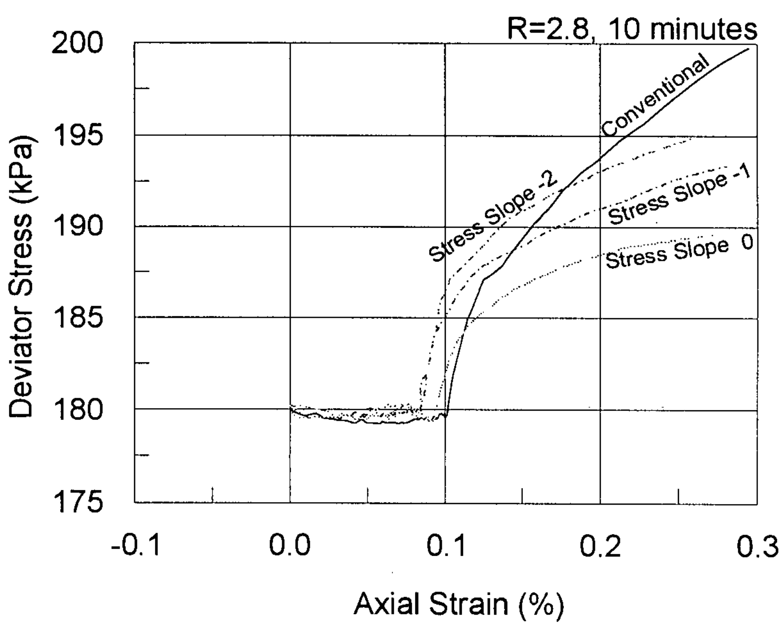

Figure A35. Axial strain development on various applied stress paths through Phase 4 and Phase 5 for 10-min. holding duration at R=2.8

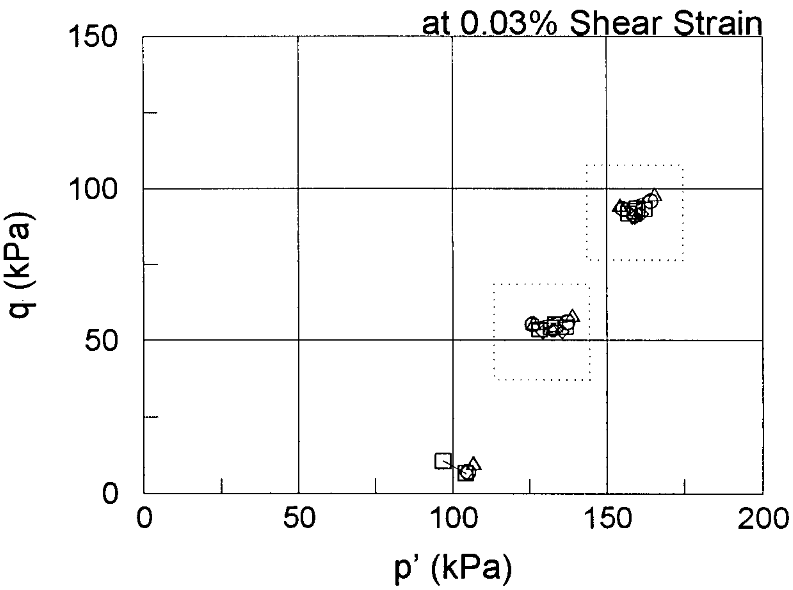

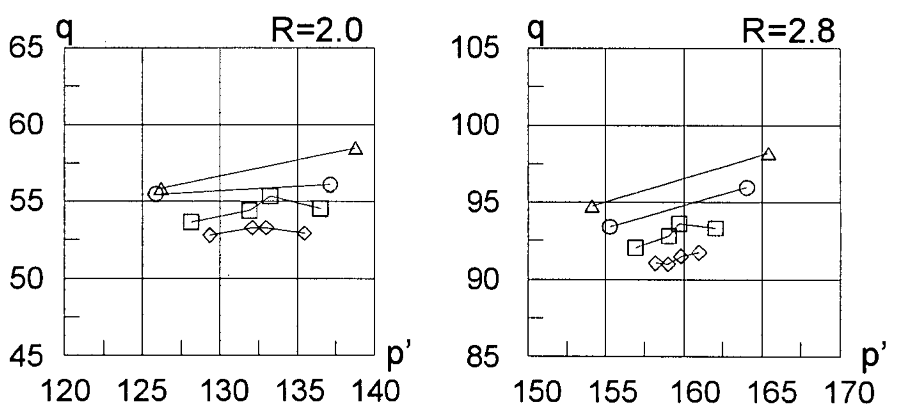

Figure A36. Strain contour at 0.03% in shear strain

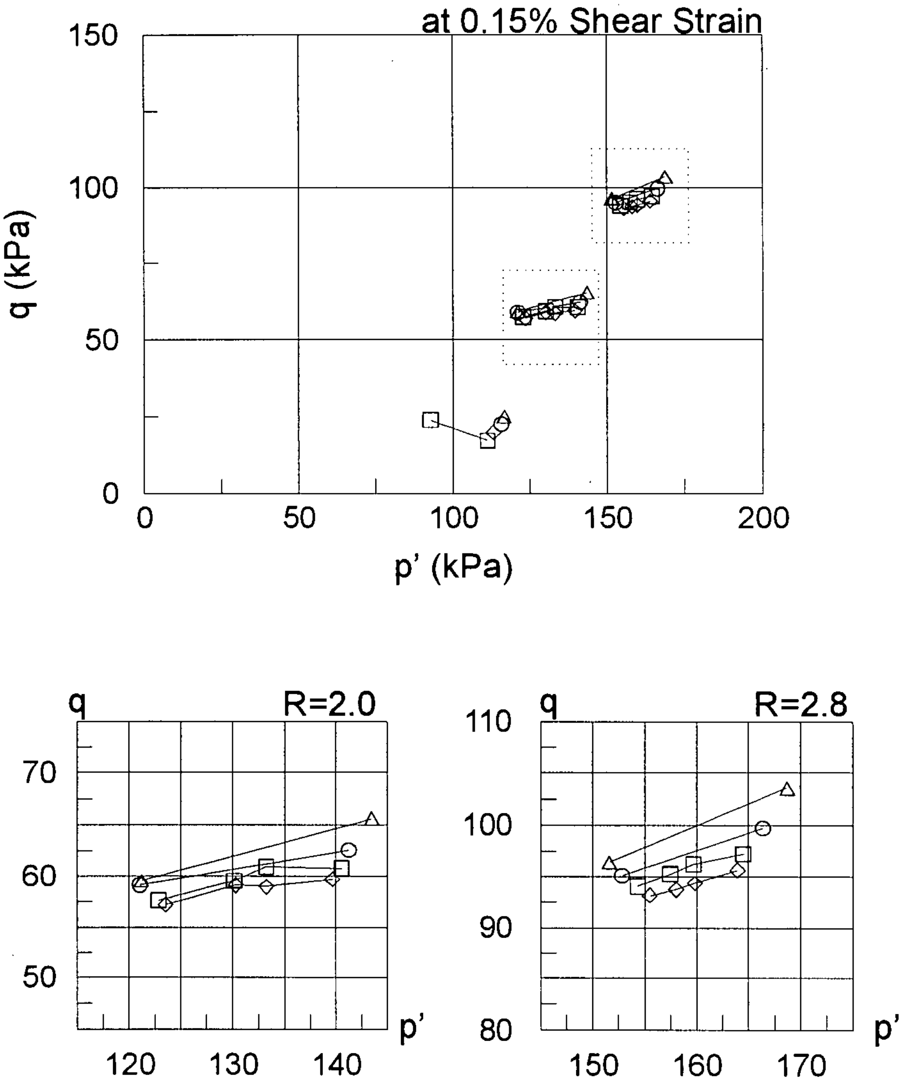

Figure A37. Strain contour at 0.15% in shear strain

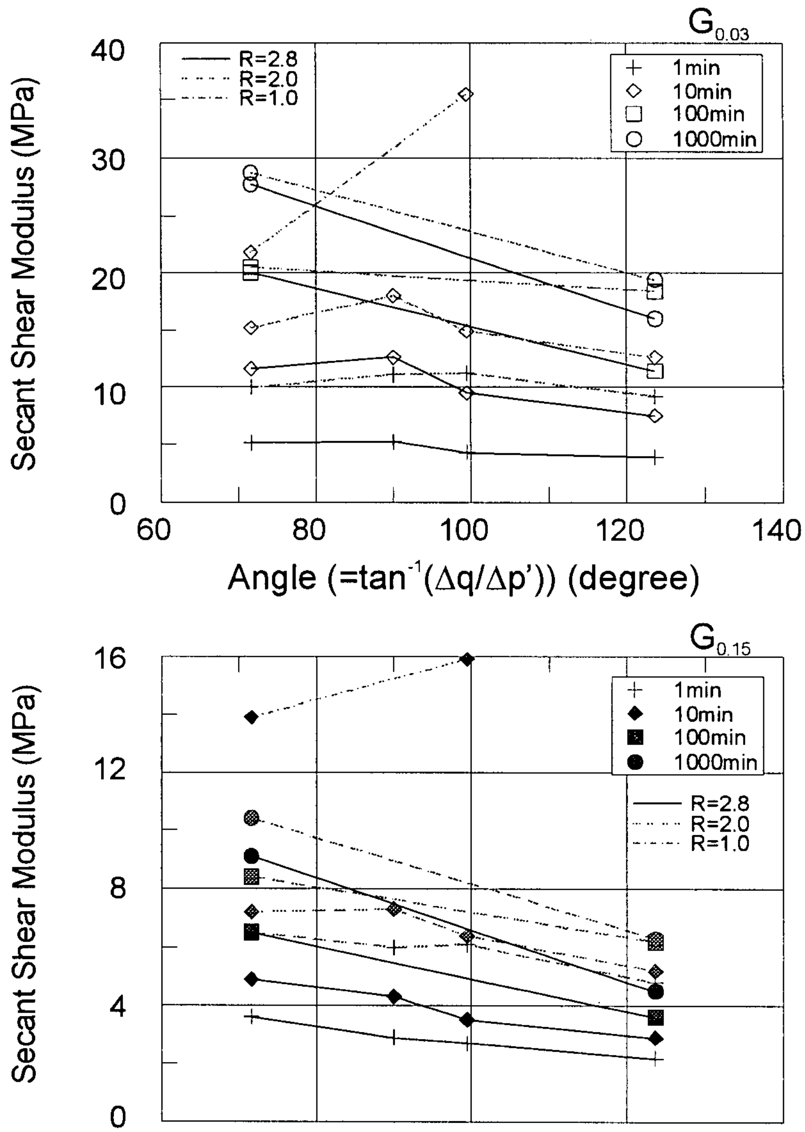

Figure A38. Shear Modulus and Stress Slope on p'-q space

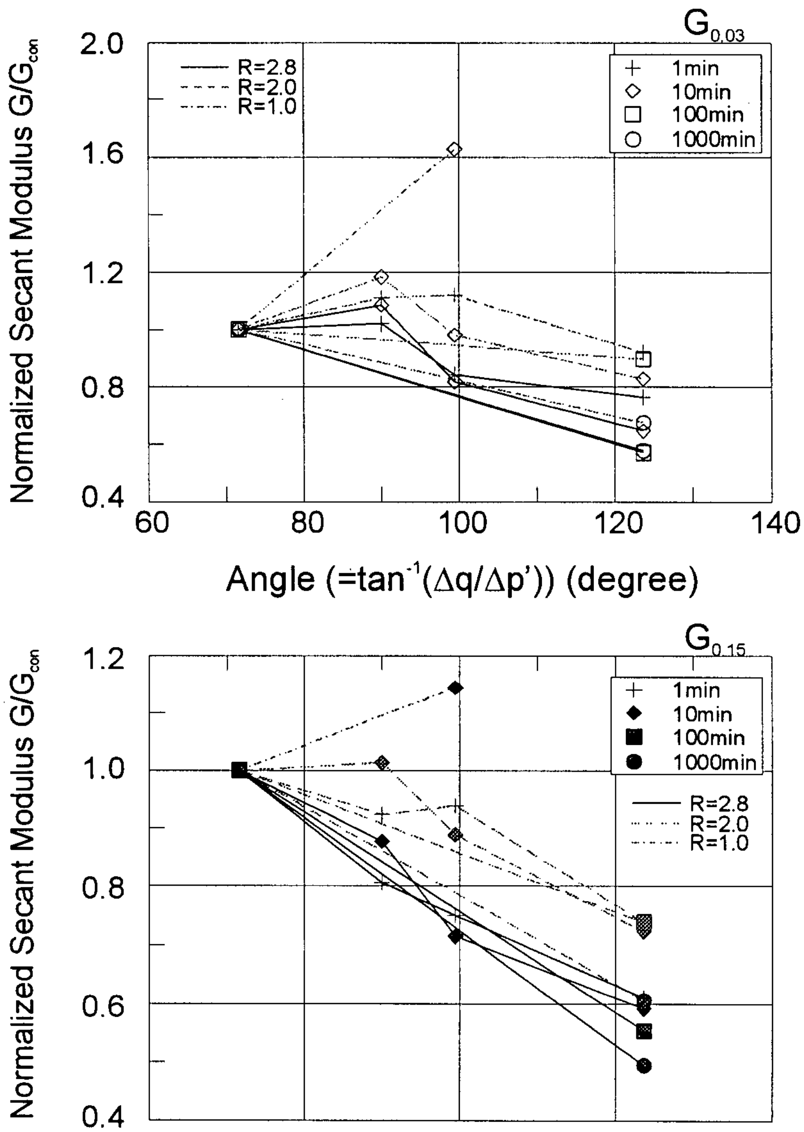

Figure A39. Normalized Shear Modulus and Stress Slope on p'-q space